Cell Replacement Therapy for Parkinson's Disease - Evaluating the potential of autologous grafting.

Nilsson, Fredrik

2023

Document Version:
Publisher's PDF, also known as Version of record

Academic dissertation

Cell Replacement Therapy for Parkinson's Disease -Evaluating the Potential of Autologous Grafting

Fredrik Nilsson

LUND
UNIVERSITY

DOCTORAL DISSERTATION

With approval of the Faculty of Medicine of Lund University,
this thesis will be defended
at 09.00 on May 10th, 2023 in Belfragesalen
Biomedical Center, Lund, Sweden

Faculty opponent

Assistant Professor Merja Voutilainen
Division of Pharmacology and Pharmacotherapy
University of Helsinki

Organization
LUND UNIVERSITY

Developmental and Regenerative Neurobiology
Department of Experimental Medical Science
Faculty of Medicine
Lund University

Document name
DOCTORAL DISSERTATION

Date of issue
2023-05-10

Sponsoring organization

Author(s)
Fredrik Nilsson

Title and subtitle
Cell Replacement Therapy for Parkinson's Disease: Evaluating the Potential of Autologous Grafting

Abstract Parkinson's disease (PD) affects approximately 1% of people over the age of 60. Due to mechanisms that are still insufficiently understood, the specific degeneration of dopaminergic neurons in the *substantia nigra pars compacta* leads to resting tremor, bradykinesia, and gait- and balance deficits. Because of this local degeneration of a relatively small population of dopaminergic neurons in the midbrain, PD has been considered an especially interesting candidate for cell replacement therapy. Transplantations of fetal tissue in the 1980s and 1990s provided proof-of-concept for the potential of cell-replacement therapy for PD and some patients benefitted greatly from their transplants. However, post-mortem analysis of transplanted tissue revealed accumulation of pathological Lewy bodies in a small subset of transplanted cells over time, revealing a host-to-graft disease propagation. Lewy bodies which are intraneuronal aggregates composed mainly of misfolded alpha synuclein (α-syn) protein is a pathological hallmark seen in both sporadic and genetic forms of PD.

Today, clinical trials using stem cell-derived dopaminergic progenitors have commenced. These progenitors which are derived from either embryonic stem cells (ESCs) or healthy induced pluripotent stem cells (iPSCs) express wild-type levels of α-syn, thus making them equally susceptible to developing Lewy bodies over time. The advent of iPSCs has opened up the possibility to graft patient-specific cells which most likely would circumvent the need for immunosuppression. However, patient-derived cells may be more prone to develop disease-associated pathology after grafting. If this is the case, gene-correction presents a solution for patients with known monogenetic mutations. However, this approach is not applicable for the majority of PD patients, since 90-95% of all cases are sporadic. Instead, for sporadic patient cells alternative strategies need to be evaluated. The overall aim of this thesis has been to assess the potential of autologous grafting in cell replacement therapy for PD. First, we utilized single cell sequencing to dissect the differentiation of stem cells to midbrain dopaminergic neurons. Second, we used directly converted neurons from sporadic patient fibroblasts to study of age-related disease relevant pathology. Next, in order to study the potential of autologous cell replacement therapy we transplanted progenitors derived from a PD patient into a pre-clinical rat model. Lastly, we evaluated the strategy of knocking out α-syn as a means to protect the cells from transfer of pathology upon grafting. The data presented in this thesis may serve as valuable resources to help optimize future cell replacement therapies for patients suffering from PD.

Key words: Parkinson's disease, cell replacement therapy, dopaminergic neurons, alpha synuclein, autologous, stem cells

Classification system and/or index termes (if any):

Supplementary bibliographical information:

Language
English

ISSN and key title:
1652-8220

ISBN
978-91-8021-392-9

Recipient's notes

Number of pages
148

Price

Security classification

Cell Replacement Therapy for Parkinson's Disease -Evaluating the Potential of Autologous Grafting

Fredrik Nilsson

2023

Developmental and Regenerative Neurobiology
Department of Experimental Medical Science
Faculty of Medicine
Lund University

LUND
UNIVERSITY

Cover illustrated by Janko Kajtez

ISSN 1652-8220
ISBN 978-91-8021-392-9
Lund University, Faculty of Medicine Doctoral Dissertation Series 2023:52

Printed by Exakta Print AB, Malmö, Sweden

To my family

TABLE OF CONTENTS

ORIGINAL PAPERS AND MANUSCRIPTS INCLUDED IN THIS THESIS

Paper I

Single-Cell Profiling of Coding and Noncoding Genes in Human Dopamine Neuron Differentiation.

Nilsson F, Storm P, Sozzi E, Hidalgo Gil D, Birtele M, Sharma Y, Parmar M, Fiorenzano A.

Cells. 2021 Jan 12;10(1):137.

Paper II

Age-related pathological impairments in directly reprogrammed dopaminergic neurons derived from patients with idiopathic Parkinson's disease.

Drouin-Ouellet J, Legault EM, **Nilsson F,** Pircs K, Bouquety J, Petit F, Shrigley S, Birtele M, Pereira M, Storm P, Sharma Y, Bruzelius A, Vuono R, Kele M, Stoker TB, Ottosson DR, Falk A, Jakobsson J, Barker RA, Parmar M.

Stem Cell Reports. 2022 Oct 11;17(10):2203-2219.

Paper III

Grafts Derived from an α-Synuclein Triplication Patient Mediate Functional Recovery but Develop Disease-Associated Pathology in the 6-OHDA Model of Parkinson's Disease.

Shrigley S, **Nilsson F,** Mattsson B, Fiorenzano A, Mudannayake J, Bruzelius A, Ottosson DR, Björklund A, Hoban DB, Parmar M.

Journal of Parkinson's Disease. 2021;11(2):515-528.

Paper IV

Evaluating alpha-synuclein deletion as a universal strategy for preventing pathology in cell-replacement therapy for Parkinson's Disease.

Nilsson F, Corsi S, Kajtez J, Shrigley S, Bruzelius A, Sharma Y, Sozzi E, Chen Y, Mattsson B, Ottosson D, Fiorenzano A, Luk K, Hoban D, Björklund A, Kunath T, Parmar M.

Submitted manuscript.

ADDITIONAL ORIGINAL PAPERS NOT INCLUDED IN THIS THESIS

I)

Single-cell transcriptomics captures features of human midbrain development and dopamine neuron diversity in brain organoids.

Fiorenzano A, Sozzi E, Birtele M, Kajtez J, Giacomoni J, **Nilsson F,** Bruzelius A, Sharma Y, Zhang Y, Mattsson B, Emnéus J, Ottosson DR, Storm P, Parmar M.

Nature Communications. 2022 Jun 8;13(1):3312.

II)

Single-cell transcriptional and functional analysis of dopaminergic neurons in organoid-like cultures derived from human fetal midbrain.

Birtele M, Storm P, Sharma Y, Kajtez J, Wahlestedt JN, Sozzi E, **Nilsson F,** Stott S, He XL, Mattsson B, Ottosson DR, Barker RA, Fiorenzano A, Parmar M.

Development. 2022 Dec 1;149(23):dev200504.

III)

Silk scaffolding drives self-assembly of functional and mature human brain organoids.

Sozzi E, Kajtez J, Bruzelius A, Wesseler MF, **Nilsson F,** Birtele M, Larsen NB, Ottosson DR, Storm P, Parmar M, Fiorenzano A.

Frontiers in Cell and Developmental Biology. 2022 Oct 14;10:1023279.

IV)

Generation of human ventral midbrain organoids derived from pluripotent stem cells.

Sozzi E, **Nilsson F,** Kajtez J, Parmar M, Fiorenzano A.

Current Protocols. 2022 Sep;2(9):e555.

REVIEW ARTICLES NOT INCLUDED IN THIS THESIS

I)

3D biomaterial models of human brain disease.

Kajtez J, **Nilsson F,** Fiorenzano A, Parmar M, Emnéus J.

Neurochem Int. 2021 Jul;147:105043.

II)

A Combined α-Synuclein/Fibril (SynFib) Model of Parkinson-Like Synucleinopathy Targeting the Nigrostriatal Dopamine System.

Björklund A, **Nilsson F,** Mattsson B, Hoban DB, Parmar M.

Journal of Parkinson's Disease. 2022;12(8):2307-2320.

ABSTRACT

Parkinson's disease (PD) affects approximately 1% of people over the age of 60. Due to mechanisms that are still insufficiently understood, the specific degeneration of dopaminergic neurons in the *substantia nigra pars compacta* leads to resting tremor, bradykinesia, and gait- and balance deficits. Because of this local degeneration of a relatively small population of dopaminergic neurons in the midbrain, PD has been considered an especially interesting candidate for cell-replacement therapy. Transplantations of fetal tissue in the 1980s and 1990s provided proof-of-concept for the potential of cell replacement therapy for PD and some patients benefitted greatly from their transplants. However, post-mortem analysis of transplanted tissue revealed accumulation of pathological Lewy bodies in a small subset of transplanted cells over time, revealing a host-to-graft disease propagation. Lewy bodies which are intraneuronal aggregates composed mainly of misfolded alpha synuclein (α-syn) protein is a pathological hallmark seen in both sporadic and genetic forms of PD.

Today, clinical trials using stem cell-derived dopaminergic progenitors have commenced. These progenitors which are derived from either embryonic stem cells (ESCs) or healthy induced pluripotent stem cells (iPSCs) express wild-type levels of α-syn, thus making them equally susceptible to developing Lewy bodies over time. The advent of iPSCs has opened up the possibility to graft patient-specific cells which most likely would circumvent the need for immunosuppression. However, patient-derived cells may be more prone to develop disease-associated pathology after grafting. If this is the case, gene-correction presents a solution for patients with known monogenetic mutations. However, this approach is not applicable for the majority of PD patients, since 90-95% of all cases are sporadic. Instead, for sporadic patient cells alternative strategies need to be evaluated. The overall aim of this thesis has been to assess the potential of autologous grafting in cell replacement therapy for PD. First, we utilized single cell sequencing to dissect the differentiation of stem cells to midbrain dopaminergic neurons. Second, we used directly converted neurons from sporadic patient fibroblasts to study of age-related disease relevant pathology. Next, in order to study the potential of autologous cell replacement therapy we transplanted progenitors derived from a PD patient into a pre-clinical rat model. Lastly, we evaluated the strategy of knocking out α-syn as a means to protect the cells from transfer of pathology upon grafting. The data presented in this thesis may serve as valuable resources to help optimize future cell replacement therapies for patients suffering from PD.

LAY SUMMARY

Parkinson's disease (PD) is the second most common neurodegenerative disorder and affects approximately 1 in 100 persons over the age of 60. Degeneration of dopamine producing neurons in the midbrain causes motor symptoms such as resting tremor, slowness to initiate movement and gait- and balance deficits. Current treatments mainly focus on increasing the dopamine levels in the brain using pharmacological intervention. However, these strategies do not cure the disorder and over time lose their effectiveness and cause side-effects. Since the motor symptoms that arise in PD are due to the specific degeneration of dopaminergic neurons in a single region of the brain, PD has always been a promising candidate for cell replacement therapy. By replacing the degenerated dopamine neurons with healthy and functional ones, the motor symptoms can be treated. Clinical trials in the 1980s and 1990s using dopaminergic neurons from aborted fetuses showed that these could survive, integrate and alleviate motor symptoms in some of the recipients. However, due to ethical concerns and issues related to logistics, this cell source was non-sustainable. Also, from post-mortem analyses it was observed that the transplanted cells over time developed disease-associated inclusions called Lewy bodies. These pathological inclusions which are found in the brains of PD patients are mainly composed of a misfolded version of a protein called alpha synuclein (α-syn).

Today, thanks to advances in developmental biology we can easily and reproducibly produce dopamine neurons in the lab from stem cells. Clinical trials using these stem cell-derived dopamine cells have now begun. Moreover, scientific breakthroughs allow us today to generate stem cells from any individual. This makes it possible to transplant patients with their own cells. Because the cells are coming from the patients themselves, this treatment would most likely by-pass the need to immunosuppress the patient in order to prevent graft rejection. However, since the cells will carry a disease background, they might be prone to develop pathology quicker.

The focus of my thesis has been to evaluate the potential of patient-specific cell replacement therapy for PD. In the first paper we analyzed the differentiation of stem cells to dopaminergic neurons on a single cell level using single cell sequencing. In the second paper we set up a cellular system where we can study age-related disease phenotypes. Next, in the third paper, we transplanted patient-derived cells into a pre-clinical model of PD to assess their potential for motor recovery. In the fourth and final paper we studied the effect of deleting the gene that encodes for α-syn as part of a strategy to help protect the cells from developing Lewy body pathology after transplantation. The results presented here can help improve future cell replacement therapies for PD.

POPULÄRVETENSKAPLIG SAMMANFATTNING

Parkinsons sjukdom är den näst vanligaste neurodegenerativa sjukdomen och drabbar en procent av alla över 60 års ålder. Degenerationen av dopaminproducerande celler i mitthjärnan leder till motorsymptom såsom skakningar, svårigheter att initiera rörelser samt gång- och balanssvårigheter. Den vanligaste behandlingen fokuserar på att öka dopaminnivåerna i hjärnan genom medicinering. Detta botar dock inte sjukdomen och med tid tappar sin effekt samt leder till biverkningar. Eftersom motorsymptomen som uppstår vid Parkinsons sjukdom beror på den specifika degenerationen av dopaminerga nervceller i en specifik del av hjärnan har Parkinsons sjukdom alltid varit en attraktiv kandidat för cellterapi. Genom att ersätta de döda och skadade nervcellerna med friska och funktionella så kan motorsymptomen behandlas. Kliniska försök som gjordes på 1980- och 1990-talet med dopaminerga nervceller från aborterade foster visade att dessa kan överleva och integrera sig i hjärnan, och vissa patienter fick goda resultat från sina transplantat. Denna cellkälla är dock ohållbar på grund av etiska och logistiska problem. Från post-mortem-undersökningar såg man att de transplanterade cellerna över tid utvecklade patologiska ansamlingar, kallade Lewy kroppar. Dessa Lewy kroppar består till största del av en felvecklad version av proteinet alpha synuclein (α-syn).

Tack vare framsteg i utvecklingsbiologi kan vi omvandla stamceller till dopaminerga nervceller i labbet. Kliniska försök med dessa stamcells-deriverade dopaminerga nerveller har redan gått av stapeln. Idag har vi dessutom möjligheten att göra patient-specifika behandlingar. Hudceller från patienter kan omvandlas till stamceller som sedan differentieras till dopaminerga nervceller som i sin tur transplanteras tillbaka in i patienten. Eftersom cellerna är patient-egna så är det väldigt liten risk att patientens immunförsvar kommer stöta bort de transplanterade cellerna. Dock så är det möjligt att dessa celler, på grund av sin sjukdomsbakgrund, utvecklar patologi snabbare som kan kompromissa den kliniska effekten.

Fokuset för min avhandling har varit att studera potentialen av patient-specifik cellterapi för Parkinsons sjukdom. I den första studien så analyserade vi differentieringen av stamceller till dopaminerga nerveller på en singel-cellnivå. I den andra studien så etablerade vi en modell som kan användas för att bättre studera åldersrelaterade sjukdomsfenotyper. I den tredje studien studerade vi ifall patient-deriverade dopaminerga celler kan återge motorförmåga i en preklinisk modell av Parkinsons sjukdom. I den fjärde och sista studien studerade vi effekten av att förhindra uttrycket av α-syn och utforskade ifall det kan vara en god strategi för att undvika patologiska Lewy kroppar i cellerna efter transplantation. Sammantaget kan resultaten från dessa studier hjälpa att förbättra framtidens cellterapibehandlingar mot Parkinsons sjukdom.

ABBREVIATIONS

AAV	adeno-associated virus
α-syn	alpha synuclein
BBB	blood-brain barrier
DA	dopamine/dopaminergic
DAB	di-aminobenzidine
DAT	dopamine transporter
DBS	deep brain stimulation
ESC	embryonic stem cell
iDAN	induced dopaminergic neuron
iN	induced neuron
i.p	intraperitoneal
iPSC	induced pluripotent stem cell
LV	lentiviral vector
MFB	medial forebrain bundle
MHC	major histocompatibility complex
MOI	multiplicity of infection
NAc	nucleus accumbens
NHP	nonhuman primate
PCR	polymerase chain reaction
PD	Parkinson's disease
PFA	paraformaldehyde
PFC	prefrontal cortex
PFFs	preformed fibrils
PSC	pluripotent stem cell
pSyn	phosphorylated alpha-synuclein
REST	RE-1 silencing transcription factor
RT	room temperature
SD	Sprague-Dawley
SNc	substantia nigra pars compacta
s.c	subcutaneous
vMB	ventral midbrain
VTA	ventral tegmental area
TH	tyrosine hydroxylase
6-OHDA	6-hydroxydopamine

INTRODUCTION

Parkinson's Disease

Parkinson's disease (PD) is the second most common neurodegenerative disorder and is characterized by the degeneration of midbrain dopaminergic (mDA) neurons of the *substantia nigra pars compacta* (SNc). These so called A9 DA neurons project to the dorsolateral striatum of the forebrain and control voluntary movements. The loss of A9 DA neurons manifests itself primarily as motor symptoms that include resting tremor, rigidity, bradykinesia and gait-and balance deficits (Jankovic, 2008). Located adjacently, just medial to the A9 DA neurons in the SNc are the A10 DA neurons of the ventral tegmental area (VTA). These neurons project to other areas such as the nucleus accumbens (NAc) and the prefrontal cortex (PFC) (Bjorklund and Dunnett, 2007). For reasons that are still insufficiently understood the A10 DA neurons tend to be spared in PD. Contrary to the A9 neurons that control voluntary movements, the degeneration of the A10 subtype is associated with cognitive impairments, depression and anxiety (Chaudhuri et al., 2006; Tye et al., 2013).

Current treatments and cell replacement therapy

There is no cure for PD and the most common treatment today is pharmacological intervention to elevate dopamine (DA) levels in the brain using drugs that can cross the blood-brain-barrier (BBB). These include DA precursors, DA receptor agonists and DA degradation enzyme inhibitors (Connolly and Lang, 2014). While these drugs tend to work well initially, over time they lose their effect and cause side-effects (Thanvi and Lo, 2004). Two more advanced treatment approaches are DuoDopa® and deep brain stimulation (DBS). DuoDopa® is an alternative treatment option for advanced PD patients with motor fluctuations and dyskinesias. A gel consisting of levodopa (a DA precursor) and carbidopa (an enzyme inhibiting peripheral dopa-decarboxylase and ensuring increased levodopa levels in the CNS) is administered via an intrajejunal tube. This helps to treat the symptoms but does not slow down the disease progression (Ciurleo et al., 2018; Nyholm, 2012). In DBS, electrodes are surgically implanted into the brain and electrical impulses are used to relieve motor symptoms (Groiss et al., 2009). Whereas this approach can be efficient in relieving motor symptoms it is an invasive treatment and can results in issues related to cognition (Rossi et al., 2018).

Since the cardinal symptoms of PD arise due to the focal degeneration of mDA neurons, it has for a long time been a particularly interesting candidate for cell replacement therapy. Back in the 1980s and 1990s, a cohort of patients were grafted with ventral midbrain fetal tissue. While the results varied, some patients showed alleviation of motor symptoms and had surviving grafts up to 24 years after transplantation, thus giving proof-of-concept for cell replacement therapy for PD (Barker et al., 2013; Kefalopoulou et al., 2014; Li et al., 2016; Ma et al., 2010). However, the use of tissue from

aborted fetuses brought issues in regard to logistics, standardization and ethical aspects. Also, some patients developed graft induced dyskinesia that were attributed to contamination of serotonergic neurons (Hagell et al., 2002; Piccini et al., 2005; Politis et al., 2010). The development of refined and well-established protocols for the differentiation of stem cells to mDA neurons addressed these issues, and today, clinical trials using stem cell-derived mDA progenitors have commenced (Barker et al., 2017; Doi et al., 2020; Piao et al., 2021; Takahashi, 2020). These trials have used mDA progenitors derived from either embryonic stem cells or induced pluripotent stem cells from a healthy donor.

Generation of midbrain dopaminergic neurons from pluripotent stem cells

While the fetal tissue transplantations represented a significant milestone in cell-replacement therapy for PD, the issues with logistics and standardization highlighted a desperate need for a sustainable and renewable source of mDA neurons. A major breakthrough to this end was the generation of human embryonic stem cell lines from the inner cell mass of human blastocysts (Thomson et al., 1998). Attempts were subsequently made to generate mDA neurons from these lines using feeder cells and the addition of SHH and FGF8 during differentiation (Park et al., 2005; Perrier et al., 2004; Zeng et al., 2004). Although this managed to generate DA neurons in *in vitro* cultures it failed to generate DA neuron rich and functional grafts after transplantation. Additionally, due to incomplete differentiations, still proliferating cells occasionally gave rise to teratomas (Brederlau et al., 2006; Roy et al., 2006; Sonntag et al., 2007). However, important discoveries in developmental biology over the next few years would lead to the development of highly efficient protocols for generating subtype specific DA neurons of a midbrain identity. First, it was discovered that mDA arise from the floorplate of the developing neural tube and not from the neuroepithelium which was believed at the time (Bonilla et al., 2008; Ono et al., 2007). Next, it was demonstrated that the addition of the dual SMAD pathway inhibitors SB431542 and noggin to inhibit the Lefty/Activin/TGFβ and BMP pathways allowed for highly efficient neuronal induction (Chambers et al., 2009). Inhibition of the dual SMAD pathways in combination with SHH for ventralization and canonical WNT activation via inhibition of GSK3 for caudalization differentiated PSCs to authentic mDA progenitors (Fasano et al., 2010; Kirkeby et al., 2012; Kriks et al., 2011; Nolbrant et al., 2017). Upon grafting these hESC-derived mDA progenitors gave rise to TH rich grafts that mediated motor recovery in pre-clinical PD models (Nolbrant et al., 2017; Piao et al., 2021; Xiong et al., 2021) and functioned *en par* with mDA progenitors derived from fetal tissue (Grealish et al., 2014). iPSCs derived from healthy donors and PD patients have been shown to generate mDA at the same capacity as embryonic stem cells (Doi et al., 2020; Doi et al., 2014; Kikuchi et al., 2017a; Kikuchi et al., 2017b; Song et al., 2020). The advantage of iPSCs compared to hESCs is the possibility of autologous grafting and also the starting source is typically skin or blood cells which is less ethically problematic compared to ESCs isolated from a blastocyst (Robinton and Daley, 2012). However, the risk of transplanting patient cells that carry a disease background in terms of developing an exacerbated Lewy body pathology needs to be further assessed. If so, genetic or modification strategies might be a necessity to protect them after grafting.

Autologous grafting

The possibility of transplanting patients with their own cells, i.e autologous transplantation was made feasible with the discovery of induced pluripotent stem cells (Takahashi et al., 2007; Takahashi and Yamanaka, 2006). In 2020 the first case-study with an autologous transplantation of a PD patient was reported (Schweitzer et al., 2020). The benefit of such autologous transplantation would be the likely circumvention of the need for immunosuppression which can come with side-effects and put the patients at risk of infection (Morizane and Takahashi, 2021). While the brain has been considered to be completely immunoprivileged, this has been shown to not hold true and a cell transplantation would inevitably have to breach the BBB, allowing infiltration of activated lymphocytes (Barker and Widner, 2004). Studies of autologous grafting in NHPs have shown that autologous cells survive and mature upon grafting (Emborg et al., 2013) and improve motor function after MPTP lesion (Hallett et al., 2015; Tao et al., 2021). Comparison of the difference in immune response after grafting between autologous and allogenic grafting revealed an acquired immune response to the allogenic graft with activated microglia and infiltrating lymphocytes (Morizane et al., 2013; Tao et al., 2021). This was either minimal or absent in the autologous grafts. Moreover, Tao and colleagues found that the autologous grafts, but not allogenic grafts, could mediate motor recovery and depressive behaviors in NHPs (Tao et al., 2021). While Morizane and colleagues found no difference in graft size between autologous and allogenic grafts, the autologous grafts had significantly higher numbers of TH+ cells and TH density (Morizane et al., 2013).

Several studies have shown that patient-derived iPSCs differentiate efficiently to mDA neurons and can alleviate motor symptoms upon grafting into rodents (Hargus et al., 2010; Kikuchi et al., 2017b; Shrigley et al., 2021; Song et al., 2020) and NHPs (Kikuchi et al., 2017a). However, a concern regarding autologous transplantation is that the transplanted cells over time might develop disease-associated pathology which can compromise graft function. Post-mortem studies of the patients in receipt of fetal tissue revealed a slowly progressive accumulation of Lewy bodies and neurites, pathological insoluble inclusions composed mainly of the protein alpha synuclein (α-syn) in some patients (Kordower et al., 2008; Li et al., 2008; Li et al., 2010). This discovery suggested a host-to-graft transfer of pathology. While this accumulation of Lewy body pathology was slow and did not seem do affect the function of the graft, it may be exacerbated in patient cells due to their disease background.

Another drawback of autologous grafting is the inherent difficulty to create an off-the-shelf product which means a higher cost per patient. Therefore, banking of 50-140 lines that can MHC-match roughly 90% of the population has been proposed as an option to combine the advantages of autologous and allogenic transplantations (Nakatsuji et al., 2008; Taylor et al., 2012). However, these numbers are based on Japan and the UK, which have high homogeneity in HLA haplotypes. For more heterogenous countries such as the US, the number of lines needed would be far higher (Zimmermann et al., 2012). A study comparing MHC-matching with MHC-mismatching revealed more surviving TH+ neurons and a lowered immune response in the matching group (Morizane et al., 2017). However, in a NHP model of Huntington's disease it was reported that MHC-matching without immunosuppression was not sufficient to allow long-term survival and more studies are needed to address this discrepancy (Aron Badin et al., 2019). Alternatively, efforts have made to produce "camouflaged" cells that have been genetically engineered to evade the immune system. However, also here more studies are needed before advancing to the clinic (Morizane and Takahashi, 2021). Nonetheless,

advances in automation, robotics and lab-on-a-chip technology may significantly reduce the time and money to the extent that autologous treatments become truly feasible on a large scale.

The role of alpha synuclein in PD

The interest in α-syn arose when mutations in the *SNCA* gene encoding α-syn were reported to cause familial PD (Polymeropoulos et al., 1997) along with the discovery that α-syn was the major component of Lewy bodies and Lewy neurites (Spillantini et al., 1998; Spillantini et al., 1997). Additionally, it was discovered that elevated α-syn levels due to duplications and triplications of the *SNCA* locus could cause PD (Chartier-Harlin et al., 2004; Singleton et al., 2003). Epidemiology studies revealed that persons with a *SNCA* locus triplication had an earlier disease-onset compared to persons with a duplication, giving further evidence of the central role of α-syn in PD (Fuchs et al., 2007). Due to this link between α-syn mutations/overexpression and PD, therapeutic approaches to target α-syn have been developed over the years.

Several studies have aimed at knocking down or out the α-syn protein. For instance, shRNA has been used to reduce α-syn levels in neural progenitor cells with a *SNCA* triplication which increased their resistance to oxidative stress (Flierl et al., 2014). Another approach to downregulate *SNCA* transcription and translation has been to hypermethylate *SNCA* intron 1 using CRISPR-deactivated Cas9. This tactic reduced mitochondrial stress and increased cell viability in dopaminergic neurons (Kantor et al., 2018). Chen et al. used CRISPR/Cas9 to knock out exon 2 of the *SNCA* gene which prevented the formation of Lewy body-like aggregates when challenged with preformed a-syn fibrils (PFFs) (Chen et al., 2019). The administration of antisense oligos targeting α-syn could rescue disease phenotypes in PFF models of PD (Cole et al., 2021). Furthermore, *SNCA*-/- primary neurons and *SNCA*-/- mice show no pathology and degeneration when challenged with PFFs (Luk et al., 2012; Volpicelli-Daley et al., 2011). Although downregulating or knocking out *SNCA* expression has been shown to recue pathological phenotypes *in vitro* and *in vivo*, the functional impact on the neurons and their clinical potential when used in cell replacement need to be further evaluated.

Modelling PD *in vivo*

Over the years, many animal models have been established to study the etiopathogenesis and potential treatments of PD. Important to know are the advantages, disadvantages as well as the limitations of each model. Invertebrates such as the common fruit fly *(Drosophila melanogaster)* and the nematode *(Caenorhabditis elegans)* or small fishes are often used for high-throughput screenings. Mammalian models are instead used for studies involving complex motor and non-motor functions. The large and convoluted brains of NHPs make them a suitable animal for modelling PD and to test treatment strategies. However, since they are expensive, ethically problematic to use and require specialized housing facilities their use is not commonplace. Rodent have instead become the most widely used model for PD because of their low cost and possibility to study complex movements, cognition and other brain functions (Cenci and Bjorklund, 2020). The following section will thus focus on rodent models.

The common denominator for clinical PD is the loss of dopaminergic innervation in the caudate putamen. Once roughly 50% of this innervation is lost, motor deficits start to appear in patients (Fearnley and Lees, 1991; Kordower et al., 2013). Many models have been established to cause this neurodegeneration and other pathological features associated with PD. In order to recreate these features and motor deficits, a significant degeneration of nigrostriatal dopamine neurons is necessary. This can be done in numerous ways, including using toxins, viral vectors, PFFs and transgenic techniques. Some of the most commonly used ones are described below.

6-hydroxydopamine and other toxin/drug models

The 6-hydroxydopamine (6-OHDA) model was the first toxin-based PD model (Ungerstedt, 1968). Intracerebral injection of 6-OHDA causes widespread dopamine neuron degeneration on the ipsilateral hemisphere. 6-OHDA is a hydroxylated analogue of dopamine that enters the dopaminergic neurons via the dopamine transporter (DAT). Once inside the cells the oxidation of 6-OHDA leads to ROS-induced degeneration (Kupsch et al., 2014; Rotman and Creveling, 1976). The imbalance in dopamine levels between the intact and lesioned side becomes apparent upon administration of amphetamine. Amphetamine induces the release of dopamine vesicles and the difference between the hemispheres will manifest itself as the biased rotation toward the injected side (Ungerstedt and Arbuthnott, 1970). Measurements of these rotations have been used extensively to study neuroprotective compounds and the functionality of xenografts. However, the 6-OHDA model does not recapitulate the progressive degeneration of DA neurons nor the accumulation of Lewy bodies.

MPTP is another toxin that has been used to recreate the degeneration of DA neurons seen in PD. Due to its lipophilic nature, MPTP can cross the BBB, unlike 6-OHDA that requires stereotaxic surgery. MPTP is oxidized in the brain to MPP+ which is structurally similar to DA and is taken up by DA neurons via DAT. MPP+ causes mitochondrial and ROS damage that ultimately leads to cell death. Similar to the 6-OHDA model, MPTP fails to recreate the slow progressive cell death and synucleinopathy. Also, since MPTP is administered systemically, both hemispheres will be affected by the toxin, making it more difficult to study its effect. This is in contrast to 6-OHDA lesions where the contralateral side acts as a control. Moreover, issues with high mortality, spontaneous recovery and resistance in rats has made the 6-OHDA the preferred choice (Cenci and Bjorklund, 2020).

Environmental toxins such as the pesticides rotenone and paraquat have also been used to model dopaminergic degeneration ever since their exposure was associated with an increased risk of PD. Both compounds can cross the BBB and cause DA neuron cell death by ROS damage and mitochondrial dysfunction. Also, cancer drugs that work by inhibiting the proteasome, such as MG132 and lactacystin have also been used to model PD by triggering α-syn accumulation and DA neuron degeneration (Bentea et al., 2017).

Alpha synuclein-based models

The toxin-based models do not faithfully reproduce the Lewy body accumulation and inflammation that is seen in PD patients. Furthermore, toxins such as 6-OHDA cause a swift and widespread nigrostriatal degeneration instead of a slower, progressive one. Therefore, efforts have been made to produce models that better mimic these features. By injecting adeno-associated viruses (AAVs) overexpressing α-syn or PFFs, a progressive degeneration accompanied by Lewy body-like accumulation of insoluble aggregates can be achieved.

The AAV model

Overexpression of α-syn using AAVs recapitulates the progressive stages of PD, making it a highly attractive disease-model. The α-syn overexpression induced by the AAVs lead to the formation of phosphorylated α-syn (pSyn) inclusions, axonal pathology, deficits in DA release and uptake and eventually DA neuron degeneration (Decressac et al., 2012b; Lundblad et al., 2012). Once >50% of the DA neurons of the nigra have been lost, motor symptoms can be measured using well-establish motor tests (Bourdenx et al., 2015; Decressac et al., 2012a; Van der Perren et al., 2015). While the AAV-α-syn model recapitulates many disease-relevant features of PD, the model has a few drawbacks. Differences in serotype, production and promotor can lead to significant batch-to-batch variation. Also, in order to elicit degeneration and motor symptoms an α-syn overexpression much higher than what is seen in patients is required (Decressac et al., 2012b; Faustini et al., 2018). Additionally, it is advantageous to do a test run of each batch since genome copies/volume does not predict effectiveness after injection and equal titers may yield different results.

The PFF model

Another common α-syn-based model is the PFF model. Injected PFFs will act as pathological seeds and recruit endogenous monomeric α-syn to create Lewy body-like pathological inclusions (Luk et al., 2012; Luk et al., 2009; Volpicelli-Daley et al., 2011). These inclusions are hyperphosphorylated, ubiquitinated, insoluble and structurally similar to those seen in patients. Because of this, the PFF model serves as a good tool to study the dynamics of seeding, aggregation and propagation. The disadvantages of the PFF model are the long time it takes to cause DA degeneration and develop motor impairments as well as the poor spreading of injected PFF which limits the number of targeted neurons, especially in rats.

The combined AAV/PFF model

By combining AAV-α-syn overexpression with PFF inoculation many of their individual shortcomings are addressed. The elevated levels of α-syn (while still within a physiologically relevant range) in combination with the PFFs will hasten and exacerbate the aggregation, toxicity and the degeneration (Hoban et al., 2020; Negrini et al., 2022; Thakur et al., 2017). For optimal toxicity in this model, the α-syn and fibrils should be from the same species (Luk et al., 2016).

Modelling PD *in vitro*

Stem cell-based models

The generation of iPSCs from PD patients along with the development of refined protocols for producing midbrain dopaminergic neurons allowed for the study of cells with a disease background in a disease relevant cell type. In the years following Yamanaka's discovery, iPSCs were generated from sporadic and familial PD patients (Devine et al., 2011; Nguyen et al., 2011; Soldner et al., 2009). These have been used to study the pathogenesis of PD and Lewy body-like pathology. However, many of these models fail to recapitulate this synucleinopathy in the absence of any challenge with toxins/PFFs/α-syn oligomers (Oh, 2019). A reason for this can be insufficient time in culture. The use of

free-floating organoids and 3-dimensional cultures has made it possible to keep cells in culture for sufficient amounts of time to allow Lewy body-like pathology to develop without the use of toxins/PFFs (Becerra-Calixto et al., 2023; Mohamed et al., 2021). Nonetheless, the ability of PSC-derived DA neurons to model the ageing brain can be questioned. As somatic cells such as skin cells or blood cells are reprogrammed to iPSCs they lose many of their ageing signature and become rejuvenated (Marion et al., 2009; Suhr et al., 2010; Vera and Studer, 2015).

Direct reprogramming

In 2010 the first successful fibroblast-to-neuron direct reprogramming was reported. Using a lentiviral cocktail of *Ascl1, Brn2* and *Myt1l,* fetal mouse fibroblasts where directly reprogrammed to neurons (Vierbuchen et al., 2010). Subsequently, this was done in human fibroblasts (Pang et al., 2011; Pfisterer et al., 2011). These so-called induced neurons (iNs) expressed neuronal markers and showed electrophysiological properties of functional neurons. By introducing factors associated with dopamine neuron generation, fibroblasts can be directly converted to induced dopaminergic neurons (iDANs) (Caiazzo et al., 2011; Jiang et al., 2015; Liu et al., 2012; Pfisterer et al., 2011). Since iNs are not going through a pluripotent intermediate, they have been shown to retain the age of the donor (Drouin-Ouellet et al., 2017; Huh et al., 2016; Mertens et al., 2015; Tang et al., 2017). This has made iNs very attractive for modelling age-related diseases of the CNS as well as for drug screening and toxicology applications.

AIMS OF THE THESIS

This thesis can be divided into four major aims:

I Dissect the differentiation of human pluripotent stem cells to functional ventral midbrain dopaminergic neurons on a single-cell level.

II Generate a relevant PD model to study age and disease-relevant phenotypes in patient derived cells using directly reprogrammed induced neurons (iNs).

III Study the functionality of patient-derived cells in a preclinical rat model of PD.

IV Evaluate the strategy of *SNCA* deletion to prevent transfer of pathology after transplantation.

SUMMARY OF RESULTS AND DISCUSSION

In **Paper I** we dissect the differentiation of human embryonic stem cells toward functional mDA neuron using single-cell sequencing. In **Paper II** we establish a platform to generate subtype-specific iDANs from directly converted human fibroblasts that can be used to study age-related disorders such as PD. In **Paper III** we study the maturation and function of patient-derived mDA neurons in a pre-clinical rat model of PD. In **Paper IV** we evaluate the potential of *SNCA* deletion as a means to prevent transfer of host-to-graft pathology with a focus on assessing the functionality and integration of *SNCA*-/- mDA neurons.

Dissect the differentiation of human pluripotent stem cells to ventral midbrain dopaminergic neurons on a single-cell level (Paper I)

Clinical trials using hPSC-derived mDA progenitors have commenced (Doi et al., 2020; Piao et al., 2021)(Lund University, 2023-02-28, First patient receives milestone stem cell-based transplant for Parkinson's Disease [Press release], https://www.lunduniversity.lu.se/article/first-patient-receives-milestone-stem-cell-based-transplant-parkinsons-disease). Since the motor symptoms that arise in PD stem from the specific degeneration of A9 dopaminergic neurons in the midbrain, it is imperative that the protocols generating these cells model mDA neurogenesis. In this study, we differentiated human embryonic stem cells toward mDA neurons in 2-dimentional cultures and performed single-cell sequencing at three stages of differentiation.

Generation of functional midbrain dopaminergic neurons from human embryonic stem cells

Human embryonic stem cells were differentiation as 2-dimensional cultures according to a well-established protocol (Nolbrant et al., 2017). This protocol relies on SB and noggin for neuroectoderm induction, SHH for ventralization and CHIR for adjusting the caudalization. Cells were collected at day 16, 30 and 60 and processed for single cell sequencing (Fig.1A-D). As the progenitors mature to functional neurons they become less proliferative (marked with Ki67) and start to upregulate neuronal marker MAP2 and dopaminergic neuron marker TH (Fig.1E-G). To assess A9 and A10 sub-specificity we stained for commonly used A9 marker Girk2 and A10 marker Calbindin, indicating that both subtypes were present in the cultures (Fig.1H-I). Electrophysiological recordings at day 60 using the patch-clamp method showed induced action potentials (Fig.1J) and induced action potentials upon brief depolarization (Fig.1K), indicative of mature neuronal activity as well as spontaneous firing (Fig.1L) characteristic of DA neurons.

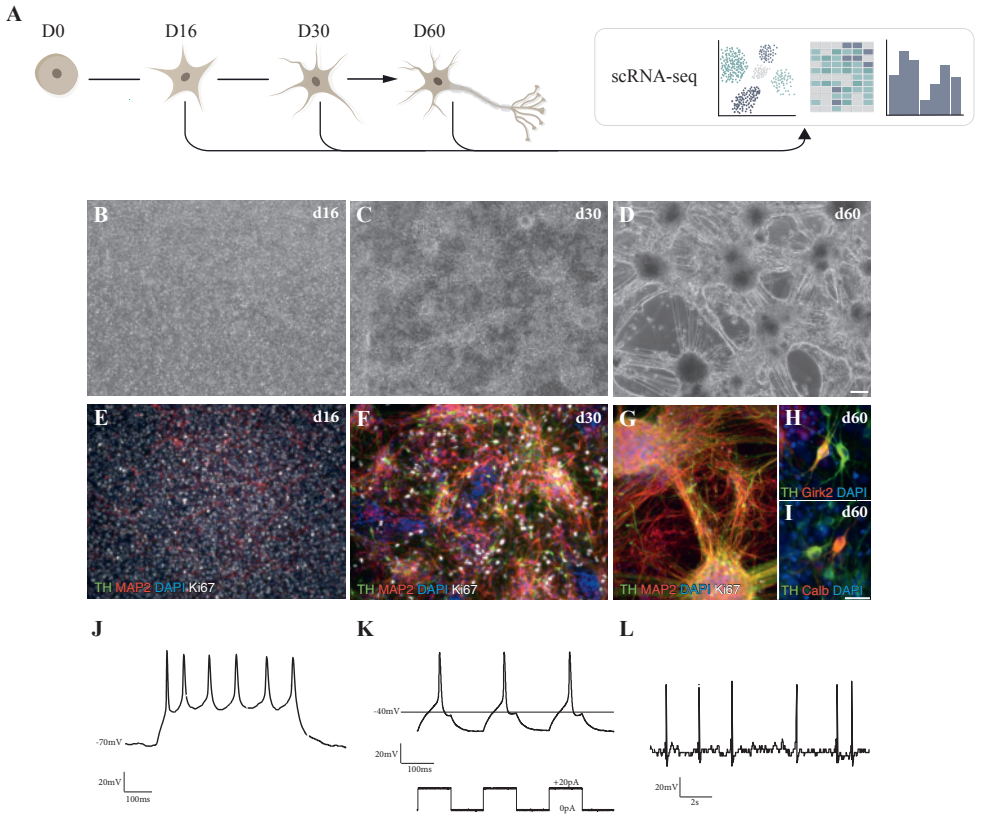

Figure 1. Generation of functional mDA neurons from hPSCs. (A) Schematic of experimental design. (B-D) Brightfield images at d16, d30 and d60. (E-G) Immunofluorescent stainings of DA neuron marker TH, neuronal marker MAP2 and proliferation marker Ki67. (H) Immunofluorescent stainings of DA neuron marker TH and A9 marker Girk2 and (I) A10 marker Calbindin. Nuclei stained with DAPI. Scale bars = 100μm. (J) Cells analyzed at d60 demonstrated induced action potentials, (K) induced action potentials upon brief depolarization and (L) spontaneous firing.

Distinct cell types are captured with single cell sequencing during neuronal differentiation and maturation.

Using single-cell sequencing we captured nearly 20.000 cells across all three time-points. These were assigned to seven clusters according to uniform manifold approximation and projection (UMAP) analysis (Fig.2A). The vast majority of the cells were assigned either a floorplate or DA progenitor/neuron identity. There was also a small cluster of vascular leptomeningal cells (VLMCs) that previously have been shown to be associated with vasculature in the brain and have been present in hESC-derived grafts (Marques et al., 2016; Tiklova et al., 2020). Separating the floorplate clusters (FP1-3) was mainly the expression of cell cycling genes (Fig.2B). One of the DA clusters had high expression of floorplate markers and was labelled DA-early. While DA-1 and DA-2 both had high expression of TH, the DA-1 cluster had higher expression of genes associated with midbrain DA neurons such as

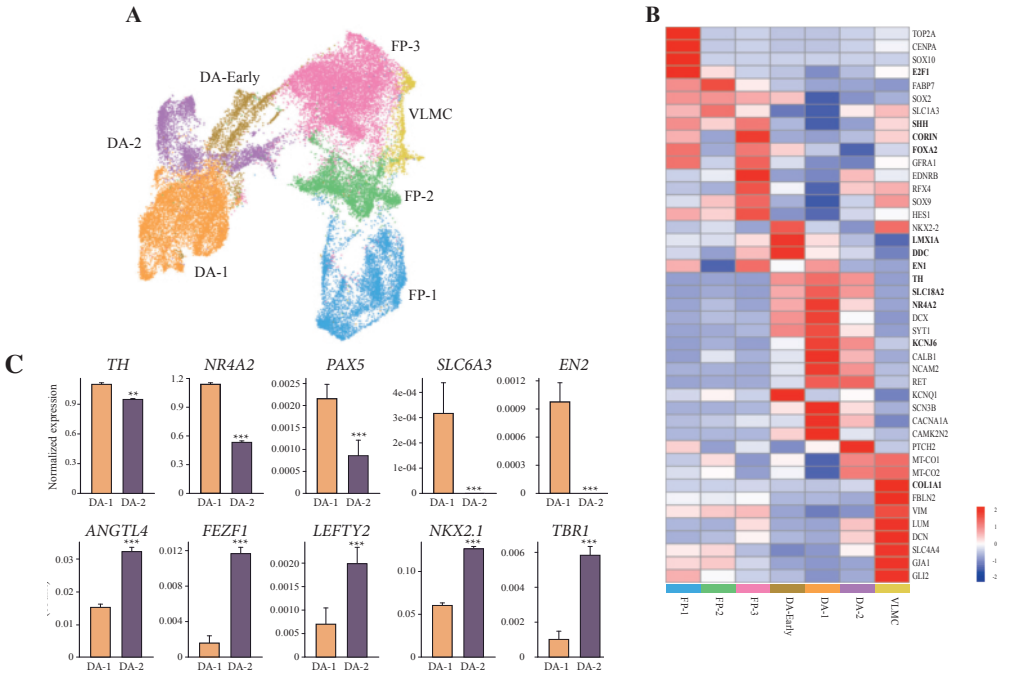

Figure 2. Dissecting the differentiation of hPSCs to mDA neurons. (A) UMAP analysis resulting in seven clusters. (B) Heatmap plot displaying the expression levels of selected genes for each assigned cluster. Values are given as standard deviations relative to average expression across all clusters. (C) Bar plots of the expression of selected markers by clusters DA-1 and DA-2. Data reported as mean +/- SEM, ** $p < 0.01$, *** $p < 0.001$.

SLC6A3 (DAT) and *NR4A2* (NURR1) (Fig.2B, C). To assess the authenticity of our captured cells we compared our data set with a human fetal VM data set comprised of almost 25.000 cells (Birtele et al., 2022). The overall prediction score was high, particularly for clusters FP-1 and the DA clusters, emphasizing the validity of the differentiation.

Fibroblast growth factor 8 (FGF8b) is important for patterning to mature DA neurons

The addition of FGF8b to the media during differentiation (day9-16) has been shown to fine-tune the patterning to a more caudal midbrain identity (Kirkeby et al., 2017; Nolbrant et al., 2017). We differentiated hESCs according the same protocol as mentioned above but removed FGF8b from one culture condition (Fig.3A). Single cell sequencing carried out at day 60 revealed significantly higher expression of genes associated with mDA neurons in the FGF8b+ condition (Fig.3B). In contrast, the FGF8b- condition had higher expression of markers that would indicate a more rostral mesencephalic/diencephalic patterning (Fig.3B). UMAP analysis further revealed that the addition of FGF8b resulted in more cells in the DA clusters (DA-1 in particular) and fewer cells in the FP clusters (FP-3 in particular) (Fig.3C, D).

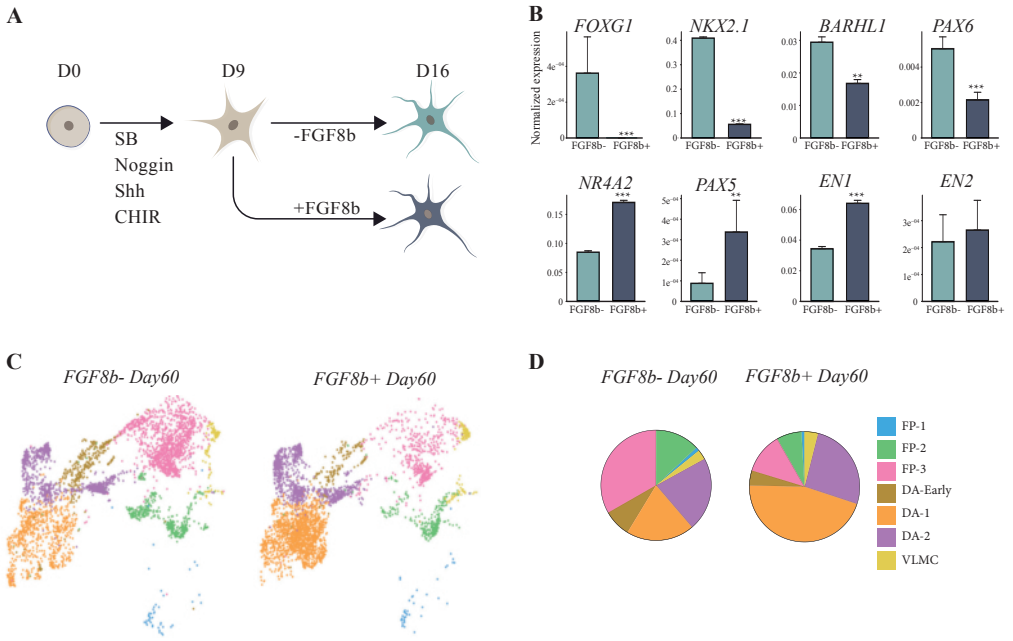

Figure 3. Addition of FGF8b improves patterning and differentiation to mDA neurons. (A) Schematic of experimental design. (B) Bar plots of selected rostral and caudal mesencephalic markers for FGF8b+/- conditions. Data reported as mean +/- SEM, ** $p < 0.01$, *** $p < 0.001$. (C) UMAP plot showing the distribution of cells across the seven clusters for FGF8b+/- conditions. (D) Pie charts showing the proportions of the seven clusters for FGF8b+/- conditions.

Reconstruction of developmental trajectories using single cell sequencing

Using our dataset of captured cells from day 16 to 60 we looked at the temporal expression of important early and late mDA markers. As the cultures matured, we saw a downregulation of progenitor markers and an upregulation of mDA neuron markers. Next, we performed a Slingshot analysis which enables lineage inference. The analysis revealed three tentative lineages, all originating

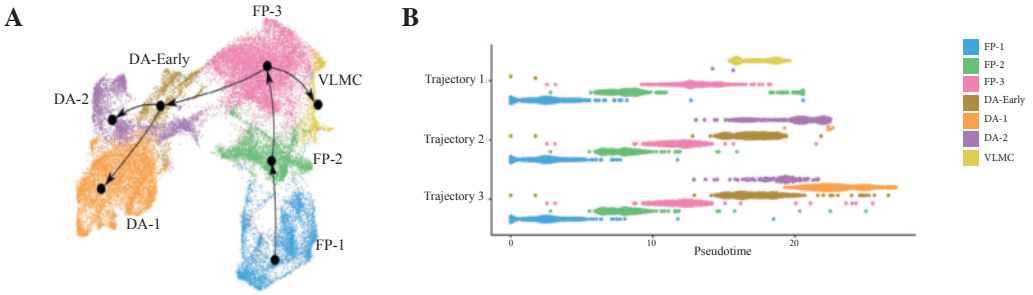

Figure 4. Developmental trajectories during mDA differentiation. (A) Slingshot analysis suggesting three tentative lineages. (B) Pseudotime inference reconstruction plot of appearing cell types.

sequentially from FP-1, FP-2 and FP-3 (Fig.4A, B). One trajectory had VLMC as the terminal trajectory while the other two went through DA-Early and had DA-1 and DA-2 as terminal trajectories (Fig.4A, B).

The data presented in **Paper I** validates the use of stem cell cultures to model human DA neurogenesis. Here we used single cell sequencing to study the differentiation and maturation of stem cell cultures patterned toward a midbrain identity. After 60 days the main cell type was DA neurons that revealed high similarity to authentic fetal DA neurons. Although, not all cells displayed a mature neuronal identity at this timepoint, giving validity to the use of 3-dimensional cultures that can be maintained in cultures for several months to ensure a more widespread maturation. The bioinformatics pipeline generated here allowed us to study the transcriptomic landscape during differentiation and help to elucidate the intricate regulatory network of coding and noncoding genes during mDA neuron differentiation. Taken together this data may serve as a valuable resource to further dissect the development and maturation of functional mDA neurons.

Generation of a relevant PD model of the ageing brain using directly reprogrammed induced neurons (iNs) (Paper II)

The first case of directly converted neurons from fibroblast were reported in 2010 (Vierbuchen et al., 2010). These so called induced neurons (iNs) have later been shown to retain ageing hallmarks of the starting fibroblast, including DNA-damage, telomere length and organelle defects (Huh et al., 2016; Kim et al., 2018; Mertens et al., 2015; Tang et al., 2017). In this study, we generated subtype specific induced dopaminergic neurons (iDANs) from sporadic and healthy fibroblast and found impairments due to their age and disease background.

Conversion of sporadic and healthy fibroblast lines to active iDANs

Fibroblasts were converted using a cocktail of eight viral vectors: five DA neuron determinants *(LMX1a, LMX1b, FoxA2, Otx2* and *Nurr1)*, two inhibitors of REST *(shREST1* &*2)* to allow for neuronal induction, as well as a pioneering factor *(Ascl1)* (Fig.5A). The iDANs expressed mature neuronal marker MAP2 and DA neuron marker TH (Fig.5B). They also expressed several other genes associated with DA neurons such as *VMAT2, AADC, DAT, GIRK2, DRD2* and *PITX3* (Fig.5C). Electrophysiological recordings with the patch-clamp methods demonstrated mature neuronal functionality (Fig.5D, E).

Conversion of sporadic and healthy iPSC lines to active iPSC-iDANs

Multiple studies have demonstrated that the reprogramming of fibroblasts to iPSCs rejuvenates the cells and erases the aging hallmarks. Therefore, to act as negative aging controls we generated iPSCs from a subset of PD and healthy donor fibroblast lines. We subjected these iPSCs to the same conversion protocol as the fibroblasts. Immunofluorescent stainings showed expression of mature neuronal markers TAU and MAP2 and DA neuron marker TH (Fig.6A). RT-qPCR analysis of gene expression showed upregulation of genes associated with DA neurons (Fig.6B) and patch-clamp recordings demonstrated mature neuronal activity (Fig.6C, D).

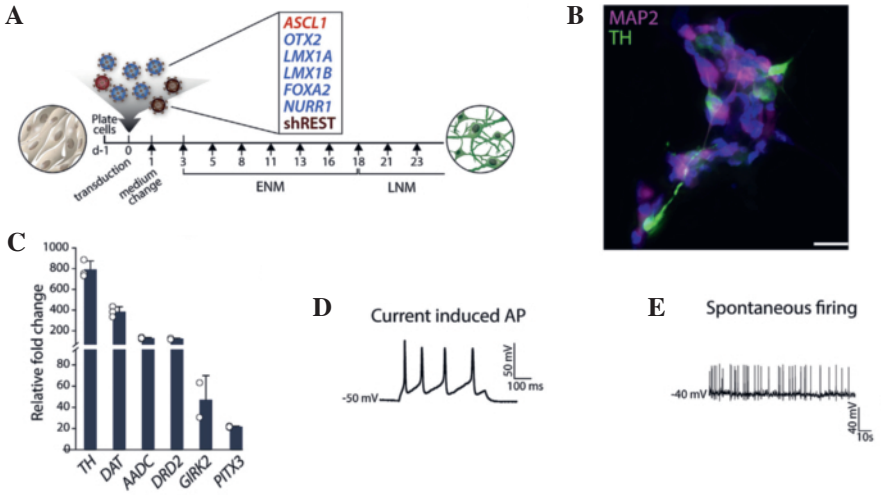

Figure 5. Generation of functional iDANs. (A) Schematic of conversion protocol. (B) Immunofluorescent staining of neuronal marker MAP2 and DA neuron marker TH. Nuclei stained with DAPI. Scale bar = 25μm. (C) RT-qPCR values for expression of selected DA neuron markers relative to unconverted fibroblasts. (D) Current induced action potential and (E) spontaneous firing demonstrating neuronal activity.

Maintenance of aging signatures in iNs

A well-documented feature of ageing is DNA damage (Mah et al., 2010; Sedelnikova et al., 2004). We stained fibroblasts, iNs and iPSC-iNs for DNA damage marker γH2AX and found numerous puncta in the fibroblasts that were maintained as the cells were converted to iNs. This level of DNA damage was not present in the iPSC-iNs from the same cell lines, suggesting a rejuvenation as the fibroblast are reprogrammed to pluripotency (Fig.7A-C). Another sign of neuronal maturity is the expression of the 4R isoform of Tau on exon 10. While the 3R version is expressed in PSC-derived neuronal cultures, the 4R version is not expressed even after 365 days *in vitro* (Sposito et al., 2015). Looking at the expression of the 4R isoform in converted neurons from adult fibroblasts, fetal fibroblast and iPSCs, only iNs from adult fibroblasts had expression of 4R Tau, again suggesting a retainment of age in iNs from adult fibroblasts (Fig.7D)

Accumulation of Lewy body like pathology in PD-iNs

Phosphorylated inclusions of α-syn is a well-documented pathological hallmark of PD. The build-up of these pathological inclusions can be attributed to a failure to clear these inclusions. Autophagy, a lysosomal degradation pathway essential for maintaining cellular homeostasis, is decreased in an age-dependent manner (Fleming et al., 2022; Rubinsztein et al., 2011). To study if stress-induced autophagy would lead to such inclusions, we starved iNs to induce macroautophagy and also inhibited autophagy flux using bafilomycin A1. While no differences were detected in healthy iNs and iDANs, an increase of inclusions were observed in PD iNs and iDANs (Fig.8A). Notably, starvation and autophagy flux blockage had no effect on iPSC-derived iNs, whether from a healthy or disease background (Fig.8B).

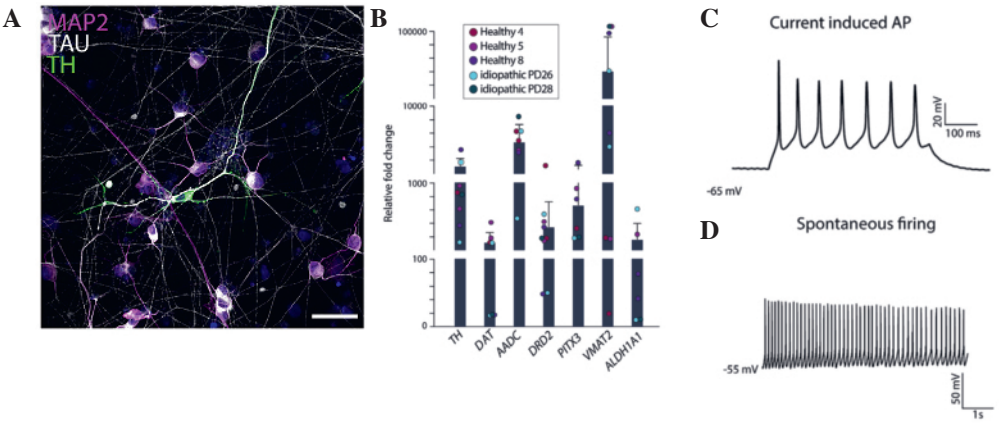

Figure 6. Generation of functional iPSC-iNs. (A) Immunofluorescent staining of neuronal markers MAP2 and TAU and DA neuron marker TH. Nuclei stained with DAPI. Scale bar = 100µm. (B) RT-qPCR values for expression of selected DA neuron markers relative to unconverted iPSCs. (C) Current induced action potential and (D) spontaneous firing demonstrating neuronal activity.

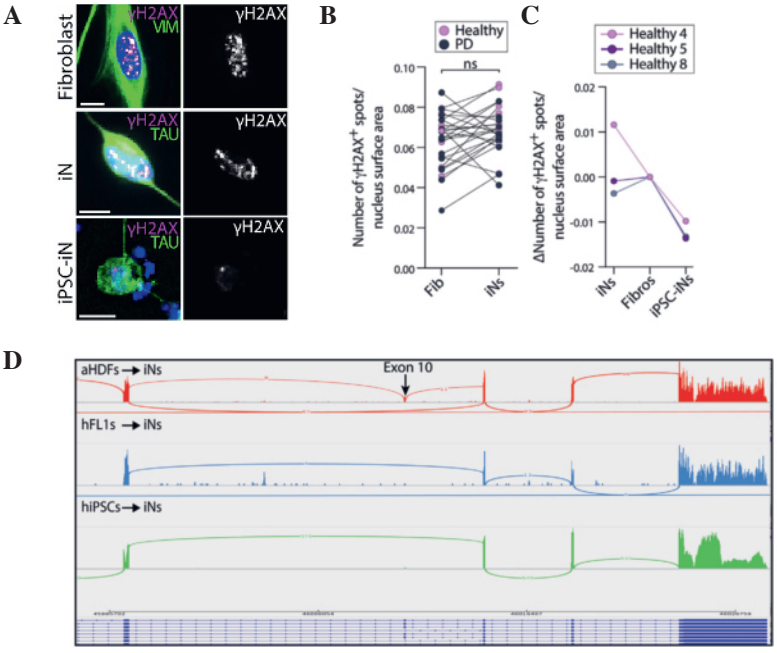

Figure 7. iNs maintain ageing hallmarks from donor fibroblasts. (A) Immunofluorescent stainings of DNA damage marker γH2AX in fibroblast, iNs and iPSC-iNs reveal a maintenance of DNA damage during direct reprogramming. (B) Quantification of γH2AX spots in fibroblast and iNs showing no difference. (C) Quantification of γH2AX spots in fibroblasts, iNs and iPSC-iNs. (D) Sashimi plots showing that only iNs from fibroblasts express the 4R Tau isoform (exon 10).

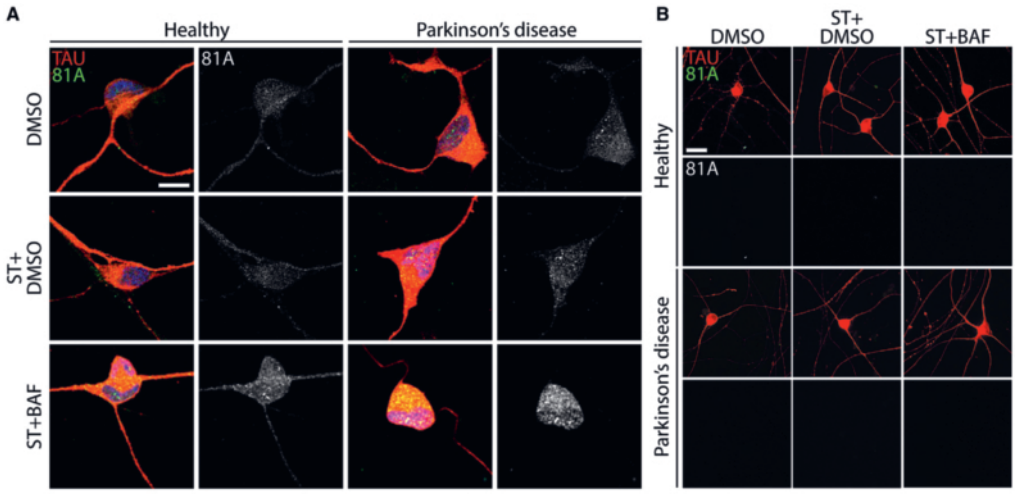

Figure 8. Autophagy impairments leading to pSyn accumulation in PD iNs. (A) Immunofluorescent stainings of neuronal marker TAU and pSyn marker 81A in iNs and (B) iPSC-iNs from a subset of individuals.

The study of the aged brain is inherently difficult. While post-mortem analyses can answer certain questions, the cells are no longer alive and it gives a mere snapshot of the end stage. Therefore, models to study aged neurons in a dish is highly sought after. Although reprogrammed iPSCs will carry the genetic background of the patient, the reprogramming resets many aging hallmarks. Therefore, iNs, that maintain these hallmarks have tremendous potential for disease modelling and drug screening. In **Paper II** we generated subtype specific iDANs that revealed autophagy impairments and accumulation of phosphorylated α-syn inclusions upon starvation-induced stress and bafilomycin A1 treatment. Moreover, unlike iPSC-iNs, the iNs retained DNA damage from the fibroblasts and expressed the 4R Tau isoform. In summary, directly reprogrammed fibroblasts can serve as a powerful tool to study the aged brain in the dish and be used to develop and assess novel therapeutic interventions.

Patient-derived mDA neurons can mediate motor recovery but demonstrate increased proneness to develop Lewy body-like pathology (Paper III and IV)

In 2020 the first PD patient underwent autologous transplantation as a medical intervention (Schweitzer et al., 2020) but there are no current ongoing clinical trials. The idea of autologous grafting is appealing from an immune-compatibility standpoint, but the use of cells with a disease background raises a few concerns. For instance, it is imperative that the patient cells can function *en par* with healthy cells and are not prone to develop disease-associated pathology to the extent that it may impact the longevity, integrity and function of the transplant. Should the latter be the case, strategies to help protect the cells after grafting need to be evaluated.

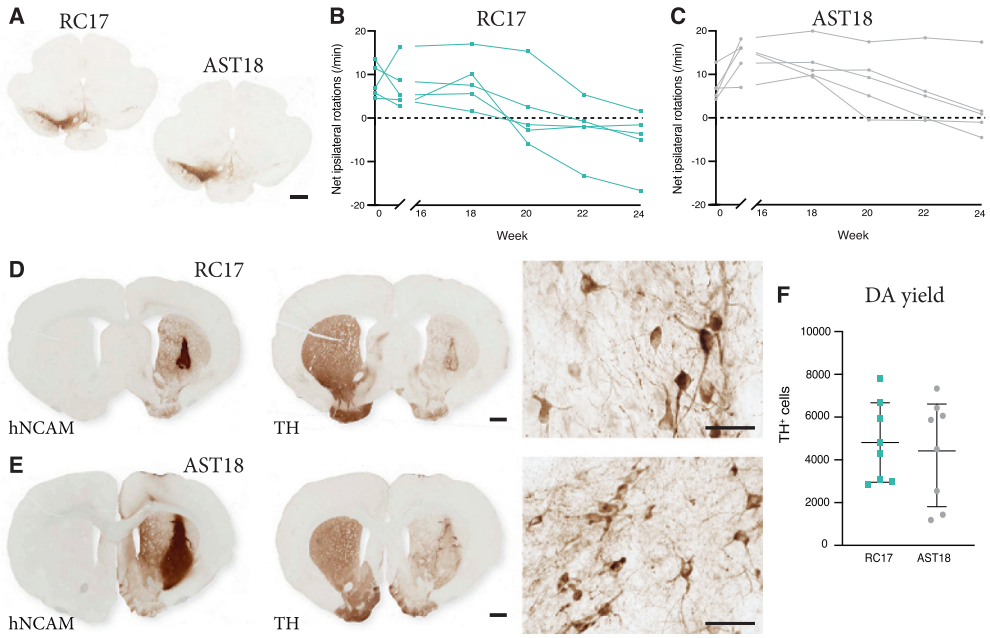

Figure 9. Long-term functional assessment of patient-derived cells carrying an *SNCA* triplication. (A) TH-DAB staining showing lesioned nigra on the right hemisphere. (B) Motor recovery seen in 5/5 of rats transplanted with RC17 and (C) 4/5 transplanted with AST18. (D) hNCAM and TH stainings of grafts with magnification of TH staining of RC17 grafts and (E) AST18 grafts. (F) No difference in DA yield between the two cell lines was observed. Scale bar sections = 1mm. Scale bar high magnification = 50μm.

Assessing the functionality of patient-derived cells

The 6-OHDA model is a well-established model to study therapeutic neuroprotection and the functionality of transplanted cells. We transplanted mDA progenitors from a patient carrying a triplication of the *SNCA* locus (called AST18) along with a healthy hESC line, RC17, into 6-OHDA lesioned rats (Fig.9A). Both cell lines mediated motor recovery as assessed by the amphetamine-induced rotation test (Fig.9B, C) and gave rise to neural and DA neuron rich grafts (Fig.9D, E). Quantification of the number of TH+ DA neurons did not reveal any differences between the lines (Fig.9F).

Lewy body-like pathology in patient-derived neurons

While the 6-OHDA model is a robust model to study behavior deficits and recovery in studies of neuroprotection and neurorestoration, it does not recapitulate some of the cardinal pathological features of PD. For instance, it does not create a pathological environment resembling that of a patient's brain. Therefore, any observed cellular pathology would be the result of intrinsic factors. Immunostainings of phosphorylated α-syn (pSyn), a marker of Lewy body-like pathology, revealed that after 24 weeks 7% of the patient derived TH+ neurons had pSyn+ inclusions (Fig.10A-F). On the contrary, no pSyn pathology was observed in the RC17 TH+ cells (Fig.10C).

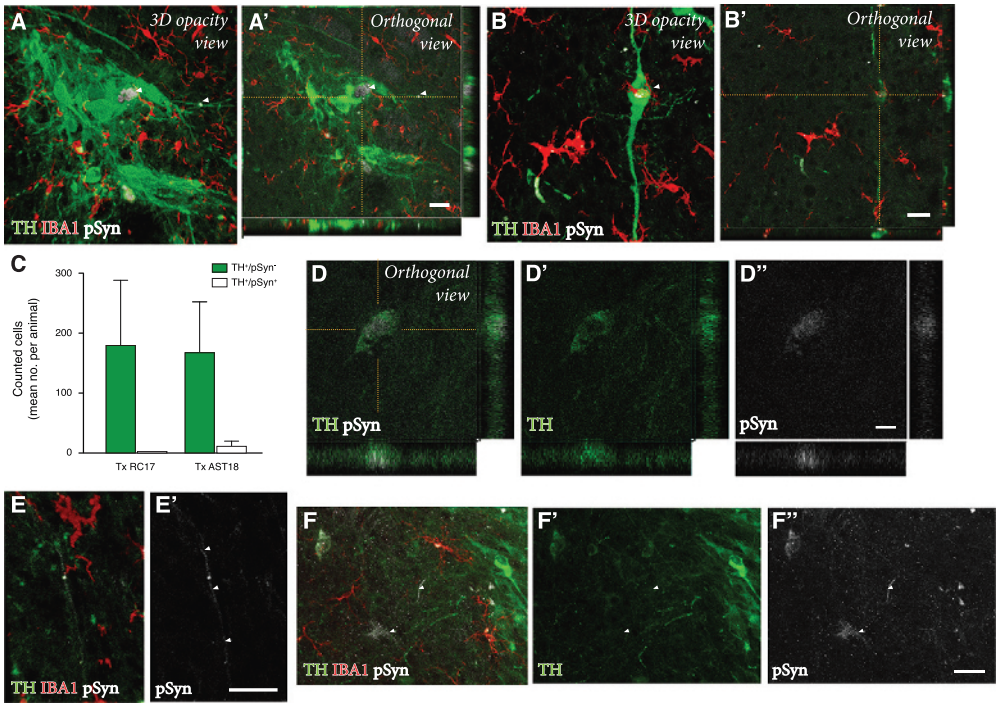

Figure 10. Long-term pathology assessment. (A,A',B,B') Stainings of DA neuron marker TH, microglia marker IBA1 and Lewy body-like pathology marker pSyn within the grafts. Scale bar = 20 μm. (C) Quantifications of number of TH+ cells harbouring pSyn inclusions. (D,D',D") TH neurons harbouring small granular inclusions of pSyn. Scale bar = 10 μm. (E,E') pSyn pathology observed in neurites. Scale bar = 20 μm. (F,F',F") Weak TH staining overlapping with pSyn, indicating down-regulation of TH. Scale bar = 20 μm.

Since the patient-derived DA neurons displayed pathological inclusions in a model that lacks a pathological environment, we wanted to see how these cells would fare in a model that recapitulates some of the pathological features observed in patient brains. To this end, we took advantage of a humanized rat model (SynFib model) where pathological features are recapitulated and transfer of pathology may be evaluated (Hoban et al., 2020). AAVs overexpressing α-syn and PFFs were injected into the SNc and VTA and four weeks later, cells were grafted into the striatum where α-syn pathology had spread (Fig.11A-C). Three patient lines, one genetic (AST18) and two sporadic (PD16 and PD22) along with hESC line RC17 were grafted and assessed after 24 weeks (Fig.11D). Comparison of the number of TH+ neurons with pSyn inclusions were markedly higher in the patient lines (Fig.11E). Also, comparison of pSyn inclusions in the AST18 line in the 6-OHDA and SynFib model reveals an exacerbated development of pathology when placed in a more pathological environment (Fig.11F).

The data presented in **Paper III** demonstrate that patient-derived mDA grafts can give rise to functional grafts that alleviate motor symptoms in the preclinical 6-OHDA model. However, even in the absence of a pathological environment the patient cells developed Lewy body-like pathology after 24 weeks. Moreover, as presented in **Paper IV,** once patient-derived cells were grafted into the

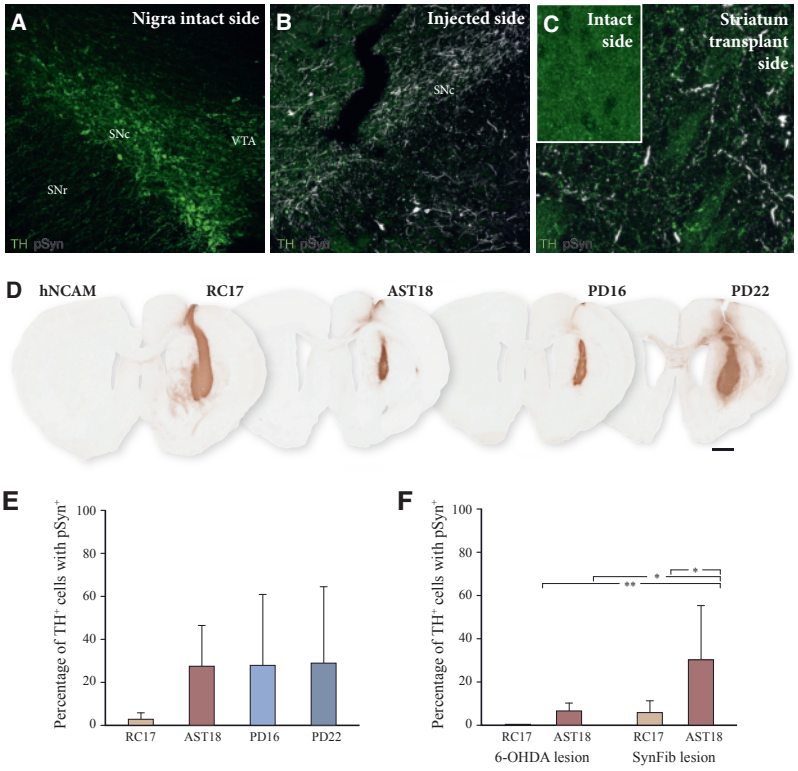

Figure 11. Patient-derived cells show exacerbated pathology. (A) No pathology is observed on the intact side. (B) In contrast the injected side show abundance of pSyn+ inclusions. (C) Spread of pathology to the striatum of the injected side while no pathology is observed on the intact side. (D) hNCAM stainings of the grafts at 24 weeks. (E) Percentage of TH+ cells with pSyn inclusions showing an increased sensitivity in the patient lines. (F) Percentage of TH+ cells with pSyn in RC17 and AST18 cells when placed in pathology free environment (6-OHDA model) and in a pathological environment (SynFib model).

SynFib model this accumulation was exacerbated. This body of data suggest that patient-derived cells might not be suitable for transplantation without prior modifications as their proneness to developed exacerbated pathology might compromise the clinical benefit of the transplant. A protective strategy could also be preferrable for patients in receipt of healthy PSCs considering the graft would need to remain functional for decades. This would be particularly important for patients that have an early disease-onset (<50 years of age) which is about 10% of all cases (Mehanna et al., 2014; Schrag and Schott, 2006).

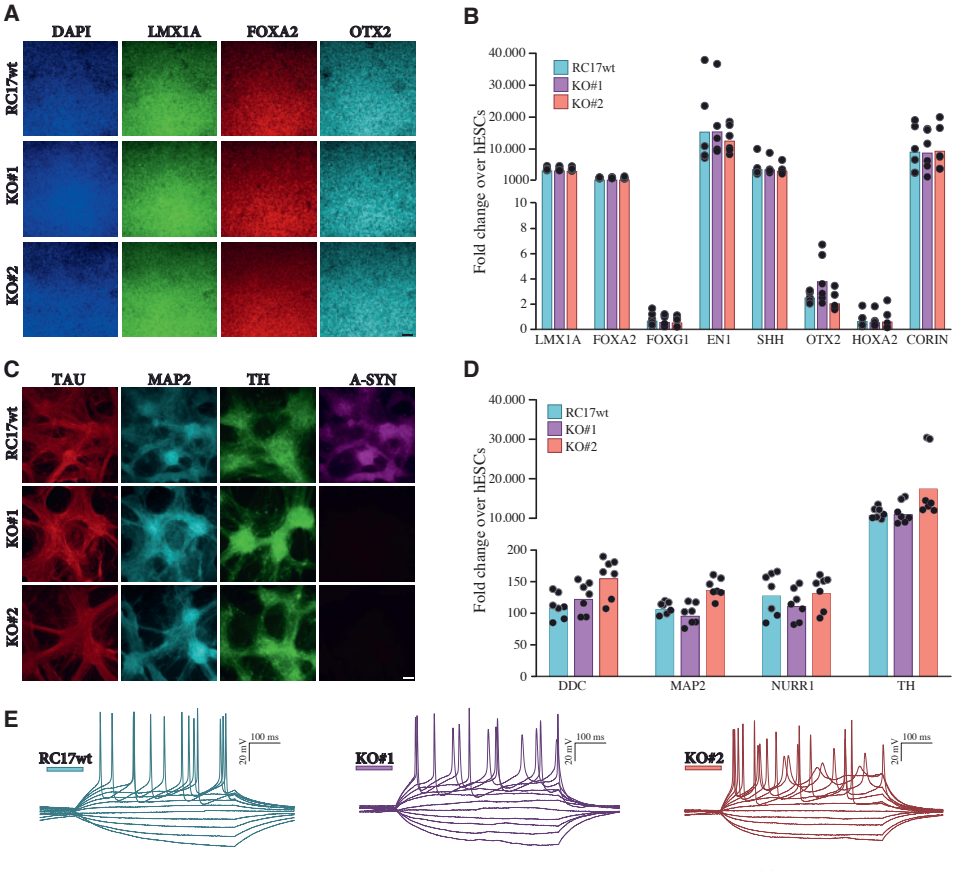

Figure 12. *SNCA*-/- hPSCs generate functional mDA neurons *en par* with parental hESC line RC17. (A) Stainings at d16 of floorplate markers LMX1a, OTX2 and FOXA2. Scale bar = 100µm. (B) RT-qPCR analysis of selected progenitor markers at d16. Values given as fold change over undifferentiated stem cells. (C) Stainings at d45 of neuronal markers TAU, MAP2, DA neuron marker TH and α-syn. Scale bar = 100µm. (D) RT-qPCR analysis of selected DA neuron markers at d45. Values given as fold change over undifferentiated stem cells. (E) Patch-clamp recordings demonstrating induced mature action potentials, indicative of neuronal functionality.

Functional and molecular assessment of *SNCA*-/- mDA neurons (Paper IV)

Several studies have demonstrated that neurons lacking α-syn expression do not develop Lewy body pathology (Chen et al., 2019; Luk et al., 2012; Volpicelli-Daley et al., 2011). This could therefore serve as a strategy to protect the transplants from host-to-graft transfer of pathology after grafting. This would be particularly important for autologous transplantation or patients with an early disease-on or aggressive synucleinopathy. However, studies on the functionality of *SNCA*-/- cells are lacking,

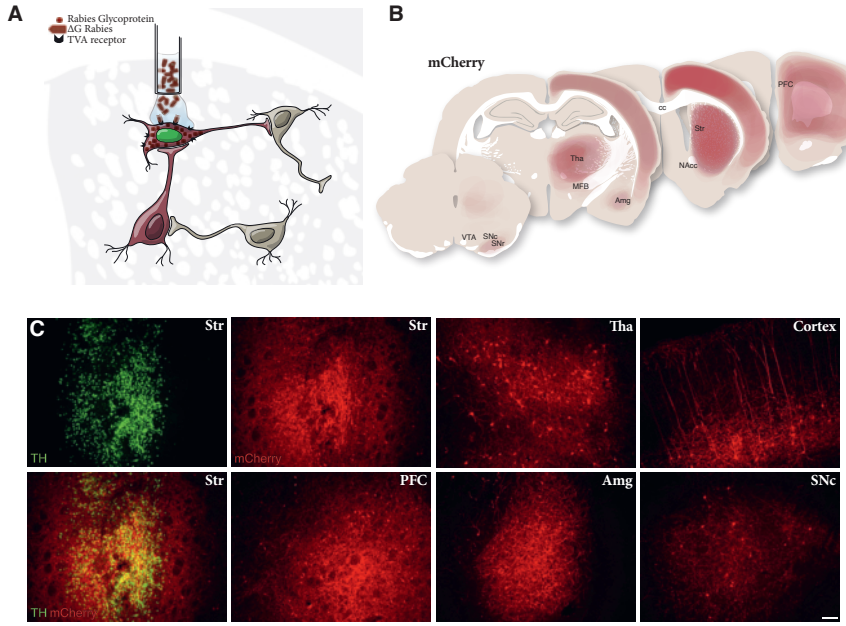

Figure 13. Tracing afferent input of grafted *SNCA*-/- progenitors. (A) Schematic of the rabies-based tracing system. (B) Mapping of the traced endogenous neuron. (C) Immunofluorescence images of traced neuron in different regions. Scale bar = 100μm.

which we aimed to address here.

SNCA-/- hPSC differentiate *en par* with hESC to mature mDA neurons

We patterned two *SNCA*-/- clones and their parental hESC line RC17 to mDA progenitors and subsequently to mDA neurons. Immunofluorescence and RT-qPCR at day 16 and day 45 showed efficient differentiation *en par* with RC17 (Fig.12A-D). Patch-clamp recordings demonstrated electrophysiological activity indicative of a mature neuronal identity (Fig.12E).

SNCA-/- mDA progenitors integrate into host striatum and receive appropriate regional input from host brain

Next, in order to study survival and integration upon grafting, we took advantage of the rabies-based monosynaptic tracing system that allows the tracing of afferent input to the grafted neurons. In short, transplanted neurons are transduced with a vector that labels them with nuclear GFP and carries the machinery to allow mCherry+ rabies infection and first-order synaptic spread. (Fig.13A). Using this approach, we transplanted *SNCA*-/- mDA progenitors and assessed the integration after 8 weeks. Stainings for mCherry revealed input from regions known to connect to the dorsolateral striatum such as the cortex, pre-frontal cortex, amygdala and thalamus (Fig.13B, C), which is in accordance with previously published data on transplanted RC17 cells (Adler et al., 2019; Grealish et al., 2015).

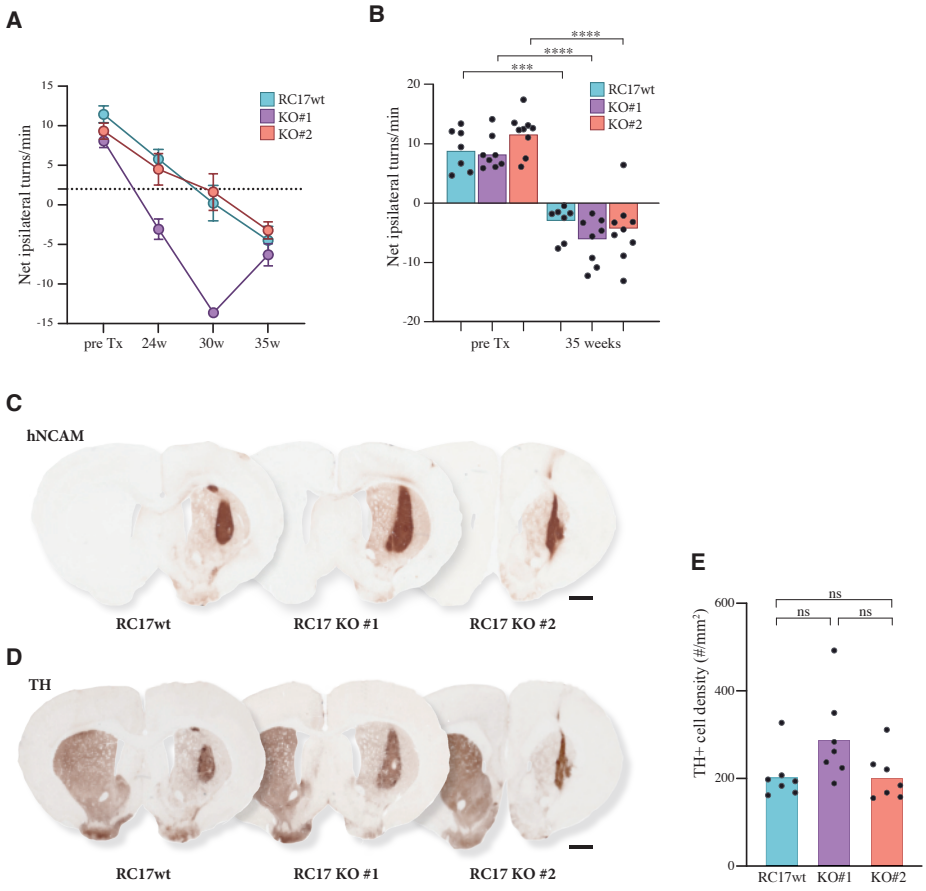

Figure 14. Long-term graft assessment after 7 months in the 6-OHDA model. (A,B) Amphetamine-induced rotations revealed motor recovery for all three lines. (C) hNCAM staining of the grafts. Scale bar = 1mm. (D) TH staining of the grafts. Scale bar = 1mm. (E) No statistically significant differences were detected in TH+ cell density among the lines.

Long-term graft assessment of *SNCA*-/- transplantations

In order for *SNCA* deletion to a viable option in a clinical setting it is essential that the absence of any α-syn expression does not interfere with the cells ability to release dopamine and alleviate motor symptoms. To answer this, we transplanted both *SNCA*-/- clones along with RC17 into 6-OHDA lesioned nude rats. Grafts isolated at 7 months and analyzed with single-nuclei sequencing revealed no population bias and the same populations that were captured (neurons, astrocytes and VLMCs) are in accordance with previously published data on stem cell-derived grafts (Tiklova et al., 2020). Furthermore, amphetamine-induced rotations demonstrated that the *SNCA*-/- lines could mediate motor recovery (Fig.14A, B) and stainings showed hNCAM and TH rich grafts (Fig.14C, D). Quantification of the DA neurons showed no difference in TH+ neuron density among the lines (Fig.14E).

In **Paper IV** we wanted to evaluate if *SNCA* deletion has the potential to serve as a universal strategy for graft protection against host-to-graft transfer of Lewy body pathology. Since α-syn serves a physiological role it is imperative to ensure that the lack of expression does not interfere with the ability to generate mDA neurons and treat motor symptoms. We demonstrate in Paper IV that the *SNCA*-/- cells differentiate and mature to mDA neurons *en par* with parent ESC line RC17. Moreover, upon grafting into the 6-OHDA lesioned rat brain the KO cells survive, integrate and mediate motor recovery. Taken together, these data suggest that *SNCA* deletion could be a viable strategy to help protect the cells after grafting and stay fully functional for the remaining lifetime of the patient.

SUMMARIZING CONCLUSIONS AND FUTURE PERSPECTIVES

The field of cell replacement therapy for PD has undoubtedly entered a very exiting era. At the time of writing this it has been four years since the hPSC-based clinical trial started in Japan, almost two years since their start in the US and this year the first patient was transplanted in Sweden. The clinical trial in Japan used iPSCs from from the same healthy donor to graft to all patients, while the trials in the US and in Sweden used hESC-derived progenitors. The breakthrough of iPSC reprogramming makes it possible to use patient-specific cell, and in 2020 the first case-study of autologous grafting was reported (Schweitzer et al., 2020) and there is a great interest to develop autologous grafting into clinical trials and new therapies. In this thesis the focus has been on evaluating the potential of autologous grafting in cell replacement therapy for PD with focus on cell quality, integrity and function without development of disease associated pathology after grafting.

In **Paper I,** we reported a single-cell sequencing data set on hPSC-derived mDA progenitors and neurons. Using this data set we could follow the differentiation from pluripotent stem cell to active, mature neurons. Also, using a fetal tissue data set we could show that the cells we generate are similar on a transcription level to authentic dopamine progenitors and neurons from human fetal brain. However, even at day 60 there were remaining cells that still had a floorplate progenitor identity which indicates that maturation was noncomplete. This speaks to use of 3-dimensional organoids cultures for studying more mature mDA neurons since their free floating nature allows for long-term cultures (Sozzi et al., 2022). We also created a pipeline where we could study long noncoding RNAs during differentiation. The data we gathered for this study can be a valuable resource to study mDA neurogenesis and further optimize and quality control stem cell differentiation toward functional mDA neurons for clinical purposes.

While pluripotent stem cell derived mDA neurons are used for cell replacement therapy, they have an inherent flaw in terms of drug screening and disease modelling using patient derived cells. Namely, as somatic cells are reprogrammed to iPSCs, they lose many hallmarks of ageing. Since age is the biggest risk factor for PD this present an issue. Directly converted induced neurons retain these ageing signatures which makes them very attractive for drug screening and disease modelling purposes. In **Paper II** we generated iDAN enriched cultures by transducing PD and healthy donor fibroblasts with an 8-viral vector cocktail. We saw that PD and healthy donor fibroblasts convert with the same efficiency, but PD iNs displayed increased autophagy impairments and vulnerability to starvation-induced stress. This was not observed with iPSC-derived neurons from the same individuals. Moreover, these iNs also maintained the DNA damage seen in the starting fibroblast. Together, these data accentuate the potential of direct reprogramming for disease modelling and drug screening applications. The maintained age means that pathology arise in a shorter time frame which is good for *in vitro* modelling of disease. Since pathology was observed in the sporadic PD-iNs but not the iPSCs

the iNs have the potential to serve as a tool to in a short period of time help predict the outcome in *in vivo* grafting of iPSCs that are meant to stay functional for decades.

The low cost and short time to generate patient-specific iNs as well as by avoiding a proliferative intermediate have sparked an interest in iNs as a therapeutic option in cell replacement therapy. However, improvements in conversion efficacy, determining the effect of using aged cells and extensive testing in animal models are required in order to make this a feasible option.

The possibility to generate patient-specific cells has generated a lot of interest in autologous grafting. Studies in NHPs have demonstrated the capacity to generate TH rich grafts that can alleviate motor symptoms all while eliciting a minimal to no immune response without the need for immune suppression (Morizane et al., 2013; Tao et al., 2021). To evaluate this type of grafting, in **Paper III,** we grafted patient-derived mDA progenitors carrying a triplication of the *SNCA* locus into the preclinical 6-OHDA model. Although the patient-derived cells gave rise to DA rich graft and could mediate motor recovery in the amphetamine-induced rotation test, we observed accumulation of pSyn+ inclusions. Since the 6-OHDA does not recapitulate the pathological features of PD, this would suggest that patient cells are intrinsically more prone to develop α-syn pathology due to their disease background independent of environment.

In **Paper IV** we aimed to assess how these patient cells would fare in a more pathological setting that is more reminiscent of the patient brain in terms of proteinopathy, inflammation and slow degeneration. We transplanted the same triplication cell line, along with two sporadic PD lines into the SynFib model. Here we found that all the patient lines displayed a much more exacerbated α-syn pathology compared to healthy hESC-derived grafts. This suggests that in order for autologous grafts to stay functional for the remaining lifetime of the patient, the cells need to be protected or made disease resistant through genetic engineering approaches or other means. Studies in rodents and hPSC-derived cultures have demonstrated that *SNCA* null cells do not develop Lewy-body like pathology (Chen et al., 2019; Luk et al., 2012; Volpicelli-Daley et al., 2011). We wanted to evaluate if *SNCA* deletion is a viable strategy to prevent host-to-graft transfer of pathology, with a focus on ensuring that its deletion does not prevent functionality and its potential use in a clinical setting. While the precise physiological role of α-syn in still not completely understood it is involved with synaptic vesicle trafficking (Burre, 2015; Burre et al., 2013; Sharma and Burre, 2023). Here, we show that the deletion of *SNCA* does not prevent the differentiation to mature, functional mDA neurons. Furthermore, upon grafting, the cells receive afferent synaptic input from the correct host brain regions and can mediate motor recovery in a preclinical rat model. These data suggest that *SNCA* deletion could serve as a valuable strategy to prevent graft pathology while maintaining the advantages of autologous grafting.

Building on past decades of efforts stem cell-based therapies have finally reached clinical trials towards developing treatments for multiple diseases, such as Parkinson's disease, macular degeneration, diabetes and heart disease. With all the reprogramming and genetic engineering tools we have at our disposal today we have the ability to custom-design the cells before transplantation. This include removing or introducing genes, induced production of neurotrophic factors and modifications to prevent immunosuppression. Together with advances in robotics and automation for production and quality control the future will see an unprecedented opportunity to deliver personalized medicine in the field of cell replacement therapy.

MATERIAL AND METHODS

In this section I will be describing the methods that have been instrumental for the work included in this thesis. For more details, I refer to the material and methods section of each individual paper.

In vitro studies

Culturing of human pluripotent stem cells

All pluripotent stem cells were maintained on laminin-521-coated (0.5μg/cm^2, Biolamina, LN-521) plates in iPS-Brew XF medium (StemMACS, Milteny) to retain pluripotency. The cells were split upon reaching a 70-90% confluency using accutase and ROCK inhibitor (10μM Y-27632) was added to the media for the first 24 hours. The stem cells were maintained in culture for at least one week before the start of differentiation.

Differentiation of human pluripotent stem cells to midbrain DA neurons in 2D and 3D

The detailed protocol for the differentiation of human pluripotent stem cells to mDA progenitors and subsequently mDA neurons can be found in Nolbrant et al., 2017 (Nolbrant et al., 2017) but will be briefly described here. On day 0, the cells are detached using accutase or EDTA, counted and plated onto laminin-111-coated plates (1μg/cm^2, Biolamina, LN-111) at a seeding density of 10.000 cells/cm^2. From day 0 to day 9 the cells were kept in N2-media supplemented with SB431542 and noggin for dual SMAD-inhibition and differentiation towards early neuroectoderm, sonic hedgehog (SHH) for ventralization and CHIR-99021 for caudalization. From day 9 to day 11 the N2 media was supplemented with only FGF8b to help with patterning towards caudal midbrain. On day 11 the cells were detached with accutase, counted and re-plated onto laminin-111-coated plates at a seeding density of 800.000 cells/cm^2 in B27-media supplemented with BDNF, AA and FGF8b. On day 16 the cells were either frozen down for later use, prepared fresh for transplantation or replated for terminal differentiation. In the later scenario, the cells were replated onto laminin-111-coated plates at a seeding density of 155.000 cells/cm^2 in B27-media supplemented with BDNF, GDNF, AA, DAPI and db-cAMP. Media was changed every 2-3 days until end of experiment. Before proceeding with transplantations and terminal differentiation it is encouraged to perform a quality control (QC) on the cells and ensuring high expression of ventral midbrain markers *FOXA2, OTX2, LMX1A, EN1, CORIN* and *SHH* by staining or RT-qPCR.

The protocol for generating 3-dimensional ventral midbrain organoids for long-term cultures is carefully explained elsewhere and resembles the protocol for 2D differentiation described above (Sozzi et al., 2022). The main difference is that the cells are seeded in ultra-low attachment plates in iPS-brew 3 days before switching to N2-media in order to allow self-aggregation and embryoid bodies to form. Also, on day 14-16 the organoids may be embedded in a hydrogel (most commonly Matrigel)

that will mimic the extracellular matrix and help with maturation and support axonal outgrowth (Fiorenzano et al., 2021). Although, the embedding can interfere with various functionality experiments such as electrophysiology and dopamine release assays.

Culturing human adult dermal fibroblasts

Skin fibroblast were cultured in uncoated flasks in fibroblast media consisting of DMEM, 10% fetal bovine serum and 1% penicillin-streptomycin. Media was changed every 2-3 days until 90-95% confluency, whereupon the cells were split using 0.05% trypsin according to Shrigley et al., 2018 (Shrigley et al., 2018).

Lentiviral production

The production of lentiviral vectors (LV) was carried out according to Zufferey et al., 1997 (Zufferey et al., 1997). In summary, HEK293 cells were transfected with the plasmids of interest along with helper plasmids necessary for the packaging of LVs and their production as well as transfection reagent polyethylenimine (PEI). After two days the media containing the LVs were collected, filtered and ultracentrifuged. The pellet of LV particles was resuspended in PBS, aliquoted and stored at -80°C.

Generation of induced neurons in 2D and 3D

For conversion in 2D fibroblasts were seeded onto plates sequentially coated with poly-ornithine, laminin and fibronectin at a density of 25.000 cells/cm^2 in fibroblast media. The following day LVs were added with new fibroblast media. For iDAN conversion 5 vectors of DA neuron fate determinants *(LMX1A, LMX1B, FOXA2, OTX2* and *NURR1)* were added along with pioneering factor *ASCL1* and *shREST1* and *shREST2* for neuronal induction at an MOI of 5 each. For general neuron conversion (yielding mostly glutamatergic neurons) a single vector termed pBpA (carrying *BRN2, ASCL1, shREST1* and *shREST2)* was used instead at an MOI of 20 (Drouin-Ouellet et al., 2017). From day 3 to day 16 the cells were maintained in early conversion media which was switched to late conversion media from day 16 until end of experiment. For *in vivo* experiments or *in vitro* experiments longer than 4 weeks the cells were converted in 3D cultures. Fibroblast were either seeded and aggregated in ultra-low attachment 96-wells, spun down in microwells to generate microspheres or embedded in collagen. In order to allow a more homogenous transduction in 3D, the LVs were mixed and added along with the cells.

Dopamine release detection using sniffer cells

To assess the potential of our cultures to produce and release dopamine, we took advantage of genetically engineered HEK293 cells, called sniffer cells (Klein Herenbrink et al., 2022). These cells have been modified to express tetracycline-induced DA sensors that through G-protein coupled receptors fluoresce upon contact with dopamine. DA neuron rich cultures were washed and put in a high NaCl solution. Following this, the solution was changed to one with a high KCl concentration to force dopamine release. This solution was then added on top of the sniffer cells that had been seeded on polyornithine-coated glass-bottom plates. The increase in fluorescence was measured by

Table 1. List of antibodies used *in vitro*.

Antigen	Species	Company (catalog)	Dilution
AADC	Rabbit	Merck Millipore (AB1569)	1:500
COL1A1	Sheep	R&D Systems (AF6220)	1:200
FOXA2	Mouse	Santa Cruz (sc-101060)	1:500
GFP	Chicken	Abcam (ab13970)	1:1000
GIRK2	Goat	Abcam (ab65096)	1:200
hGFAP (STEM123)	Mouse	Takara Bio (Y40420)	1:500
Human Nuclei (HuNu)	Mouse	Merck Millipore (MAB1281)	1:200
LMX1A	Rabbit	Merck Millipore (AB10533)	1:1000
MAP2	Chicken	Abcam (ab5392)	1:5000
mCherry	Goat	Sicgen (AB0040-200)	1:500
OTX2	Goat	R&D Systems (AF1979)	1:2000
TAU	Rabbit	DAKO (A0024)	1:1000
TH	Rabbit	Merck Millipore (AB152)	1:1000
TUBB3	Mouse	Biolegend (801202)	1:500

acquiring images before and after the addition of the solution and was presented as a percentage of maximum fluorescence (measured after addition of highly concentrated DA solution to reach saturation of sensors).

Immunocytochemistry

Cells were washed 3x in PBS and fixed with 4% paraformaldehyde for 15 min at room temperature (4 hours for organoids) and washed 3x again. Organoids were left in 30% sucrose overnight, cryopreserved in blocks of OCT Cryomount, sectioned with a cryostat and stained as slices on glass slides. The cells were incubated in blocking solution (5% serum and 0.1% Triton in PBS) for 1-2 hours to avoid any unspecific binding and left overnight incubating in primary antibodies diluted in blocking solution. The following day the cells were washed 2x and put in blocking solution for 30min and subsequently in blocking solution with secondary antibodies and DAPI for 1 hour in RT. Lastly the cells were washed 3x and stored in PBS at 4°C until imaging. For full list of antibodies that were used *in vitro*, see table 1.

mRNA extraction, cDNA conversion and RT-qPCR

Gene expression analysis was carried out using reverse transcription quantitative real-time PCR (RT-qPCR). Cells were washed twice in PBS and mRNA was collected and extracted according to manufacturer instructions (QIAGEN RNeasy Micro Kit, #74004). The concentration of mRNA was measured with a NanoDrop™ spectrophotometer and roughly 1μg of mRNA was reverse transcribed to cDNA using Maxima First Strand cDNA Synthesis Kit (Thermo Scientific, #K1642). The samples, primers of interest and SYBR Green (Roche, #04887352001) were mixed using a Bravo

Table 2. List of primers used for RT-qPCR gene expression analysis.

Gene	Full gene name	Primer Sequence (fwd/rev)
ACTB	Actin beta	CCTTGCACATGCCGGAG GCACAGAGCCTCGCCTT
CORIN	Corin, serine peptidase	CATATCTCCATCGCCTCAGTTG GGCAGGAGTCCATGACTGT
EN1	Engrailed homeobox 1	CGTGGCTTACTCCCCATTTA TCTCGCTGTCTCTCCCTCTC
FOXA2	Forkhead box A2	CCGTTCTCCATCAACAACCT GGGGTAGTGCATCACCTGTT
FOXG1	Forkhead box G1	TGGCCCATGTCGCCCTTCCT GCCGACGTGGTGCCGTTGTA
GAPDH	Glyceraldehyde-3-phosphate dehydrogenase	TTGAGGTCAATGAAGGGGTC GAAGGTGAAGGTCGGAGTCA
HOXA2	Homeobox A2	CGTCGCTCGCTGAGTGCCTG TGTCGAGTGTGAAAGCGTCGAGG
LMX1A	LIM homeobox transcription factor 1 alpha	CGCATCGTTTCTTCTCCTCT CAGACAGACTTGGGGCTCAC
LMX1B	LIM homeobox transcription factor beta	CTTAACCAGCCTCAGCGACT TCAGGAGGCGAAGTAGGAAC
NURR1 (NR4A2)	Nuclear Receptor Subfamily 4 Group A Member 2	CAGGCGTTTTCGAGGAAAT GAGACGCGGAGAACTCCTAA
SHH	Sonic Hedgehog Signalling Molecule	CCAATTACAACCCCGACATC AGTTTCACTCCTGGCCACTG
TH	Tyrosine Hydroxylase	CGGGCTTCTCGGACCAGGTGTA CTCCTCGGCGGTGTACTCCACA

Automated Liquid Handling Platform (Agilent) and analysed with a LightCycler 480 II (Roche). The gene expression was normalized to two housekeeping genes *(actin beta* and *GAPDH)* and compared to undifferentiated/unconverted cells.

In vivo studies

Animals

All experiments conducted using live animals were carried out in full accordance with the European Union Directive 2010/63/EU and were approved by Jordbruksverket (the Swedish Department of Agriculture) and the local ethics committee at Lund University. For experiment shorter than 18 weeks, procedures were conducted in adult female Sprague-Dawley (SD) rats purchased from Charles River Laboratories. Since SD rats have a fully functional immune system, they received daily injections of Ciclosporin A (10mg/kg) intraperitoneally (i.p.) starting 2 days prior to cell transplantation in order to keep them immune-suppressed and prevent graft rejection. For long-term experiments lasting longer than 18 weeks adult female athymic rats from Envigo were used instead, which did not require daily Ciclosporin injections. All rats weighed at least 225g before any surgical procedure and were kept in ventilated cages under 12-hour light/dark cycles with free access to food and water.

Table 3. Coordinates, volumes, rate of injection and diffusion times for all surgical procedures.

Procedure	A/P	M/L	D/V	Details
MFB Lesion	-4.4	-1.1	-7.8	3µl, 0.3µl/min
SD rats				No diff. time
MFB Lesion	-3.9	-1.2	-7.3	3µl, 0.3µl/min
Nude rats				No diff. time
Striatum transplantation	+1.2	-3.0	-4.5 / -5.5	75.000 cells/µl
SD rats	+0.5	-2.6	-4.5 / -5.5	1µl/min
				1µl/deposit, 2 min diff.time
Striatum transplantation	+1.4	-3.0	-4.0 / -5.0	75.000 cells/µl
Nude rats	+0.9	-2.6	-4.0 / -5.0	1µl/min
				1µl/deposit, 2 min diff.time
Rabies injection	+0.8	-2.8	-4.5 / -5.5	3µl, 0.3µl/min
SD rats				No diff. time
Rabies injection	+1.1	-2.8	-4.0 / -5.0	3µl, 0.3µl/min
Nude rats				No diff. time
Nigral/VTA	-5.0	-2.6	-6.1	2µl, 2µl, 1µl. 0.2µl/min
SynFib Lesion	-5.0	-1.6	-6.8	No diff. time
Nude rats	-5.0	-0.8	-6.6	

Surgeries

All surgical procedures took place under general anaesthesia via i.p. injection of a mixture of ketaminol® (ketamine hydrochloride, 45mg/kg) and domitor® (medetomidine, 0.3mg/kg) with the addition of Marcain® (bupivacaine, 0.1ml) injected subcutaneous (s.c.) as a local anaesthesia. The rats were carefully placed in stereotaxic frames and placed in a "flat head" position, i.e. the dorso-ventral difference between bregma and 8.0mm posteriorly is less than ± 0.3mm. After the surgery the anaesthesia was reversed with Antisedan® (atipamezole, 0.28mg/kg) and Temgesic® (buprenorphine, 0.04mg/kg) was given as analgesia. All coordinates for the different procedures and rat strains can be found in Table 3.

6-OHDA model

The ability to mediate motor recovery was assessed in the well-established 6-OHDA model. In this preclinical model, the toxin 6-OHDA is injected into the medial forebrain bundle (MFB) of the animals to achieve a complete dopamine degeneration on the injected hemisphere. The 6-OHDA was prepared by diluting 6-OHDA (3.5µg/µL free base SigmaH481-1G) in ascorbic acid (0.02% in saline) and put on ice. This imbalance in DA can be assessed by the administration of amphetamine, which causes the release of DA vesicles and prevents its update via DAT (Sulzer et al., 1995). Upon amphetamine administration the rats will (if well-lesioned) turn toward the lesioned side and this can be quantified by placing the rats in a harness inside a bowl and record their turning behaviour (Ungerstedt and Arbuthnott, 1970).

The rats were given an i.p. injection of dexamphetamine (3.5mg/kg), put in a harness and placed in a rotometer bowl. Their movements were recorded for 90 minutes and each clockwise turn was registered as a positive value and each counterclockwise turn as a negative value. The results were measured as net turns per minute. The criterium for a well-lesioned rat was set to 4 net turns per minutes. In experiments to evaluate if a cell line could mediate motor recovery, this criterion was set to the following: (1) statistically significant decrease in net turns per minute on a group level and (2) more than 50% of the group should record 2 turns per minute or less.

SynFib model

AAV6 expressing α-syn under the synapsin promoter were produced as previously described (Decressac et al., 2011). For the experiments included in this thesis the titer was measured to $4.7x10^{14}$ genome copies/mL and diluted to 20%. The PPFs were made by sonicating 5mg/mL of full-length recombinant human α-syn protein (gifted by Kelvin Luk) at pulses of 6x 5 seconds (Volpicelli-Daley et al., 2014). The AAVs and PFFs were mixed at a ratio of 1:1 to yield a final concentration of 10% AAVs and 2.5mg/mL PFFs. The preparation, including the sonication was made on the day of surgery and put on ice when not in use.

Cell preparation for transplantation

On the day of transplantation, cells were prepared either from fresh cultures or frozen vials. The cells were counted and prepared to a final concentration of 75.000 cells per µL in HBSS and DNase (1:10). The cells were placed on ice and resuspended each time before injection.

Perfusion and histology

At the end of the experiment the rats were administered a terminal anesthetic dose of pentobarbital i.p. and transcardially perfused with room-temperature 0.9% saline followed by ice-cold 4% PFA for 5 minutes. Subsequently, the brains were taken out from the skull and put in 4% PFA for post-fixation overnight at 4ºC. The following day the PFA was replaced with 25% sucrose in PBS and left for 2-3 days or until the brain had sunk to the bottom of the vial. Lastly, the brains were sectioned with a freezing microtome at a thickness of 35 µm per section, in series of 1:8 and were ready for staining. The sections to be analyzed at a later timepoint were stored in anti-freeze at 4ºC.

All sections were stained as free-floating slices in glass vials. The sections were washed 3x in KPBS and then incubated in TRIS-EDTA (pH 9) for 30 min at 80ºC. Sections to be DAB-stained were put in a quenching solution (10% methanol, 3% H_2O_2 in KPBS) for 15 min and washed 3x. Next, the sections were incubated in blocking solution (5% serum, 0.25% triton) for 1 hour to prevent unspecific binding and lastly the sections were left to incubate in blocking solution with added primary antibodies at room temperature overnight.

The following day the sections were washed twice and put in blocking solution for 30 min. For immunofluorescence staining, the sections were incubated with fluorophore-conjugated secondary antibodies (5µl/ml) and DAPI (1:1000) for 1-2 hours at RT, washed 3x, mounted onto gelatine-coated glass slides and coverslipped with PVA-DABCO. The DAB-sections were instead incubated in biotinylated secondary antibodies (5µl/ml), washed 3x, left in an avidin-biotin complex (ABC complex)

Table 4. List of antibodies used *in vivo*.

Antibody	Host species	Company and catalogue number	Dilution
AADC	Rabbit	Merck Millipore (AB1569)	1:500
COL1A1	Sheep	R&D Systems (AF6220)	1:200
FOXA2	Mouse	Santa Cruz (sc-101060)	1:500
GFP	Chicken	Abcam (ab13970)	1:1000
GIRK2	Goat	Abcam (ab65096)	1:200
hGFAP (STEM123)	Mouse	Takara Bio (Y40420)	1:500
Ki67	Mouse	BD Biosciences (ab550 609	1:500
mCherry	Goat	Sicgen (AB0040-200)	1:500
TH	Rabbit	Merck Millipore (AB152)	1:1000
TUBB3	Mouse	Biolegend (801202)	1:500

for 1 hour and washed 3x. Next, the sections were incubated in DAB solution (20µl/ml) for 2 minutes prior to adding 20µl of 3% H_2O_2 solution to allow the colour to develop. The sections were washed 3x, mounted onto gelatine-coated glass slides, dehydrated in an ascending order of alcohol concentration, cleared with xylene and coverslipped with DPX mountant.

DA neuron quantification

TH+ DA neurons were quantified using TH DAB-staining. Following the staining, the sections were imaged with an Olympus CKX53 brightfield microscope with a 20x objective at two different focal planes. The images were imported onto ImageJ and quantified.

REFERENCES

Adler, A.F., Cardoso, T., Nolbrant, S., Mattsson, B., Hoban, D.B., Jarl, U., Wahlestedt, J.N., Grealish, S., Bjorklund, A., and Parmar, M. (2019). hESC-Derived Dopaminergic Transplants Integrate into Basal Ganglia Circuitry in a Preclinical Model of Parkinson's Disease. Cell Rep 28, 3462-3473 e3465. 10.1016/j.celrep.2019.08.058.

Aron Badin, R., Bugi, A., Williams, S., Vadori, M., Michael, M., Jan, C., Nassi, A., Lecourtois, S., Blancher, A., Cozzi, E., et al. (2019). MHC matching fails to prevent long-term rejection of iPSC-derived neurons in non-human primates. Nat Commun 10, 4357. 10.1038/s41467-019-12324-0.

Barker, R.A., Barrett, J., Mason, S.L., and Bjorklund, A. (2013). Fetal dopaminergic transplantation trials and the future of neural grafting in Parkinson's disease. Lancet Neurol 12, 84-91. 10.1016/S1474-4422(12)70295-8.

Barker, R.A., Parmar, M., Studer, L., and Takahashi, J. (2017). Human Trials of Stem Cell-Derived Dopamine Neurons for Parkinson's Disease: Dawn of a New Era. Cell Stem Cell 21, 569-573. 10.1016/j.stem.2017.09.014.

Barker, R.A., and Widner, H. (2004). Immune problems in central nervous system cell therapy. NeuroRx 1, 472-481. 10.1602/neurorx.1.4.472.

Becerra-Calixto, A., Mukherjee, A., Ramirez, S., Sepulveda, S., Sinha, T., Al-Lahham, R., De Gregorio, N., Gherardelli, C., and Soto, C. (2023). Lewy Body-like Pathology and Loss of Dopaminergic Neurons in Midbrain Organoids Derived from Familial Parkinson's Disease Patient. Cells 12. 10.3390/cells12040625.

Bentea, E., Verbruggen, L., and Massie, A. (2017). The Proteasome Inhibition Model of Parkinson's Disease. J Parkinsons Dis 7, 31-63. 10.3233/JPD-160921.

Birtele, M., Storm, P., Sharma, Y., Kajtez, J., Wahlestedt, J.N., Sozzi, E., Nilsson, F., Stott, S., He, X.L., Mattsson, B., et al. (2022). Single-cell transcriptional and functional analysis of dopaminergic neurons in organoid-like cultures derived from human fetal midbrain. Development 149. 10.1242/dev.200504.

Bjorklund, A., and Dunnett, S.B. (2007). Dopamine neuron systems in the brain: an update. Trends Neurosci 30, 194-202. 10.1016/j.tins.2007.03.006.

Bonilla, S., Hall, A.C., Pinto, L., Attardo, A., Gotz, M., Huttner, W.B., and Arenas, E. (2008). Identification of midbrain floor plate radial glia-like cells as dopaminergic progenitors. Glia 56, 809-820. 10.1002/glia.20654.

Bourdenx, M., Dovero, S., Engeln, M., Bido, S., Bastide, M.F., Dutheil, N., Vollenweider, I., Baud, L., Piron, C., Grouthier, V., et al. (2015). Lack of additive role of ageing in nigrostriatal neurodegeneration triggered by alpha-synuclein overexpression. Acta Neuropathol Commun 3, 46. 10.1186/s40478-015-0222-2.

Brederlau, A., Correia, A.S., Anisimov, S.V., Elmi, M., Paul, G., Roybon, L., Morizane, A., Bergquist, F., Riebe, I., Nannmark, U., et al. (2006). Transplantation of human embryonic stem cell-derived cells to a rat model of Parkinson's disease: effect of in vitro differentiation on graft survival and teratoma formation. Stem Cells 24, 1433-1440. 10.1634/stemcells.2005-0393.

Burre, J. (2015). The Synaptic Function of alpha-Synuclein. J Parkinsons Dis 5, 699-713. 10.3233/JPD-150642.

Burre, J., Vivona, S., Diao, J., Sharma, M., Brunger, A.T., and Sudhof, T.C. (2013). Properties of native brain alpha-synuclein. Nature 498, E4-6; discussion E6-7. 10.1038/nature12125.

Caiazzo, M., Dell'Anno, M.T., Dvoretskova, E., Lazarevic, D., Taverna, S., Leo, D., Sotnikova, T.D., Menegon, A., Roncaglia, P., Colciago, G., et al. (2011). Direct generation of functional dopaminergic neurons from mouse and human fibroblasts. Nature 476, 224-227. 10.1038/nature10284.

Cenci, M.A., and Bjorklund, A. (2020). Animal models for preclinical Parkinson's research: An update and critical appraisal. Prog Brain Res 252, 27-59. 10.1016/bs.pbr.2020.02.003.

Chambers, S.M., Fasano, C.A., Papapetrou, E.P., Tomishima, M., Sadelain, M., and Studer, L. (2009). Highly efficient neural conversion of human ES and iPS cells by dual inhibition of SMAD signaling. Nat Biotechnol 27, 275-280. 10.1038/nbt.1529.

Chartier-Harlin, M.C., Kachergus, J., Roumier, C., Mouroux, V., Douay, X., Lincoln, S., Levecque, C., Larvor, L., Andrieux, J., Hulihan, M., et al. (2004). Alpha-synuclein locus duplication as a cause of familial Parkinson's disease. Lancet 364, 1167-1169. 10.1016/S0140-6736(04)17103-1.

Chaudhuri, K.R., Healy, D.G., Schapira, A.H., and National Institute for Clinical, E. (2006). Non-motor symptoms of Parkinson's disease: diagnosis and management. Lancet Neurol 5, 235-245. 10.1016/S1474-4422(06)70373-8.

Chen, Y., Dolt, K.S., Kriek, M., Baker, T., Downey, P., Drummond, N.J., Canham, M.A., Natalwala, A., Rosser, S., and Kunath, T. (2019). Engineering synucleinopathy-resistant human dopaminergic neurons by CRISPR-mediated deletion of the SNCA gene. Eur J Neurosci 49, 510-524. 10.1111/ejn.14286.

Ciurleo, R., Corallo, F., Bonanno, L., Lo Buono, V., Di Lorenzo, G., Versaci, R., Allone, C., Palmeri, R., Bramanti, P., and Marino, S. (2018). Assessment of Duodopa((R)) effects on quality of life of patients with advanced Parkinson's disease and their caregivers. J Neurol 265, 2005-2014. 10.1007/s00415-018-8951-3.

Cole, T.A., Zhao, H., Collier, T.J., Sandoval, I., Sortwell, C.E., Steece-Collier, K., Daley, B.F., Booms, A., Lipton, J., Welch, M., et al. (2021). alpha-Synuclein antisense oligonucleotides as a disease-modifying therapy for Parkinson's disease. JCI Insight 6. 10.1172/jci.insight.135633.

Connolly, B.S., and Lang, A.E. (2014). Pharmacological treatment of Parkinson disease: a review. JAMA 311, 1670-1683. 10.1001/jama.2014.3654.

Decressac, M., Kadkhodaei, B., Mattsson, B., Laguna, A., Perlmann, T., and Bjorklund, A. (2012a). alpha-Synuclein-induced down-regulation of Nurr1 disrupts GDNF signaling in nigral dopamine neurons. Sci Transl Med 4, 163ra156. 10.1126/scitranslmed.3004676.

Decressac, M., Mattsson, B., and Bjorklund, A. (2012b). Comparison of the behavioural and histological characteristics of the 6-OHDA and alpha-synuclein rat models of Parkinson's disease. Exp Neurol 235, 306-315. 10.1016/j.expneurol.2012.02.012.

Decressac, M., Ulusoy, A., Mattsson, B., Georgievska, B., Romero-Ramos, M., Kirik, D., and Bjorklund, A. (2011). GDNF fails to exert neuroprotection in a rat alpha-synuclein model of Parkinson's disease. Brain 134, 2302-2311. 10.1093/brain/awr149.

Devine, M.J., Ryten, M., Vodicka, P., Thomson, A.J., Burdon, T., Houlden, H., Cavaleri, F., Nagano, M., Drummond, N.J., Taanman, J.W., et al. (2011). Parkinson's disease induced pluripotent stem cells with triplication of the alpha-synuclein locus. Nat Commun 2, 440. 10.1038/ncomms1453.

Doi, D., Magotani, H., Kikuchi, T., Ikeda, M., Hiramatsu, S., Yoshida, K., Amano, N., Nomura, M., Umekage, M., Morizane, A., and Takahashi, J. (2020). Pre-clinical study of induced pluripotent stem cell-derived dopaminergic progenitor cells for Parkinson's disease. Nat Commun 11, 3369. 10.1038/s41467-020-17165-w.

Doi, D., Samata, B., Katsukawa, M., Kikuchi, T., Morizane, A., Ono, Y., Sekiguchi, K., Nakagawa, M., Parmar, M., and Takahashi, J. (2014). Isolation of human induced pluripotent stem cell-derived dopaminergic progenitors by cell sorting for successful transplantation. Stem Cell Reports 2, 337-350. 10.1016/j.stemcr.2014.01.013.

Drouin-Ouellet, J., Lau, S., Brattas, P.L., Rylander Ottosson, D., Pircs, K., Grassi, D.A., Collins, L.M., Vuono, R., Andersson Sjoland, A., Westergren-Thorsson, G., et al. (2017). REST suppression mediates neural conversion of adult human fibroblasts via microRNA-dependent and -independent pathways. EMBO Mol Med 9, 1117-1131. 10.15252/emmm.201607471.

Emborg, M.E., Liu, Y., Xi, J., Zhang, X., Yin, Y., Lu, J., Joers, V., Swanson, C., Holden, J.E., and Zhang, S.C. (2013). Induced pluripotent stem cell-derived neural cells survive and mature in the nonhuman primate brain. Cell Rep 3, 646-650. 10.1016/j.celrep.2013.02.016.

Fasano, C.A., Chambers, S.M., Lee, G., Tomishima, M.J., and Studer, L. (2010). Efficient derivation of functional floor plate tissue from human embryonic stem cells. Cell Stem Cell 6, 336-347. 10.1016/j.stem.2010.03.001.

Faustini, G., Longhena, F., Varanita, T., Bubacco, L., Pizzi, M., Missale, C., Benfenati, F., Bjorklund, A., Spano, P., and Bellucci, A. (2018). Synapsin III deficiency hampers alpha-synuclein aggregation, striatal synaptic damage and nigral cell loss in an AAV-based mouse model of Parkinson's disease. Acta Neuropathol 136, 621-639. 10.1007/s00401-018-1892-1.

Fearnley, J.M., and Lees, A.J. (1991). Ageing and Parkinson's disease: substantia nigra regional selectivity. Brain 114 (Pt 5), 2283-2301. 10.1093/brain/114.5.2283.

Fiorenzano, A., Sozzi, E., Birtele, M., Kajtez, J., Giacomoni, J., Nilsson, F., Bruzelius, A., Sharma, Y., Zhang, Y., Mattsson, B., et al. (2021). Single-cell transcriptomics captures features of human midbrain development and dopamine neuron diversity in brain organoids. Nat Commun 12, 7302. 10.1038/s41467-021-27464-5.

Fleming, A., Bourdenx, M., Fujimaki, M., Karabiyik, C., Krause, G.J., Lopez, A., Martin-Segura, A., Puri, C., Scrivo, A., Skidmore, J., et al. (2022). The different autophagy degradation pathways and neurodegeneration. Neuron 110, 935-966. 10.1016/j.neuron.2022.01.017.

Flierl, A., Oliveira, L.M., Falomir-Lockhart, L.J., Mak, S.K., Hesley, J., Soldner, F., Arndt-Jovin, D.J., Jaenisch, R., Langston, J.W., Jovin, T.M., and Schule, B. (2014). Higher vulnerability and stress sensitivity of neuronal precursor cells carrying an alpha-synuclein gene triplication. PLoS One 9, e112413. 10.1371/journal.pone.0112413.

Fuchs, J., Nilsson, C., Kachergus, J., Munz, M., Larsson, E.M., Schule, B., Langston, J.W., Middleton, F.A., Ross, O.A., Hulihan, M., et al. (2007). Phenotypic variation in a large Swedish pedigree due to SNCA duplication and triplication. Neurology 68, 916-922. 10.1212/01.wnl.0000254458.17630.c5.

Grealish, S., Diguet, E., Kirkeby, A., Mattsson, B., Heuer, A., Bramoulle, Y., Van Camp, N., Perrier, A.L., Hantraye, P., Bjorklund, A., and Parmar, M. (2014). Human ESC-derived dopamine neurons show similar preclinical efficacy and potency to fetal neurons when grafted in a rat model of Parkinson's disease. Cell Stem Cell 15, 653-665. 10.1016/j.stem.2014.09.017.

Grealish, S., Heuer, A., Cardoso, T., Kirkeby, A., Jonsson, M., Johansson, J., Bjorklund, A., Jakobsson, J., and Parmar, M. (2015). Monosynaptic Tracing using Modified Rabies Virus Reveals Early and Extensive Circuit Integration of Human Embryonic Stem Cell-Derived Neurons. Stem Cell Reports 4, 975-983. 10.1016/j.stemcr.2015.04.011.

Groiss, S.J., Wojtecki, L., Sudmeyer, M., and Schnitzler, A. (2009). Deep brain stimulation in Parkinson's disease. Ther Adv Neurol Disord 2, 20-28. 10.1177/1756285609339382.

Hagell, P., Piccini, P., Bjorklund, A., Brundin, P., Rehncrona, S., Widner, H., Crabb, L., Pavese, N., Oertel, W.H., Quinn, N., et al. (2002). Dyskinesias following neural transplantation in Parkinson's disease. Nat Neurosci 5, 627-628. 10.1038/nn863.

Hallett, P.J., Deleidi, M., Astradsson, A., Smith, G.A., Cooper, O., Osborn, T.M., Sundberg, M., Moore, M.A., Perez-Torres, E., Brownell, A.L., et al. (2015). Successful function of autologous iPSC-derived dopamine

neurons following transplantation in a non-human primate model of Parkinson's disease. Cell Stem Cell 16, 269-274. 10.1016/j.stem.2015.01.018.

Hargus, G., Cooper, O., Deleidi, M., Levy, A., Lee, K., Marlow, E., Yow, A., Soldner, F., Hockemeyer, D., Hallett, P.J., et al. (2010). Differentiated Parkinson patient-derived induced pluripotent stem cells grow in the adult rodent brain and reduce motor asymmetry in Parkinsonian rats. Proc Natl Acad Sci U S A 107, 15921-15926. 10.1073/pnas.1010209107.

Hoban, D.B., Shrigley, S., Mattsson, B., Breger, L.S., Jarl, U., Cardoso, T., Nelander Wahlestedt, J., Luk, K.C., Bjorklund, A., and Parmar, M. (2020). Impact of alpha-synuclein pathology on transplanted hESC-derived dopaminergic neurons in a humanized alpha-synuclein rat model of PD. Proc Natl Acad Sci U S A 117, 15209-15220. 10.1073/pnas.2001305117.

Huh, C.J., Zhang, B., Victor, M.B., Dahiya, S., Batista, L.F., Horvath, S., and Yoo, A.S. (2016). Maintenance of age in human neurons generated by microRNA-based neuronal conversion of fibroblasts. Elife 5. 10.7554/eLife.18648.

Jankovic, J. (2008). Parkinson's disease: clinical features and diagnosis. J Neurol Neurosurg Psychiatry 79, 368-376. 10.1136/jnnp.2007.131045.

Jiang, H., Xu, Z., Zhong, P., Ren, Y., Liang, G., Schilling, H.A., Hu, Z., Zhang, Y., Wang, X., Chen, S., et al. (2015). Cell cycle and p53 gate the direct conversion of human fibroblasts to dopaminergic neurons. Nat Commun 6, 10100. 10.1038/ncomms10100.

Kantor, B., Tagliafierro, L., Gu, J., Zamora, M.E., Ilich, E., Grenier, C., Huang, Z.Y., Murphy, S., and Chiba-Falek, O. (2018). Downregulation of SNCA Expression by Targeted Editing of DNA Methylation: A Potential Strategy for Precision Therapy in PD. Mol Ther 26, 2638-2649. 10.1016/j.ymthe.2018.08.019.

Kefalopoulou, Z., Politis, M., Piccini, P., Mencacci, N., Bhatia, K., Jahanshahi, M., Widner, H., Rehncrona, S., Brundin, P., Bjorklund, A., et al. (2014). Long-term clinical outcome of fetal cell transplantation for Parkinson disease: two case reports. JAMA Neurol 71, 83-87. 10.1001/jamaneurol.2013.4749.

Kikuchi, T., Morizane, A., Doi, D., Magotani, H., Onoe, H., Hayashi, T., Mizuma, H., Takara, S., Takahashi, R., Inoue, H., et al. (2017a). Human iPS cell-derived dopaminergic neurons function in a primate Parkinson's disease model. Nature 548, 592-596. 10.1038/nature23664.

Kikuchi, T., Morizane, A., Doi, D., Okita, K., Nakagawa, M., Yamakado, H., Inoue, H., Takahashi, R., and Takahashi, J. (2017b). Idiopathic Parkinson's disease patient-derived induced pluripotent stem cells function as midbrain dopaminergic neurons in rodent brains. J Neurosci Res 95, 1829-1837. 10.1002/jnr.24014.

Kim, Y., Zheng, X., Ansari, Z., Bunnell, M.C., Herdy, J.R., Traxler, L., Lee, H., Paquola, A.C.M., Blithikioti, C., Ku, M., et al. (2018). Mitochondrial Aging Defects Emerge in Directly Reprogrammed Human Neurons due to Their Metabolic Profile. Cell Rep 23, 2550-2558. 10.1016/j.celrep.2018.04.105.

Kirkeby, A., Grealish, S., Wolf, D.A., Nelander, J., Wood, J., Lundblad, M., Lindvall, O., and Parmar, M. (2012). Generation of regionally specified neural progenitors and functional neurons from human embryonic stem cells under defined conditions. Cell Rep 1, 703-714. 10.1016/j.celrep.2012.04.009.

Kirkeby, A., Nolbrant, S., Tiklova, K., Heuer, A., Kee, N., Cardoso, T., Ottosson, D.R., Lelos, M.J., Rifes, P., Dunnett, S.B., et al. (2017). Predictive Markers Guide Differentiation to Improve Graft Outcome in Clinical Translation of hESC-Based Therapy for Parkinson's Disease. Cell Stem Cell 20, 135-148. 10.1016/j.stem.2016.09.004.

Klein Herenbrink, C., Stoier, J.F., Reith, W.D., Dagra, A., Gregorek, M.A.C., Cola, R.B., Patriarchi, T., Li, Y., Tian, L., Gether, U., and Herborg, F. (2022). Multimodal detection of dopamine by sniffer cells expressing genetically encoded fluorescent sensors. Commun Biol 5, 578. 10.1038/s42003-022-03488-5.

Kordower, J.H., Chu, Y., Hauser, R.A., Freeman, T.B., and Olanow, C.W. (2008). Lewy body-like pathology in long-term embryonic nigral transplants in Parkinson's disease. Nat Med 14, 504-506. 10.1038/nm1747.

Kordower, J.H., Olanow, C.W., Dodiya, H.B., Chu, Y., Beach, T.G., Adler, C.H., Halliday, G.M., and Bartus, R.T. (2013). Disease duration and the integrity of the nigrostriatal system in Parkinson's disease. Brain 136, 2419-2431. 10.1093/brain/awt192.

Kriks, S., Shim, J.W., Piao, J., Ganat, Y.M., Wakeman, D.R., Xie, Z., Carrillo-Reid, L., Auyeung, G., Antonacci, C., Buch, A., et al. (2011). Dopamine neurons derived from human ES cells efficiently engraft in animal models of Parkinson's disease. Nature 480, 547-551. 10.1038/nature10648.

Kupsch, A., Schmidt, W., Gizatullina, Z., Debska-Vielhaber, G., Voges, J., Striggow, F., Panther, P., Schwegler, H., Heinze, H.J., Vielhaber, S., and Gellerich, F.N. (2014). 6-Hydroxydopamine impairs mitochondrial function in the rat model of Parkinson's disease: respirometric, histological, and behavioral analyses. J Neural Transm (Vienna) 121, 1245-1257. 10.1007/s00702-014-1185-3.

Li, J.Y., Englund, E., Holton, J.L., Soulet, D., Hagell, P., Lees, A.J., Lashley, T., Quinn, N.P., Rehncrona, S., Bjorklund, A., et al. (2008). Lewy bodies in grafted neurons in subjects with Parkinson's disease suggest host-to-graft disease propagation. Nat Med 14, 501-503. 10.1038/nm1746.

Li, J.Y., Englund, E., Widner, H., Rehncrona, S., Bjorklund, A., Lindvall, O., and Brundin, P. (2010). Characterization of Lewy body pathology in 12- and 16-year-old intrastriatal mesencephalic grafts surviving in a patient with Parkinson's disease. Mov Disord 25, 1091-1096. 10.1002/mds.23012.

Li, W., Englund, E., Widner, H., Mattsson, B., van Westen, D., Latt, J., Rehncrona, S., Brundin, P., Bjorklund, A., Lindvall, O., and Li, J.Y. (2016). Extensive graft-derived dopaminergic innervation is maintained 24 years after transplantation in the degenerating parkinsonian brain. Proc Natl Acad Sci U S A 113, 6544-6549. 10.1073/pnas.1605245113.

Liu, X., Li, F., Stubblefield, E.A., Blanchard, B., Richards, T.L., Larson, G.A., He, Y., Huang, Q., Tan, A.C., Zhang, D., et al. (2012). Direct reprogramming of human fibroblasts into dopaminergic neuron-like cells. Cell Res 22, 321-332. 10.1038/cr.2011.181.

Luk, K.C., Covell, D.J., Kehm, V.M., Zhang, B., Song, I.Y., Byrne, M.D., Pitkin, R.M., Decker, S.C., Trojanowski, J.Q., and Lee, V.M. (2016). Molecular and Biological Compatibility with Host Alpha-Synuclein Influences Fibril Pathogenicity. Cell Rep 16, 3373-3387. 10.1016/j.celrep.2016.08.053.

Luk, K.C., Kehm, V., Carroll, J., Zhang, B., O'Brien, P., Trojanowski, J.Q., and Lee, V.M. (2012). Pathological alpha-synuclein transmission initiates Parkinson-like neurodegeneration in nontransgenic mice. Science 338, 949-953. 10.1126/science.1227157.

Luk, K.C., Song, C., O'Brien, P., Stieber, A., Branch, J.R., Brunden, K.R., Trojanowski, J.Q., and Lee, V.M. (2009). Exogenous alpha-synuclein fibrils seed the formation of Lewy body-like intracellular inclusions in cultured cells. Proc Natl Acad Sci U S A 106, 20051-20056. 10.1073/pnas.0908005106.

Lundblad, M., Decressac, M., Mattsson, B., and Bjorklund, A. (2012). Impaired neurotransmission caused by overexpression of alpha-synuclein in nigral dopamine neurons. Proc Natl Acad Sci U S A 109, 3213-3219. 10.1073/pnas.1200575109.

Ma, Y., Tang, C., Chaly, T., Greene, P., Breeze, R., Fahn, S., Freed, C., Dhawan, V., and Eidelberg, D. (2010). Dopamine cell implantation in Parkinson's disease: long-term clinical and (18)F-FDOPA PET outcomes. J Nucl Med 51, 7-15. 10.2967/jnumed.109.066811.

Mah, L.J., El-Osta, A., and Karagiannis, T.C. (2010). gammaH2AX: a sensitive molecular marker of DNA damage and repair. Leukemia 24, 679-686. 10.1038/leu.2010.6.

Marion, R.M., Strati, K., Li, H., Tejera, A., Schoeftner, S., Ortega, S., Serrano, M., and Blasco, M.A. (2009). Telomeres acquire embryonic stem cell characteristics in induced pluripotent stem cells. Cell Stem Cell 4, 141-154. 10.1016/j.stem.2008.12.010.

Marques, S., Zeisel, A., Codeluppi, S., van Bruggen, D., Mendanha Falcao, A., Xiao, L., Li, H., Haring, M., Hochgerner, H., Romanov, R.A., et al. (2016). Oligodendrocyte heterogeneity in the mouse juvenile and adult central nervous system. Science 352, 1326-1329. 10.1126/science.aaf6463.

Mehanna, R., Moore, S., Hou, J.G., Sarwar, A.I., and Lai, E.C. (2014). Comparing clinical features of young onset, middle onset and late onset Parkinson's disease. Parkinsonism Relat Disord 20, 530-534. 10.1016/j.parkreldis.2014.02.013.

Mertens, J., Paquola, A.C.M., Ku, M., Hatch, E., Bohnke, L., Ladjevardi, S., McGrath, S., Campbell, B., Lee, H., Herdy, J.R., et al. (2015). Directly Reprogrammed Human Neurons Retain Aging-Associated Transcriptomic Signatures and Reveal Age-Related Nucleocytoplasmic Defects. Cell Stem Cell 17, 705-718. 10.1016/j.stem.2015.09.001.

Mohamed, N.V., Sirois, J., Ramamurthy, J., Mathur, M., Lepine, P., Deneault, E., Maussion, G., Nicouleau, M., Chen, C.X., Abdian, N., et al. (2021). Midbrain organoids with an SNCA gene triplication model key features of synucleinopathy. Brain Commun 3, fcab223. 10.1093/braincomms/fcab223.

Morizane, A., Doi, D., Kikuchi, T., Okita, K., Hotta, A., Kawasaki, T., Hayashi, T., Onoe, H., Shiina, T., Yamanaka, S., and Takahashi, J. (2013). Direct comparison of autologous and allogeneic transplantation of iPSC-derived neural cells in the brain of a non-human primate. Stem Cell Reports 1, 283-292. 10.1016/j.stemcr.2013.08.007.

Morizane, A., Kikuchi, T., Hayashi, T., Mizuma, H., Takara, S., Doi, H., Mawatari, A., Glasser, M.F., Shiina, T., Ishigaki, H., et al. (2017). MHC matching improves engraftment of iPSC-derived neurons in non-human primates. Nat Commun 8, 385. 10.1038/s41467-017-00926-5.

Morizane, A., and Takahashi, J. (2021). Evading the Immune System: Immune Modulation and Immune Matching in Cell Replacement Therapies for Parkinson's Disease. J Parkinsons Dis 11, S167-S172. 10.3233/JPD-212608.

Nakatsuji, N., Nakajima, F., and Tokunaga, K. (2008). HLA-haplotype banking and iPS cells. Nat Biotechnol 26, 739-740. 10.1038/nbt0708-739.

Negrini, M., Tomasello, G., Davidsson, M., Fenyi, A., Adant, C., Hauser, S., Espa, E., Gubinelli, F., Manfredsson, F.P., Melki, R., and Heuer, A. (2022). Sequential or Simultaneous Injection of Preformed Fibrils and AAV Overexpression of Alpha-Synuclein Are Equipotent in Producing Relevant Pathology and Behavioral Deficits. J Parkinsons Dis 12, 1133-1153. 10.3233/JPD-212555.

Nguyen, H.N., Byers, B., Cord, B., Shcheglovitov, A., Byrne, J., Gujar, P., Kee, K., Schule, B., Dolmetsch, R.E., Langston, W., et al. (2011). LRRK2 mutant iPSC-derived DA neurons demonstrate increased susceptibility to oxidative stress. Cell Stem Cell 8, 267-280. 10.1016/j.stem.2011.01.013.

Nolbrant, S., Heuer, A., Parmar, M., and Kirkeby, A. (2017). Generation of high-purity human ventral midbrain dopaminergic progenitors for in vitro maturation and intracerebral transplantation. Nat Protoc 12, 1962-1979. 10.1038/nprot.2017.078.

Nyholm, D. (2012). Duodopa(R) treatment for advanced Parkinson's disease: a review of efficacy and safety. Parkinsonism Relat Disord 18, 916-929. 10.1016/j.parkreldis.2012.06.022.

Oh, Y. (2019). Patient-specific pluripotent stem cell-based Parkinson's disease models showing endogenous alpha-synuclein aggregation. BMB Rep 52, 349-359. 10.5483/BMBRep.2019.52.6.142.

Ono, Y., Nakatani, T., Sakamoto, Y., Mizuhara, E., Minaki, Y., Kumai, M., Hamaguchi, A., Nishimura, M., Inoue, Y., Hayashi, H., et al. (2007). Differences in neurogenic potential in floor plate cells along an anteroposterior location: midbrain dopaminergic neurons originate from mesencephalic floor plate cells. Development 134, 3213-3225. 10.1242/dev.02879.

Pang, Z.P., Yang, N., Vierbuchen, T., Ostermeier, A., Fuentes, D.R., Yang, T.Q., Citri, A., Sebastiano, V., Marro, S., Sudhof, T.C., and Wernig, M. (2011). Induction of human neuronal cells by defined transcription factors. Nature 476, 220-223. 10.1038/nature10202.

Park, C.H., Minn, Y.K., Lee, J.Y., Choi, D.H., Chang, M.Y., Shim, J.W., Ko, J.Y., Koh, H.C., Kang, M.J., Kang, J.S., et al. (2005). In vitro and in vivo analyses of human embryonic stem cell-derived dopamine neurons. J Neurochem 92, 1265-1276. 10.1111/j.1471-4159.2004.03006.x.

Perrier, A.L., Tabar, V., Barberi, T., Rubio, M.E., Bruses, J., Topf, N., Harrison, N.L., and Studer, L. (2004). Derivation of midbrain dopamine neurons from human embryonic stem cells. Proc Natl Acad Sci U S A 101, 12543-12548. 10.1073/pnas.0404700101.

Pfisterer, U., Kirkeby, A., Torper, O., Wood, J., Nelander, J., Dufour, A., Bjorklund, A., Lindvall, O., Jakobsson, J., and Parmar, M. (2011). Direct conversion of human fibroblasts to dopaminergic neurons. Proc Natl Acad Sci U S A 108, 10343-10348. 10.1073/pnas.1105135108.

Piao, J., Zabierowski, S., Dubose, B.N., Hill, E.J., Navare, M., Claros, N., Rosen, S., Ramnarine, K., Horn, C., Fredrickson, C., et al. (2021). Preclinical Efficacy and Safety of a Human Embryonic Stem Cell-Derived Midbrain Dopamine Progenitor Product, MSK-DA01. Cell Stem Cell 28, 217-229 e217. 10.1016/j.stem.2021.01.004.

Piccini, P., Pavese, N., Hagell, P., Reimer, J., Bjorklund, A., Oertel, W.H., Quinn, N.P., Brooks, D.J., and Lindvall, O. (2005). Factors affecting the clinical outcome after neural transplantation in Parkinson's disease. Brain 128, 2977-2986. 10.1093/brain/awh649.

Politis, M., Wu, K., Loane, C., Quinn, N.P., Brooks, D.J., Rehncrona, S., Bjorklund, A., Lindvall, O., and Piccini, P. (2010). Serotonergic neurons mediate dyskinesia side effects in Parkinson's patients with neural transplants. Sci Transl Med 2, 38ra46. 10.1126/scitranslmed.3000976.

Polymeropoulos, M.H., Lavedan, C., Leroy, E., Ide, S.E., Dehejia, A., Dutra, A., Pike, B., Root, H., Rubenstein, J., Boyer, R., et al. (1997). Mutation in the alpha-synuclein gene identified in families with Parkinson's disease. Science 276, 2045-2047. 10.1126/science.276.5321.2045.

Robinton, D.A., and Daley, G.Q. (2012). The promise of induced pluripotent stem cells in research and therapy. Nature 481, 295-305. 10.1038/nature10761.

Rossi, M., Bruno, V., Arena, J., Cammarota, A., and Merello, M. (2018). Challenges in PD Patient Management After DBS: A Pragmatic Review. Mov Disord Clin Pract 5, 246-254. 10.1002/mdc3.12592.

Rotman, A., and Creveling, C.R. (1976). A rationale for the design of cell-specific toxic agents: the mechanism of action of 6-hydroxydopamine. FEBS Lett 72, 227-230. 10.1016/0014-5793(76)80974-x.

Roy, N.S., Cleren, C., Singh, S.K., Yang, L., Beal, M.F., and Goldman, S.A. (2006). Functional engraftment of human ES cell-derived dopaminergic neurons enriched by coculture with telomerase-immortalized midbrain astrocytes. Nat Med 12, 1259-1268. 10.1038/nm1495.

Rubinsztein, D.C., Marino, G., and Kroemer, G. (2011). Autophagy and aging. Cell 146, 682-695. 10.1016/j.cell.2011.07.030.

Schrag, A., and Schott, J.M. (2006). Epidemiological, clinical, and genetic characteristics of early-onset parkinsonism. Lancet Neurol 5, 355-363. 10.1016/S1474-4422(06)70411-2.

Schweitzer, J.S., Song, B., Herrington, T.M., Park, T.Y., Lee, N., Ko, S., Jeon, J., Cha, Y., Kim, K., Li, Q., et al. (2020). Personalized iPSC-Derived Dopamine Progenitor Cells for Parkinson's Disease. N Engl J Med 382, 1926-1932. 10.1056/NEJMoa1915872.

Sedelnikova, O.A., Horikawa, I., Zimonjic, D.B., Popescu, N.C., Bonner, W.M., and Barrett, J.C. (2004). Senescing human cells and ageing mice accumulate DNA lesions with unrepairable double-strand breaks. Nat Cell Biol 6, 168-170. 10.1038/ncb1095.

Sharma, M., and Burre, J. (2023). alpha-Synuclein in synaptic function and dysfunction. Trends Neurosci 46, 153-166. 10.1016/j.tins.2022.11.007.

Shrigley, S., Nilsson, F., Mattsson, B., Fiorenzano, A., Mudannayake, J., Bruzelius, A., Ottosson, D.R., Bjorklund, A., Hoban, D.B., and Parmar, M. (2021). Grafts Derived from an alpha-Synuclein Triplication Patient Mediate Functional Recovery but Develop Disease-Associated Pathology in the 6-OHDA Model of Parkinson's Disease. J Parkinsons Dis 11, 515-528. 10.3233/JPD-202366.

Shrigley, S., Pircs, K., Barker, R.A., Parmar, M., and Drouin-Ouellet, J. (2018). Simple Generation of a High Yield Culture of Induced Neurons from Human Adult Skin Fibroblasts. J Vis Exp. 10.3791/56904.

Singleton, A.B., Farrer, M., Johnson, J., Singleton, A., Hague, S., Kachergus, J., Hulihan, M., Peuralinna, T., Dutra, A., Nussbaum, R., et al. (2003). alpha-Synuclein locus triplication causes Parkinson's disease. Science 302, 841. 10.1126/science.1090278.

Soldner, F., Hockemeyer, D., Beard, C., Gao, Q., Bell, G.W., Cook, E.G., Hargus, G., Blak, A., Cooper, O., Mitalipova, M., et al. (2009). Parkinson's disease patient-derived induced pluripotent stem cells free of viral reprogramming factors. Cell 136, 964-977. 10.1016/j.cell.2009.02.013.

Song, B., Cha, Y., Ko, S., Jeon, J., Lee, N., Seo, H., Park, K.J., Lee, I.H., Lopes, C., Feitosa, M., et al. (2020). Human autologous iPSC-derived dopaminergic progenitors restore motor function in Parkinson's disease models. J Clin Invest 130, 904-920. 10.1172/JCI130767.

Sonntag, K.C., Pruszak, J., Yoshizaki, T., van Arensbergen, J., Sanchez-Pernaute, R., and Isacson, O. (2007). Enhanced yield of neuroepithelial precursors and midbrain-like dopaminergic neurons from human embryonic stem cells using the bone morphogenic protein antagonist noggin. Stem Cells 25, 411-418. 10.1634/stemcells.2006-0380.

Sozzi, E., Nilsson, F., Kajtez, J., Parmar, M., and Fiorenzano, A. (2022). Generation of Human Ventral Midbrain Organoids Derived from Pluripotent Stem Cells. Curr Protoc 2, e555. 10.1002/cpz1.555.

Spillantini, M.G., Crowther, R.A., Jakes, R., Hasegawa, M., and Goedert, M. (1998). alpha-Synuclein in filamentous inclusions of Lewy bodies from Parkinson's disease and dementia with lewy bodies. Proc Natl Acad Sci U S A 95, 6469-6473. 10.1073/pnas.95.11.6469.

Spillantini, M.G., Schmidt, M.L., Lee, V.M., Trojanowski, J.Q., Jakes, R., and Goedert, M. (1997). Alpha-synuclein in Lewy bodies. Nature 388, 839-840. 10.1038/42166.

Sposito, T., Preza, E., Mahoney, C.J., Seto-Salvia, N., Ryan, N.S., Morris, H.R., Arber, C., Devine, M.J., Houlden, H., Warner, T.T., et al. (2015). Developmental regulation of tau splicing is disrupted in stem cell-derived neurons from frontotemporal dementia patients with the 10 + 16 splice-site mutation in MAPT. Hum Mol Genet 24, 5260-5269. 10.1093/hmg/ddv246.

Suhr, S.T., Chang, E.A., Tjong, J., Alcasid, N., Perkins, G.A., Goissis, M.D., Ellisman, M.H., Perez, G.I., and Cibelli, J.B. (2010). Mitochondrial rejuvenation after induced pluripotency. PLoS One 5, e14095. 10.1371/journal.pone.0014095.

Sulzer, D., Chen, T.K., Lau, Y.Y., Kristensen, H., Rayport, S., and Ewing, A. (1995). Amphetamine redistributes dopamine from synaptic vesicles to the cytosol and promotes reverse transport. J Neurosci 15, 4102-4108. 10.1523/JNEUROSCI.15-05-04102.1995.

Takahashi, J. (2020). iPS cell-based therapy for Parkinson's disease: A Kyoto trial. Regen Ther 13, 18-22. 10.1016/j.reth.2020.06.002.

Takahashi, K., Tanabe, K., Ohnuki, M., Narita, M., Ichisaka, T., Tomoda, K., and Yamanaka, S. (2007). Induction of pluripotent stem cells from adult human fibroblasts by defined factors. Cell 131, 861-872. 10.1016/j.cell.2007.11.019.

Takahashi, K., and Yamanaka, S. (2006). Induction of pluripotent stem cells from mouse embryonic and adult fibroblast cultures by defined factors. Cell 126, 663-676. 10.1016/j.cell.2006.07.024.

Tang, Y., Liu, M.L., Zang, T., and Zhang, C.L. (2017). Direct Reprogramming Rather than iPSC-Based Reprogramming Maintains Aging Hallmarks in Human Motor Neurons. Front Mol Neurosci 10, 359. 10.3389/fnmol.2017.00359.

Tao, Y., Vermilyea, S.C., Zammit, M., Lu, J., Olsen, M., Metzger, J.M., Yao, L., Chen, Y., Phillips, S., Holden, J.E., et al. (2021). Autologous transplant therapy alleviates motor and depressive behaviors in parkinsonian monkeys. Nat Med 27, 632-639. 10.1038/s41591-021-01257-1.

Taylor, C.J., Peacock, S., Chaudhry, A.N., Bradley, J.A., and Bolton, E.M. (2012). Generating an iPSC bank for HLA-matched tissue transplantation based on known donor and recipient HLA types. Cell Stem Cell 11, 147-152. 10.1016/j.stem.2012.07.014.

Thakur, P., Breger, L.S., Lundblad, M., Wan, O.W., Mattsson, B., Luk, K.C., Lee, V.M.Y., Trojanowski, J.Q., and Bjorklund, A. (2017). Modeling Parkinson's disease pathology by combination of fibril seeds and alpha-synuclein overexpression in the rat brain. Proc Natl Acad Sci U S A 114, E8284-E8293. 10.1073/pnas.1710442114.

Thanvi, B.R., and Lo, T.C. (2004). Long term motor complications of levodopa: clinical features, mechanisms, and management strategies. Postgrad Med J 80, 452-458. 10.1136/pgmj.2003.013912.

Thomson, J.A., Itskovitz-Eldor, J., Shapiro, S.S., Waknitz, M.A., Swiergiel, J.J., Marshall, V.S., and Jones, J.M. (1998). Embryonic stem cell lines derived from human blastocysts. Science 282, 1145-1147. 10.1126/science.282.5391.1145.

Tiklova, K., Nolbrant, S., Fiorenzano, A., Bjorklund, A.K., Sharma, Y., Heuer, A., Gillberg, L., Hoban, D.B., Cardoso, T., Adler, A.F., et al. (2020). Single cell transcriptomics identifies stem cell-derived graft composition in a model of Parkinson's disease. Nat Commun 11, 2434. 10.1038/s41467-020-16225-5.

Tye, K.M., Mirzabekov, J.J., Warden, M.R., Ferenczi, E.A., Tsai, H.C., Finkelstein, J., Kim, S.Y., Adhikari, A., Thompson, K.R., Andalman, A.S., et al. (2013). Dopamine neurons modulate neural encoding and expression of depression-related behaviour. Nature 493, 537-541. 10.1038/nature11740.

Ungerstedt, U. (1968). 6-Hydroxy-dopamine induced degeneration of central monoamine neurons. Eur J Pharmacol 5, 107-110. 10.1016/0014-2999(68)90164-7.

Ungerstedt, U., and Arbuthnott, G.W. (1970). Quantitative recording of rotational behavior in rats after 6-hydroxy-dopamine lesions of the nigrostriatal dopamine system. Brain Res 24, 485-493. 10.1016/0006-8993(70)90187-3.

Van der Perren, A., Toelen, J., Casteels, C., Macchi, F., Van Rompuy, A.S., Sarre, S., Casadei, N., Nuber, S., Himmelreich, U., Osorio Garcia, M.I., et al. (2015). Longitudinal follow-up and characterization of a robust rat model for Parkinson's disease based on overexpression of alpha-synuclein with adeno-associated viral vectors. Neurobiol Aging 36, 1543-1558. 10.1016/j.neurobiolaging.2014.11.015.

Vera, E., and Studer, L. (2015). When rejuvenation is a problem: challenges of modeling late-onset neurodegenerative disease. Development 142, 3085-3089. 10.1242/dev.120667.

Vierbuchen, T., Ostermeier, A., Pang, Z.P., Kokubu, Y., Sudhof, T.C., and Wernig, M. (2010). Direct conversion of fibroblasts to functional neurons by defined factors. Nature 463, 1035-1041. 10.1038/nature08797.

Volpicelli-Daley, L.A., Luk, K.C., and Lee, V.M. (2014). Addition of exogenous alpha-synuclein preformed fibrils to primary neuronal cultures to seed recruitment of endogenous alpha-synuclein to Lewy body and Lewy neurite-like aggregates. Nat Protoc 9, 2135-2146. 10.1038/nprot.2014.143.

Volpicelli-Daley, L.A., Luk, K.C., Patel, T.P., Tanik, S.A., Riddle, D.M., Stieber, A., Meaney, D.F., Trojanowski, J.Q., and Lee, V.M. (2011). Exogenous alpha-synuclein fibrils induce Lewy body pathology leading to synaptic dysfunction and neuron death. Neuron 72, 57-71. 10.1016/j.neuron.2011.08.033.

Xiong, M., Tao, Y., Gao, Q., Feng, B., Yan, W., Zhou, Y., Kotsonis, T.A., Yuan, T., You, Z., Wu, Z., et al. (2021). Human Stem Cell-Derived Neurons Repair Circuits and Restore Neural Function. Cell Stem Cell 28, 112-126 e116. 10.1016/j.stem.2020.08.014.

Zeng, X., Cai, J., Chen, J., Luo, Y., You, Z.B., Fotter, E., Wang, Y., Harvey, B., Miura, T., Backman, C., et al. (2004). Dopaminergic differentiation of human embryonic stem cells. Stem Cells 22, 925-940. 10.1634/stemcells.22-6-925.

Zimmermann, A., Preynat-Seauve, O., Tiercy, J.M., Krause, K.H., and Villard, J. (2012). Haplotype-based banking of human pluripotent stem cells for transplantation: potential and limitations. Stem Cells Dev 21, 2364-2373. 10.1089/scd.2012.0088.

Zufferey, R., Nagy, D., Mandel, R.J., Naldini, L., and Trono, D. (1997). Multiply attenuated lentiviral vector achieves efficient gene delivery in vivo. Nat Biotechnol 15, 871-875. 10.1038/nbt0997-871.

ACKNOWLEDGEMENTS

First and foremost, I would like to thank my supervisor **Malin** for giving me the opportunity to do a PhD in "the most respected lab in the world". These years have been incredibly fun and rewarding. I could not have asked for a better PI and a better group.

I would also like to extend my sincere thanks to my co-supervisors, **Dee** and **Johan**, for your valuable contributions to my research projects and always being there for me. Also, I would like to thank **Anders** for all the interesting and helpful discussions and microscope sessions.

To all the past and current members of the Parmar group, thank you all for making these years absolutely fantastic. To **Ulla, Bengt** and **Micke**: your help these years have been tremendously appreciated and I cannot thank you enough. To **Alessandro, Janko, Petter, Edo, Jessica, Jenny, Yogita, Sara C & Mette**: I could not have asked for better colleagues. Thank you for all the jokes and memories. To the newer members of the Parmar group, **Malin Å, Kerstin, Maria G & Jana**: it has been a pleasure getting to know you and best of luck in the future. To **Paulina**: thank you so much for all the help these years that have made my life so much easier. **Marie PV, Sol, Jenny J & Anna H**: your help has been invaluable and I am very grateful for all your assistance. I would also like to thank all the past members of the Parmar Lab that I have had the pleasure to meet over the years: **Sara N, Tiago, Andrew, Marcella, Yu, Olof, Janitha, Janelle** and **Shelby**.

I want to thank **Andreas, Efrain and Daniella** from the Daniella Ottosson group that have helped us with their expertise throughout the years. I also want to thank **Karolina P**, the Johan Jakobsson group, the Anna Falk group, the Cecilia Lundberg group and the Christopher Douse group. I want to thank **Raquel** and **Ofelia** for being such great office companions. A big thank you to everyone on A11, A10 and B10 that has made this place a fantastic and fun workplace. A special thank you to my padel compadres **Janko, Petter, Martino, Edo, Andreas E** and **Gunnar Gunnarsson**.

Lastly, I would like to thank my family for their continuous and invaluable support throughout these years.

PAPER I

cells

MDPI

Article

Single-Cell Profiling of Coding and Noncoding Genes in Human Dopamine Neuron Differentiation

Fredrik Nilsson, Petter Storm, Edoardo Sozzi, David Hidalgo Gil, Marcella Birtele, Yogita Sharma, Malin Parmar * and Alessandro Fiorenzano *

Developmental and Regenerative Neurobiology, Wallenberg Neuroscience Center, Lund Stem Cell Centre, Department of Experimental Medical Science, Lund University, 22184 Lund, Sweden; fredrik.nilsson.5372@med.lu.se (F.N.); petter.storm@med.lu.se (P.S.); edoardo.sozzi@med.lu.se (E.S.); da4206hi-s@student.lu.se (D.H.G.); marcella.birtele@med.lu.se (M.B.); yogita.sharma@med.lu.se (Y.S.)

* Correspondence: malin.parmar@med.lu.se (M.P.); alessandro.fiorenzano@med.lu.se (A.F.); Tel.: +46-46-222-0620 (M.P.); +46-46-222-0549 (A.F.)

Abstract: Dopaminergic (DA) neurons derived from human pluripotent stem cells (hPSCs) represent a renewable and available source of cells useful for understanding development, developing disease models, and stem-cell therapies for Parkinson's disease (PD). To assess the utility of stem cell cultures as an in vitro model system of human DA neurogenesis, we performed high-throughput transcriptional profiling of ~20,000 ventral midbrain (VM)-patterned stem cells at different stages of maturation using droplet-based single-cell RNA sequencing (scRNAseq). Using this dataset, we defined the cellular composition of human VM cultures at different timepoints and found high purity DA progenitor formation at an early stage of differentiation. DA neurons sharing similar molecular identities to those found in authentic DA neurons derived from human fetal VM were the major cell type after two months in culture. We also developed a bioinformatic pipeline that provided a comprehensive long noncoding RNA landscape based on temporal and cell-type specificity, which may contribute to unraveling the intricate regulatory network of coding and noncoding genes in DA neuron differentiation. Our findings serve as a valuable resource to elucidate the molecular steps of development, maturation, and function of human DA neurons, and to identify novel candidate coding and noncoding genes driving specification of progenitors into functionally mature DA neurons.

Keywords: human pluripotent stem cells; dopamine neuron differentiation; single-cell RNA sequencing

Citation: Nilsson, F.; Storm, P.; Sozzi, E.; Hidalgo Gil, D.; Birtele, M.; Sharma, Y.; Parmar, M.; Fiorenzano, A. Single-Cell Profiling of Coding and Noncoding Genes in Human Dopamine Neuron Differentiation. *Cells* **2021**, *10*, 137. https://doi.org/10.3390/cells10010137

Received: 17 December 2020
Accepted: 9 January 2021
Published: 12 January 2021

1. Introduction

Dopaminergic (DA) neurons in the ventral midbrain (VM) are essential for controlling key functions such as control of voluntary movement, reward processing, and working memory. Dysfunction of DA neurons in the ventral tegmental area (VTA), which projects into corticolimbic structures, is associated with the development of neuropsychiatric disorders, drug addiction, and depression while degeneration of DA neurons in the substantia nigra compacta (SNc) is the main pathology in Parkinson's disease (PD). Over the last three decades, scientific endeavors have focused on designing a novel cell-based therapy for PD via replacement of lost cells with new healthy DA neurons [1]. Major efforts have thus focused on generating ventral midbrain DA neurons from human pluripotent stem cells (hPSCs) for use in disease models and diagnostics [2] as well as in cell-based therapies for PD [3,4]. It is now possible to obtain mature and functional DA neurons from hPSCs for disease modeling and therapeutics [5–7], and these 2D culture systems could potentially also be used as stem cell models of human VM DA neurogenesis.

We previously reported a standardized differentiation approach based on floor-plate transition with the addition of dual-SMAD inhibition (Noggin and SB431542) combined with i) sonic hedgehog (SHH) to induce differentiation into ventral neural fates and ii) glycogen synthase kinase 3 inhibitor (GSK3i) to progressively pattern hPSCs toward a

caudal VM progenitor phenotype [8]. Our protocol also included the timed delivery of fibroblast growth factor 8b (FGF8b) to drive a more fine-tuned control of rostro-caudal patterning of VM progenitors, which subsequently gave rise to mature DA neurons [9,10].

In this study, we assessed the potential of long-term in vitro differentiation as a stem-cell model of human DA neuron specification and maturation. We used 10× single-cell RNA sequencing (scRNAseq) to perform high-throughput transcriptional profiling of a large number of hPSCs (19,841) at different developmental stages of VM patterning and differentiation. To better dissect the DA developmental program, we examined the cellular composition of VM-patterned stem-cell cultures at the progenitor state, and after one and two months, when functionally mature DA neurons have been formed. Based on single-cell data obtained at different timepoints of DAgenesis, we reconstructed developmental trajectories able to deduce the origin and timing of cell type appearance during VM differentiation. The advent of single-cell resolution technologies has brought unprecedented insights into the complexity and diversity of cell types during brain development [11,12]. However, most scRNAseq studies of neural differentiation currently focus on coding genes, failing to consider the vast amount of noncoding RNA. Long noncoding RNAs (lncRNAs) are a class of noncoding transcripts longer than 200 nucleotides that have emerged as key transcriptional and posttranscriptional regulators acting at multiple levels of gene expression [13–16]. We therefore developed a bioinformatic pipeline for profiling the expression of lncRNA and obtained a single-cell landscape of these noncoding genes during DA differentiation in the 10× Genomics dataset by mapping their temporal and cell-type-specific expression.

Together, our findings constitute a valuable resource that may help identify both candidate lncRNAs and coding genes involved in regulatory mechanisms during DA neurogenesis. This single-cell dataset will serve as a powerful tool to elucidate human DA neuron development, maturation, and function, and will contribute to establishing more refined DA differentiation protocols.

2. Materials and Methods

2.1. hPSC Culture and 2D Differentiation

Undifferentiated RC17 (Roslin Cells, #hPSCreg RCe021-A) were maintained on 0.5 μg/cm^2 Lam-521 (BioLamina, #LN-521)-coated plates in iPS Brew 4 medium (Miltenyi, #130-104-368) until the start of differentiation. They were passaged with 0.5mM EDTA (ethylenediaminetetraacetic acid) roughly every 7 days (with 10μM Y-27632 and seeding density 2500 cells/cm^2) or when becoming confluent. The cells were differentiated into 2D VM-patterned progenitors using our good manufacturing practice (GMP)-grade protocol [9]. On day 0 of the differentiation the cells were detached with EDTA and seeded (10,000 cells/cm^2) onto Lam-111 (BioLamina, #LN-111)-coated plates (1 μg/cm^2) in N2 medium with SB431542 (10 μM), Noggin (100 ng/mL), Shh-C24II (300 ng/mL), CHIR99021 (0.9 μM), and Y-27632 (10 μM). Media was changed on days 2, 4, 7. On day 9 the media was changed to either N2 medium with FGF8b (fibroblast growth factor 8b, 100 ng/mL) or solely N2 medium. The cells were detached with accutase on day 11 and replated (800,000 cells/cm^2) on Lam-111-coated plates (1 μg/cm^2) in B27 medium with BDNF (brain-derived neurotrophic factor, 20 ng/mL), AA (ascorbic acid, 0.2 mM), and Y-27632 (10 μM), either with or without FGF8b (100 ng/mL). Media was changed on day 14. On day 16 the cells were either taken for analysis or replated for terminal differentiation. For long-term culture the cells were detached with accutase and replated at a lower density (155,000 cells/cm^2) on Lam-111-coated plates in B27 medium with BDNF (20 ng/mL), AA (0.2 mM), GDNF (glial cell line-derived neurotrophic factor, 10 ng/mL) + db-cAMP (dibutyryl cyclic adenosine monophosphate, 500 μM), DAPT (notch inhibitor, 1 μM), and Y-27632 (10 μM). Media was changed every 2–3 days until the end of the experiment. For the long-term cultures the cells were plated on Lam-111 with double concentration (2 μg/cm^2) and after day 25 only 50–75% of the media was changed in order to minimize the risk of detachment.

2.2. scRNA-Seq Analysis

Cell suspensions were loaded into a 10× Genomics Chromium Single Cell System (10× Genomics) and libraries were generated using version 3 chemistry according to the manufacturer's instructions. Libraries were sequenced on Illumina NextSeq500 (400 million reads flow cells) using the recommended read length. Sequencing data was first pre-processed through the Cell Ranger pipeline (10× Genomics, Cellranger count v2) with default parameters (expect-cells set to number of cells added to 10× system), aligned to GrCH38 (v3.1.0) and resulting matrix files were used for subsequent bioinformatic analysis. Seurat (version 3.1.1 and R version 3.6.1, R, Vienna, Austria) was utilized for downstream analysis. Batch effects were removed using the Harmony algorithm (1.0), treating individual 10× runs as a batch. Cells with at least 200 detected genes were retained and the data was normalized to transcript copies per 10,000, and log-normalized to reduce sequencing depth variability. For visualization and clustering, manifolds were calculated using UMAP methods (RunUMAP, Seurat) on 20 precomputed principal components. Clusters were identified by calculating a shared-neighbor graph and then defined (FindClusters, Seurat) with a resolution of 0.2. Identification of differentially expressed genes between clusters was carried out using the default Wilcoxon rank sum test (Seurat). For pseudotime and trajectory analysis Slingshot (1.4) was adopted. For comparison with fetal data Seurats LabelTransfer was used with fetal data as reference object projected the PCA structure onto the data.

2.3. LncRNA Quantification

Cell populations identified on the basis of protein-coding genes were used to quantify lncRNA from each cell type across three time points. The expression of lncRNAs was analyzed by extracting cell barcodes for all clusters using Seurat function WhichCells and the original .bam files obtained from the Cellranger pipeline were used to subset aligned files for each cluster (subset-bam tool provided by 10×. Each cluster-specific .bam file was then used as input to count LncRNA expression using FeatureCounts (forward strand). The LncRNA annotation file was downloaded from Gencode (release 36, assembly GRCh38). Differential lncRNA expression analysis was performed using DeSeq2 for both cell types (DA neuron and floor-plate progenitors (FP)) and time points (days 16 and 60) as design (p adj < 0.01). This tool creates a general linear model, assuming a negative binomial distribution. LncRNA that overlapped within a 5kb distance to a protein-coding gene were defined as intragenic. Nearby correlation analysis was performed computing Pearson correlation coefficient using change in protein coding gene expression and lncRNA expression. All data visualization was performed using tidyverse (V1.3), ggplot2 (V3.3.0), and genomic ranges (V1.40.0) running on R (V. 4.0).

2.4. qRT-PCR

Total RNAs were isolated on day of analysis using the RNeasy Micro Kit (QIAGEN#74004) according to manufacturer instructions. Approximately 1 μg of RNA was reverse transcribed using Maxima First Strand cDNA Synthesis Kit (Thermo Fisher 2#K1642In vitrogen). cDNA was prepared together with SYBR Green Master mix (Roche#04887352001) using the Bravo instrument (Agilent) and analyzed by quantitative PCR on a LightCycler 480 II instrument (Roche) using a 2-step protocol with a 95 °C, 0.5 min denaturation step followed by a 60 °C, 1 min annealing/elongation step for 40 cycles in total. All quantitative RT-PCR (qRT-PCR) samples were run in technical triplicates, analyzed with the ΔΔCt-method, normalized against the two housekeeping genes ACTB (actin-beta) and GAPDH (glyceraldehyde-3-phosphate dehydrogenase) and results are given as a fold change of expression over undifferentiated hPSCs. Details and list of primers are reported in Supplementary Table S1.

2.5. Electrophysiology

Prior to recording, cells on coverslips were transferred to a recording chamber containing Krebs solution gassed with 95% O_2 and 5% CO_2 at RT and exchanged every 20 min during recordings. The standard solution was composed of (in mM): 119 NaCl, 2.5 KCl, 1.3 $MgSO_4$, 2.5 $CaCl_2$, 25 glucose, and 26 $NaHCO_3$. For recordings, a Multiclamp 700B Microelectrode Amplifier (Molecular Devices) was used together with borosilicate glass pipettes (3–7 MOhm) filled with the following intracellular solution (in mM): 122.5 potassium gluconate, 12.5 KCl, 0.2 EGTA (egtazic acid), 10 HEPES (N-2-hydroxyethylpiperazine-N-ethanesulfonic acid), 2 MgATP, 0.3 Na_3GTP, and 8 NaCl adjusted to pH 7.3 with KOH, as previously described. Data acquisition was performed with pCLAMP 10.2 software (Molecular Devices, San Jose, CA, United States); current was filtered at 0.1 kHz and digitized at 2 kHz. Cells with neuronal morphology and round cell body were selected for recordings. Resting membrane potentials were monitored immediately after breaking-in in current-clamp mode. Thereafter, cells were kept at a membrane potential of −60 mV to −80 mV, and 500 ms currents were injected from −85 pA to +165 pA with 20 pA increments to induce action potentials. For inward sodium and delayed rectifying potassium current measurements, cells were clamped at −70 mV and voltage-depolarizing steps were delivered for 100 ms at 10 mV increments.

2.6. Immunocytochemistry

The cells were washed with PBS and fixed in 4% paraformaldehyde solution for 15 min at room temperature (RT) prior to staining. The cells were pre-incubated in a blocking solution containing 0.1 M PBS with potassium (KPBS) +0.1% Triton +5% serum (of secondary antibody host species) for 1–3 h before the primary antibody solution was added.

The cells were incubated with the primary antibodies overnight at 4 °C and the following day they were washed with KPBS before adding the secondary antibody solution containing fluorophore-conjugated antibodies (1:200, Jackson ImmunoResearch Laboratories, West Grove, PA, USA) and DAPI (4′,6-diamidino-2-phenylindole) (1:500). The cells were incubated with the secondary antibodies for 2 h at RT and finally washed with KPBS. Primary antibodies used were: rabbit anti-TH(tyrosine hydroxylase) (1:1000, AB152, Merck Millipore, Burlington, MA, USA), chicken anti-MAP2 (1:10,000, ab5392, Abcam, Cambridge, United Kingdom), mouse anti-Ki67 (1: 500, ab550609, BD Biosciences, San Jose, CA, USA), mouse anti-FOXA2 (1:1000, ab101060, Santa Cruz, Dallas, TX, USA), rabbit anti-LMX1A (1:1000, AB10533, Merck Millipore), goat anti-OTX2 (1:2000, AF1979, R&D Systems, Minneapolis, MN, USA), rabbit anti-TAU (1:2000, A0024, DAKO, Glostrup, Denmark), rabbit anti-GIRK2 (G-protein-regulated inward-rectifier potassium channel 2) (1:500, APC006, Alomone Labs, Jerusalem, Israel), rabbit anti-AADC (aromatic L-amino acid decarboxylase) (1:500, Merck Millipore AB1519), rabbit anti-CALB (calbindin) (1:200, cb38, Swant Inc., Marly, Fribourg, Switzerland), and mouse anti-GFAP (glial fibrillary acidic protein) (1:200 SMI 21, BioLegend San Diego, CA, USA).

2.7. Microscopy

Fluorescent images were captured using a Leica DMI6000B widefield microscope with a Leica 12V 100W Lamphouse 11,504,103 BZ: 00 light source. The images were either taken with a 10× objective (HC PL FLUOTAR 10×, NA = 0.30, immersion = DRY) or a 20× objective (HC FLUOTAR L 20x, NA = 0.4, immersion = DRY). The channels and filters used were DAPI (EX=excitation (nm), EM= emissions (nm); EX: 320–400, EM: 430-510), Cy2 (EX: 430–510, EM: 475–575), Cy3 (EX: 485–585, EM: 535-685), and Cy5 (EX: 560–680, EM: 625–775). Image acquisition software was Leica LAS X and images were processed using Adobe Photoshop CC 2020 (Adobe, San Jose, CA, USA). Any adjustments were applied equally across the entire image, and without the loss of any information. All brightfield images were taken with an Olympus CKX53 with a 4x objective (UPlanFL N 4×/0.13 NA, immersion = DRY) and the software used was OLYMPUS cellSens Standard V1.18.

2.8. Statistical Analysis

All data are expressed as mean ± standard error of the mean (SEM). A Shapiro–Wilk normality test was used to assess the normality of the distribution and parametric or nonparametric tests were performed accordingly. Statistical analyses were conducted using GraphPad Prism 8.0 (GraphPad, San Diego, CA, USA).

2.9. Code Availability

Code for bioinformatics pipeline used in this analysis is available at GitHub https://github.com/davhg96/SC_lncRNA.git.

3. Results

3.1. hPSCs Are Patterned into Functionally Mature DA Neurons

We used a well-established differentiation protocol [9] that relies on dual-SMAD inhibition for neuralization, combined with exposure to the ventralizing secreted factor SHH and to GSK3i for caudalization in order to efficiently drive hPSC differentiation into DA progenitors and subsequently into mature VM DA neurons for single-cell sequencing (Figure 1A). This protocol results in the formation of a homogeneous VM progenitor population after 16 days, as assessed by immunostaining for FOXA2, LMX1a, and OTX2 (Figure 1B,E and Supplementary Figure S1A,B). Subsequent differentiation (Figure 1C,D) led to downregulation of the progenitor markers *SOX2* and *SHH1*, and upregulation of the DA transcripts *NURR1* and *TH* (Supplementary Figure S1E and Supplementary Table S1). The progressive formation of DA neurons was confirmed by staining for TH/MAP2, TAU/MAP2 and AADC/MAP2 (Figure 1F,G and Supplementary Figure S1C,D), showing an increase in morphological complexity of cultures over time as DA progenitors exited from cell cycle and differentiated into postmitotic DA neurons. Immunocytochemistry for Ki67 showed that cells were highly proliferative at days 16 and 30, but that proliferation was minimal at day 60 (Figure 1E–G). At this later timepoint, DA neurons had acquired a subtype identity, expressing GIRK2 (Figure 1H) and CALB (Figure 1I), and had reached functional maturity, as confirmed by whole-cell patch-clamp electrophysiological recordings (Figure 1J–L). Patched cells (n = 5) exhibited functional properties such as hyperpolarized resting membrane potentials (−47.12 mV) and presence of inward sodium (Na^+)-outward delayed-rectifier potassium (K^+) currents (Supplementary Figure S1F,G). Neuronal function was confirmed by the ability to fire multiple induced-action potentials (APs) upon current injections (n = 4/5) (Figure 1J) with majority of the cells (n = 4/5) showing rebound APs after brief depolarization (Figure 1K), characteristic of midbrain DA neurons in vitro [17]. Furthermore, some cells (n = 3/5) displayed the ability to fire APs without current injection, as shown by spontaneous firing (Figure 1L), indicative of functional neuronal maturation.

3.2. scRNAseq Reveals Cell-Type Specificity and Developmental Trajectories During VM Differentiation

We next performed a 10× Genomics droplet-based single-cell time course transcriptomic analysis at days 16, 30, and 60 of differentiation (Figure 1A and Supplementary Figure S2C), and a total of 19,841 cells were retained for analysis following quality control (QC). Uniform manifold approximation and projection (UMAP) and graph-based clustering assigned the majority of cells to either a floor plate or a DA progenitor/neuron identity in the integrated dataset (Figure 2A,B). A few cells with features of vascular leptomeningal cells (VLMCs), a new cell type associated with vasculature in the brain [18], but none with a glia cell signature were detected (Figure 2A,B). These findings were confirmed at protein level by immunocytochemistry (Supplementary Figure S2A,B). Cell cycle analysis corroborated immunostaining data (Figure 1E–G), with 33%, 6%, and <1% of cells in active cell cycle at day 15, 30, and 60, respectively (Figure 2C,D). A large population of floor-plate cells was also detected, and further analysis of cell cycle showed that the major segregation within this population was due to cycling genes (Figure 2B–D). UMAP distinguished three clusters,

which we named FP-1, FP-2, and FP-3 (Figure 2A). We then identified the most highly differentially expressed genes using the Wilcoxon rank sum test for each cell cluster. FP-1 and FP-2 shared key molecular features of radial glial (RG) cells, characterized by expression of *SOX2*, *PLP1*, *EDNRB*, and *SOX9* (Figure 2B and Supplementary Figure S2D,E). FP-1 differed primarily from FP-2 in that it included cycling cells with a highly proliferative signature (*TOP2A* and *CENPA*), as visualized by UMAP cell cycle score (S.Score and G2M.Score) as well as in expression of the pro-neural gene *SOX2* and the chromatin-associated gene *E2F1*(Figure 2B–D and Supplementary Figure S2D,E). The FP-3 cluster was instead highly enriched by expression of the morphogens *SHH*, *CORIN*, and *WNt5A* as well as *FOXA2*, *LMX1A*, and *OTX2*, which define the VM floor plate (Figure 2B and Supplementary Figure S2D,E). Furthermore, the scRNAseq data revealed the absence of pluripotency-associated genes (*NANOG* and *OCT4*) as well as forebrain (*FOXG1* and *SIX6*) and hindbrain (HOXA2 and GBX2) cells, showing efficient VM patterning (Supplementary Figure S2F).

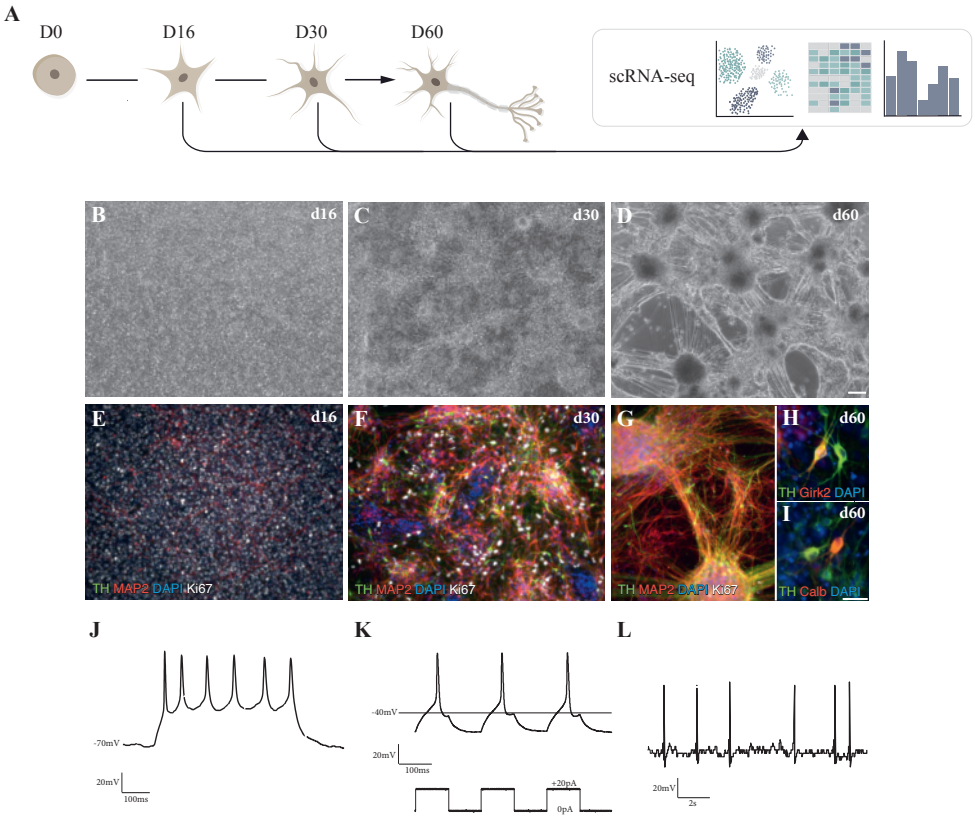

Figure 1. VM-patterned hPSC differentiation generates functionally mature dopaminergic (DA) neurons. (**A**) Schematic overview of the experimental design. (**B**–**D**) Representative bright-field images of ventral midbrain (VM) differentiation cultures at different time points (16, 30, and 60 days). Scale bars, 100 µm. (**E**–**G**) Immunofluorescence staining of tyrosine hydroxylase (TH), MAP2, and Ki67 at days 16, 30, and 60. Scale bars, 100 µm. Nuclei were stained with 4′,6-diamidino-2-phenylindole (DAPI). (**H**) Immunofluorescence staining of DA markers TH/GIRK2. (**I**) TH/calbindin (CALB) at day 60. Scale bars, 25 µm. Nuclei were stained with DAPI. (**J**–**L**) Electrophysiological assessment of DA neuron-rich cultures using patch-clamp analysis. (**J**) Cells analyzed at day 60 displayed induced action potentials. (**K**) Induced action potentials upon brief depolarization. (**L**) Spontaneous firing characteristic of DA neurons.

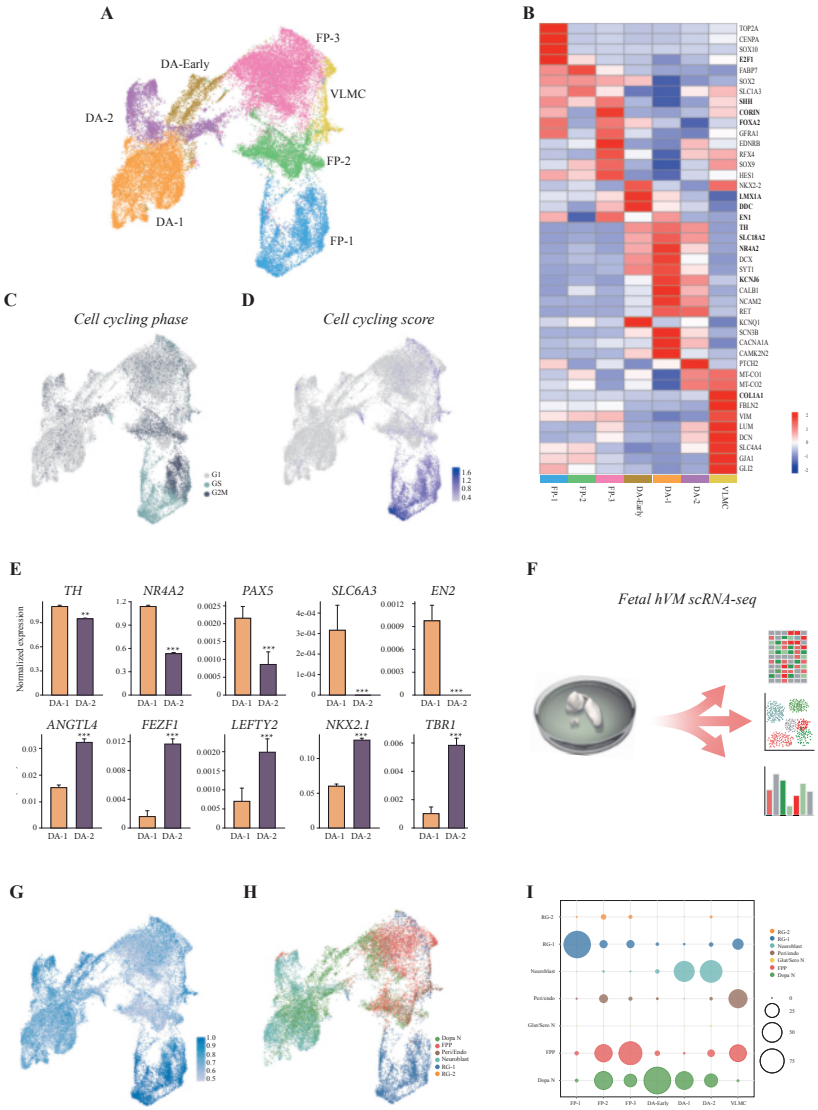

Figure 2. Single-cell RNA sequencing (ScRNAseq) captures distinct cell-type identities during human pluripotent stem cell DA neuron differentiation. (**A**) Uniform manifold approximation and projection (UMAP) plot embeddings of 19,841 cells from VM cultures at day 16, 30, and 60. Cell-type assignments are indicated. (**B**) Heat map showing expression levels of selected genes for each cluster. Values are given as standard deviations relative to average expression across all clusters. (**C**) UMAP embeddings showing the predicted cell cycle phase. (**D**) Cell-cycling score (S.Score + G2M.Score) calculated using Seurat CellCycleScoring function. (**E**) Bar plot of DA-1 and DA-2 clusters showing expression of meso/diencephalic markers. Data represent mean ± SEM, ** $p < 0.01$, *** $p < 0.001$. (**F**) Schematic overview of the experimental design. (**G**) UMAP embeddings of prediction score for human fetal VM cells from three separate fetuses (6, 8, and 11 weeks post-conception) vs. hPSC VM-derived culture cell types. (**H**) Predicted cell types using fetal derived cell types as reference. (**I**) Relative overlapping quantification (% cells overlapping) of human fetal midbrain vs. hPSC VM culture datasets.

We also identified a large neuronal cluster (8989 cells) with increased expression of *MAP2*, *DCX*, *POU2F2,* and *RBFIX1* (all upregulated with an adjusted *p*-value $<10^{-30}$ compared to FPs) (Figure 2B and Supplementary Figure S2C–E). This neuronal cluster was further refined into three subclusters, which we called DA-early, DA-1, and DA-2 (Figure 2A and Supplementary Figure S2C). DA-early differed mainly from the DA-1 and DA-2 clusters in its retained expression of the floor-plate markers *LMX1A* and *FOXA2*, but was starting to gain additional expression of the neuronal precursor markers *DCX* and *SYT1*, and the late DA progenitor markers *Nurr1* and *DDC* (Figure 2B and Supplementary Figure S2D). DA-1 and DA-2 subclusters both expressed *TH* (Figure 2B,C). DA-1 (orange in Figure 2A and Supplementary Figure S2C) was characterized by key markers of VM DA neurons such as *TH*, *NR4A2*, *PAX5*, *SLC6A3*, and *EN2* (Figure 2E), while the smaller DA-2 cluster (purple in Figure 2A) displayed lower or no expression of most DA-related genes (Figure 2E). This latter cluster was instead enriched for non-DA genes such as *ANGLT4*, *FEZF1*, *LEFTY2*, *NKX2.1*, and *TBR1* (Figure 2E).

We next compared the molecular identity of the cells in our 2D VM cultures to a newly generated single-cell dataset of human fetal VM from fetuses dissected 6–11 weeks post conception using the Seurats data projection method in order to assess how well the in vitro stem-cell system captures human VM development (Figure 2F). The fetal dataset comprised 23,438 cells, including ~12,400 progenitors and almost 4000 cells classified as DA neurons (Birtele et al) [19]. Overall prediction quality between the 2D VM-patterned stem-cell culture and fetal VM was high, with a median prediction score of 0.67. Accuracy was higher for the FP-1 and the neuronal clusters, and lower for FP-2 (Figure 2G). Focusing on the two DA clusters in 2D culture revealed 43% of the cells in DA-1 and 25% in DA-2 predicted to be in the fetal DA neuron cluster (median prediction score 0.70 and 0.60, respectively) (Figure 2H,I). However, 56% of DA cells in DA-1 and 68% in DA-2 were also predicted to be fetal neuroblasts, suggesting that not all DA neurons fully mature under 2D culture conditions (Figure 2H,I).

The fine-tuned balance of patterning factors is crucial for ensuring homogeneous VM cell commitment. We previously showed that addition of FGF8b to VM progenitors at days 9–16 resulted in more robust and precise DA neuron formation after transplantation in a PD rat model [8,9]. In this study, we compared the cellular composition of terminally differentiated VM cultures patterned with or without FGF8b at single-cell level (Figure 3A). scRNAseq showed that the absence of FGF8b correlated with ectopic expression of rostral meso/diencephalic markers (*BARHL1*, *NKX2.1*, *PAX6*, and *FOXG1*) accompanied by downregulation of caudal VM markers (*PAX5*, *EN1*, and *NR4A2*) (Figure 3B).

Further investigation of the cellular composition of VM culture with and without FGF8b at day 60 showed that in this 2D model, the timed and dosed delivery of FGF8b also resulted in an increased yield of the DA neuron population (Figure 3C,D).

Interestingly, after two months, over twice the number of cells were found in the DA-1 cluster cultured under FGF8b+ conditions than in the FGF8b- culture (45% vs. 20%, respectively) (Figure 3D). In contrast, a larger DA-early and floor-plate clusters were found in the FGF8b- (DA-early, 8%; FP clusters, 47%) than in the FGF8b+ (DA-early, 4%; floor plate, 20%) (Figure 3C,D) cultures, pointing to the fact that a considerable number of cells with immature identities were still present in 2D cultures grown without FG8b. Single-cell analysis (Figure 3E) and immunohistochemistry of early and late DA markers also confirmed that the absence of FGF8b affected the recapitulation of more mature human DA neurons (Figure 3F,G).

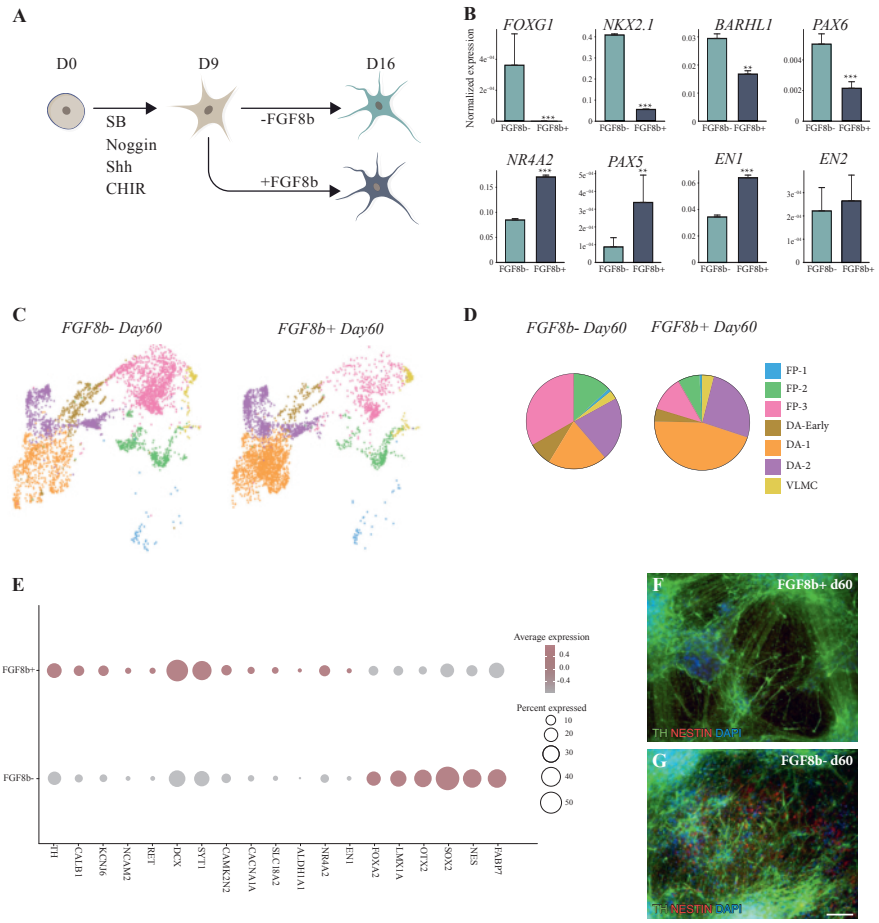

Figure 3. Fibroblast growth factor 8 (FGF8b) facilitates progenitor transition into mature DA neurons. (**A**) Schematic overview of the experimental design. (**B**) Bar plots showing expression of rostral and caudal mesencephalic markers with and without FGF8b treatment at 2 months from single-cell dataset. Data represent mean ± SEM, ** $p < 0.01$, *** $p < 0.001$. (**C**) UMAP embeddings showing cells from 60-day VM culture with and without FGF8b colored by cell types. (**D**) Pie chart showing cell-type proportion with and without FGF8b at 2 months. (**E**) Dot plot showing percent of cells expressing early and late DA markers in VM culture with and without FGF8b at 2 months. (**F**) Immunofluorescence staining of TH/NESTIN with and (**G**) without FGF8b treatment at 2 months VM culture. Scale bars, 100 µm. Nuclei were stained with DAPI.

Together, these findings underscore the pivotal role of FGF8b in the induction and specification of DA progenitors into functionally mature DA neurons during VM differentiation.

We also assessed the dynamics of DA neuron development in our stem-cell-based model. Time-based expression analysis of progenitor markers including *CORIN*, *SHH*, and *SOX2* decreased from day 16 to day 60, whereas markers for maturing neurons increased over time (Figure 4A). This prompted us to exploit our a single-cell dataset to temporally reconstruct human DA neurogenesis in in vitro 2D culture using Slingshot on integrated data from all timepoints of differentiation (Figure 4B). Slingshot performs lineage inference using a cluster-based minimum spanning tree, constructing simultaneous principal curves for branching paths through the tree. Three tentative lineages were

identified, all originating from the floor-plate population (Figure 4B). Specifically, the resulting plots placed the cells along a continuous path, identifying first FP-1 and then FP-2 as the parent lineage, which subsequently underwent gradual transcriptional changes projecting into three different tentative trajectories (Figure 4B,C). Two of the trajectories shared the same four progenitors (FP-1, FP-2, FP-3, and DA-early), but with DA-1 and DA-2 as terminal states, respectively (Figure 4C,D). In the third trajectory, VLMC was the terminal state, with FP-1, FP-2, and FP-3 as progenitors (Figure 4C,D). Overall, these data confirm that key molecular aspects of DA neurogenesis are recapitulated along a temporal axis in 2D VM culture following a precise developmental program, which eventually gives rise to the generation of functionally mature DA neurons. Interestingly, we also found that the VLMC and DA neuron clusters originated from the same VM floor-plate cells and did not diverge until terminally differentiated into DA neurons or VLMCs, respectively.

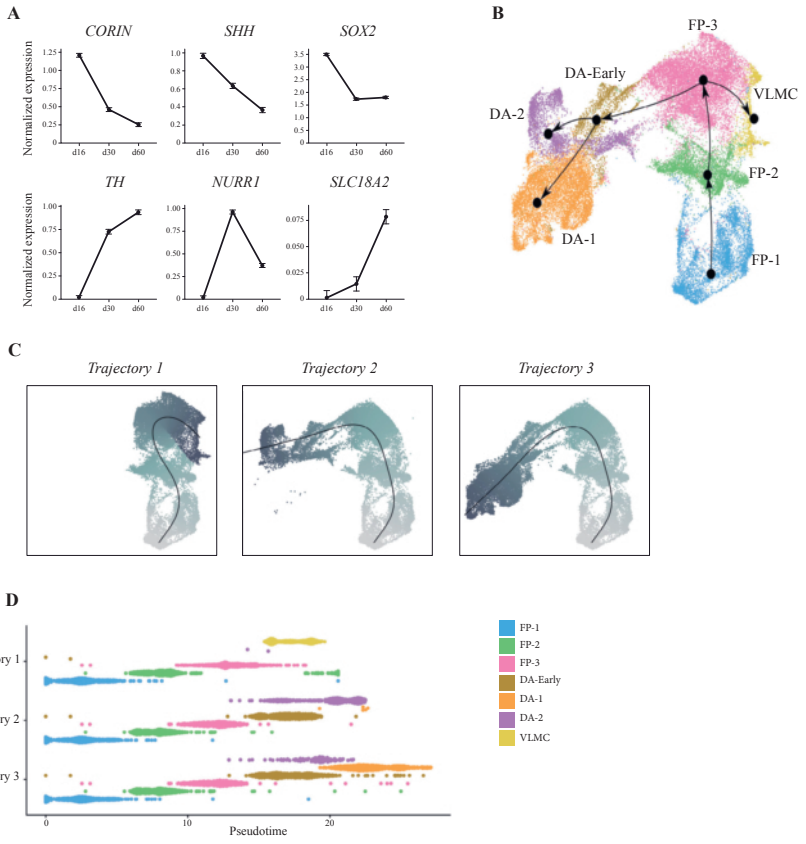

Figure 4. ScRNAseq reconstructs developmental trajectories during VM-patterned hPSC differentiation. (**A**) Temporal expression pattern of early and late DA markers during hPSC VM differentiation (16–60 days). (**B**) Slingshot-based pseudotime trajectories calculated from UMAP embeddings showing combined developmental trajectories of all identified cell types and, (**C**) individual trajectory curves colored by pseudotime. (**D**), Pseudotime inference reconstruction plot showing the appearance and temporal progression of cell-types along a pseudotemporal axis.

3.3. 10× Genomics Captures a Repertoire of lncRNAs during VM Differentiation

In order to study tissue-specific expression of lncRNAs and their functional importance as critical regulators in key biological processes we developed a pipeline to examine the developmental dynamics and cell-type specificity of lncRNAs during DA neuron differentiation. The pipeline was designed to comprehensively profile differentially expressed lncRNAs at different timepoints or according to cell-type specificity based on the clusters previously defined using coding gene markers. To identify lncRNAs expressed during VM differentiation, we merged the reads from each cluster and performed lncRNA quantification in a strand-specific manner (see Materials and Methods and Figure 5A). By comparing the expression of lncRNAs and mRNAs, we found that the average number of mapped lncRNA genes at each timepoint was significantly lower than that of mRNA genes. However, no significant changes were detected from day 16 to day 60 (Figure 5B). Our pipeline detected 3802 lncRNA genes, including 1961 sense and 1842 antisense (expression base mean $\geq$1), and distance matrix of lncRNA expression showed a correlation between cell types and differentiation timepoints (Figure 5C,D and Supplementary Figure S3A,B). Since lncRNAs can exert either repressive or promoting activities on target genes by coordinating protein and RNA interactions both in cis (on neighboring genes) and in trans (on distant loci), we investigated their genomic distribution. Among 3803 identified lncRNA genes, the majority were intragenic (Supplementary Figure S3C). Pearson's pairwise correlation analysis showed that lncRNAs exhibited a higher change in expression correlation with their nearest protein coding gene (<5 kb, Figure 5E). Specifically, we found a higher percentage of positive correlations between cis pairs. Length distribution showed that the majority of lncRNAs detected in this pipeline ranged from 300 to 2500 base pairs (Figure 5F). This confirms that the pipeline is able to profile lncRNAs during VM differentiation regardless of genomic location, length of transcript, or transcriptional direction.

3.4. Single-Cell Analysis Reveals Dynamics and Cell-Type Specificity of LncRNAs During VM Differentiation

scRNAseq based on coding gene analysis distinguished cell types and defined their developmental dynamics during differentiation. We therefore investigated whether the expression of captured lncRNAs correlated to that of molecularly distinct cell clusters identified during DA neuron specification. C (PCA) clustered 456 single cells into three distinct populations, in line with the three different stages of human VM differentiation analyzed, showing that lncRNAs exhibit high stage specificity following VM developmental dynamics (Figure 6A). The MA plot showed significantly differentially expressed lncRNAs (p value adjusted < 0.01) between day 16 and day 60 (Figure 6B). As expected, during VM differentiation we found downregulated well-known lncRNAs such as *NR2F2-AS1,* and *LHX5-AS1* were shown to play regulatory roles in neural stem-cell differentiation (Figure 6B,E and Supplementary Figure S3D) [20,21]. *LINC01833* (also called *SIX3os*), the long noncoding opposite strand transcript of homeodomain factor *Six3,* known to be involved in neuronal differentiation and retinal cell specification, was also downregulated (Figure 6B,E) [22]. Captured downregulated lncNRAs also included annotated transcripts not yet associated with neurodevelopment, such as *LINC01918* and *AL139393.2*, implicated in thyroid and medulloblastoma carcinoma, respectively [23,24], as well as *SMCR2*, also known as *lncSREBF1*, which plays a role in lipid metabolism (Figure 6B,E and Supplementary Figure S3D) [25].

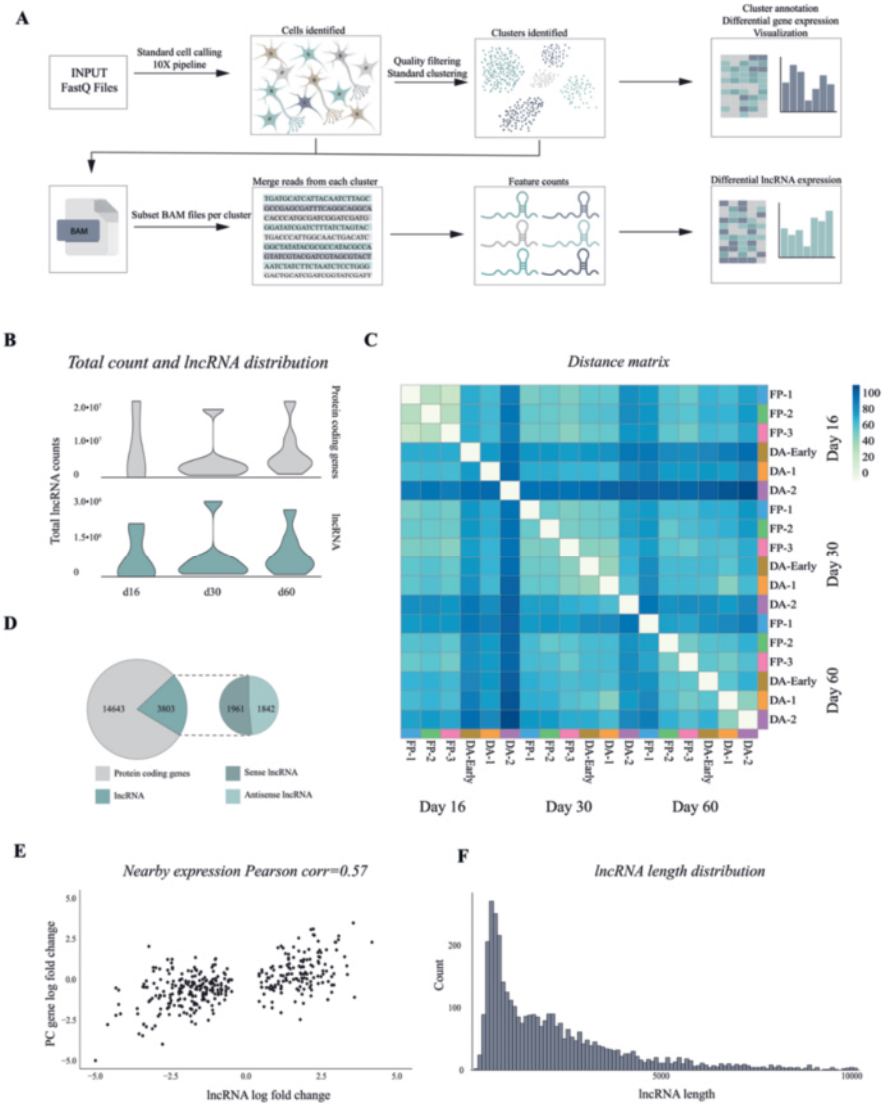

Figure 5. Bioinformatic pipeline detects lncRNAs from 10x Genomics single cell dataset (**A**) Schematic overview of pipeline designed for lncRNA quantification. (**B**) Count distribution of protein-coding genes and lncRNAs from each sample at three time points of hPSC DA neuron differentiation (day 16, 30, 60). (**C**) Heatmap of Euclidean distance across different cell types and time points (log2 normalized counts). (**D**) Number and distribution of protein-coding genes and lncRNAs expressed (baseMean >1), strand (sense "+", antisense "−"). (**E**) Pearson correlation of change in expression of protein-coding genes and lncRNAs (±5Kb, p adj < 0.01). The x-axis shows the log fold change of the lncRNA and the y-axis the log fold change of the overlapping protein-coding gene. (**F**) Length distribution of expressed lncRNAs (x-axis).

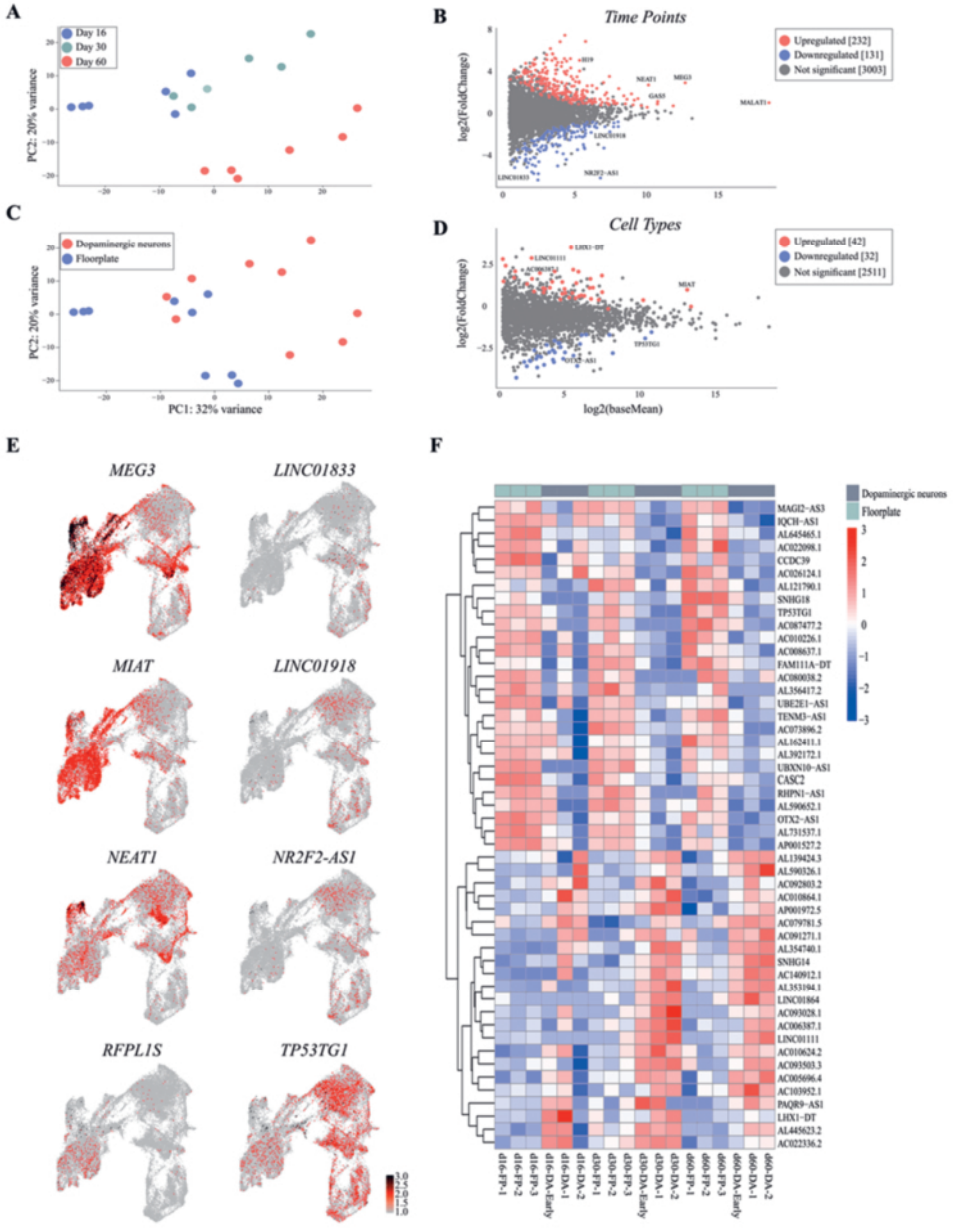

Figure 6. Catalogue of lncRNA time and cell-type specificity. (**A**) Principal component analysis (PCA) plot of lncRNA expression across timepoints in hPSC DA neuron differentiation. (**B**) MA plot of lncRNAs showing their log2 fold change and log2 baseMean expression across time points (p adj < 0.01). (**C**) PCA plot of lncRNA expression across cell types in hPSC DA neuron differentiation. (**D**) MA plot of lncRNAs showing their log2 fold change and log2 baseMean expression across cell type (p adj < 0.01). (**E**) Expression map of candidate lncRNAs projected on UMAP plot. (**F**) Expression heatmap of the top 50 most differentially expressed lncRNAs across cell types (log2 vst, p adj < 0.01).

Differentially expressed upregulated lncRNAs in long-term VM culture included the well-known nuclear paraspeckle assembly transcript 1 (*NEAT1*), overexpressed in the substantia nigra, as well as *H19*, *MALAT1*, and *SNHG12*, previously reported to be enriched at early stages of PD pathogenesis (Figure 6B,E and Supplementary Table S2) [26–28]. We also found upregulated expression of *AC005062.1* and *AL590302.1*, as well as *LINC02019* and the antisense *SPRY4-AS1*, previously associated with tumorigenesis (Supplementary Figure S3D and Supplementary Table S2) [29].

We next examined lncRNA expression based on cell-type specificity by combining single-cell data from days 16, 30, and 60. PCA revealed that lncRNAs clearly segregated into DA and floor-plate clusters, and 140 lncRNAs were found significantly differentially expressed in these two molecularly distinct cell types (Figure 6C). Consistent with these findings, we found lncRNAs associated with brain development to be upregulated in the DA cluster, such as the nuclear-localized *MIAT*, also known as *Gomafu*, reported to be expressed in postmitotic neurons (Figure 6C,D) [30]. The imprinted lncRNA *Meg3* [31] (Figure 6E and Supplementary Figure S3A), expressed in the cortex, was also found enriched in DA neurons, similarly to its neighbor gene *DLK1*, which plays a critical role in DA specification. *LINC01111*, identified as an oncosuppressor in pancreatic cancer [32], and the annotated *LHX1-DT* and *AC006387.1* transcripts were also significantly enriched in the DA population (Figure 6F and Supplementary Table S3). Noteworthy, ~80% of lncRNAs detected in the DA cell type were also found upregulated at day 60 of VM differentiation. In contrast, *OTX2-AS1* was significantly enriched in the floor-plate cluster together with *TP53TG1*, implicated in carcinoma but not as yet associated with a neuronal phenotype [33] (Figure 6D–F and Supplementary Figure S3E). This cluster of immature cells was also characterized by *SNHG18* [34], known to play an oncogenic role in glioma, *LINC0052* [35], which acts as a sponge for miR-608, and the annotated transcripts *AC026124.1*, *AL132780.2*, and *AC026401.3* (Figure 6D–F and Supplementary Figure S3E).

4. Discussion

In this study, we used single-cell sequencing to assess the validity and potential use of stem-cell-based differentiation to model human DA neuron development. By transcriptionally profiling almost 20,000 cells at different time points, spanning the transition from progenitor stage to functionally mature DA neurons, we were able to assess the extent to which this culture system recapitulates DA neuron development. Our findings prompt a number of important observations. Firstly, clustering analysis shows that cell types present during stem-cell differentiation are similar to those present during fetal VM development and that no aberrant cell types are found in the cultures. Secondly, the temporal appearance of different cell types corresponds to the order of progression previously observed in human fetal VM [11] and in xenograft models [10]. Thirdly, the molecular profile of the resulting DA neurons closely matches that of fetal VM-derived DA neurons. Taken together, these considerations support the use of stem-cell-based models to study aspects of human brain development.

When using the single-cell dataset to reconstruct lineage specification and DA neurogenesis, we were able to identify three distinct lineages all originating from the same floor-plate population. Two of the trajectories shared exactly the same progenitors (FP-1, FP-2, FP-3, and DA-early), but then diverged into a large DA population (DA-1) and a smaller population of neurons expressing TH but few other DA-associated markers (DA-2). This latter population also shared a much smaller overlap of genes with DA neurons in fetal VM, indicating that some cells in 2D culture underwent incomplete differentiation and/or insufficient patterning toward a VM regional fate or otherwise aberrantly express TH in non-DAergic cells as is commonly observed in in vitro cultures [36–39]. Interestingly, this lineage analysis also revealed that the VLMC and DA neuron clusters originated from the same VM floor-plate cells and did not diverge until terminal differentiation into DA neurons or VLMCs had occurred.

Rostro-caudal patterning in VM differentiation protocol can be more precisely controlled using timed delivery of FGF8b [9]. By quantifying cellular composition of cells patterened with and without FGF8 after two months in culture, we showed that FGF8b facilitates the conversion of progenitors into functionally mature DA neurons while enabling efficient differentiation toward a caudal VM pattern. These findings also underscore the need to identify and validate more markers able to predict functional maturation in both long-term culture and in vivo after transplantation.

In the past decades, large-scale genome-wide sequencing has revealed the tissue-specificity and functional relevance of lncRNAs as key regulators in neural development, refuting the paradigm of RNA as simply an intermediary between DNA and protein [40–42]. In this expanding view of the genomic landscape, very few scRNAseq studies have as yet provided comprehensive human lncRNA repertoires of different healthy human tissues [43–46]. Although the relatively low expression levels of lncRNAs make analysis at single-cell resolution challenging, a detailed catalog of cell-type-specific lncRNAs expressed during DA differentiation may increase our understanding of their involvement in the VM developmental program and intricate regulatory DA pathways [47,48]. Here, we exploited 3′-end high-throughput sequencing of 10× Genomics technology to capture polyadenylated noncoding genes and developed a bioinformatic pipeline that provided the first comprehensive dataset of lncRNAs showing cell-type specificity by analyzing different stages of DA neuron differentiation. 3′-end sequencing is not able to capture non polyA transcripts and is less efficient than full-length scRNAseq methodologies. Nevertheless, 10× Genomics performs high-throughput microfluidic profiling of a large number of cells. Thus, although many lncRNAs may individually have low expression levels, the extensive number of cells that is possible to sequence with this method also allows lncRNA expression to be analyzed and mapped to distinct clusters defined by the coding gene expresssion.

We found that many lncRNAs are specific to distinct cell types associated with either progenitors or functionally mature DA neurons. Interestingly, we identified new lncRNAs potentially involved in early steps of DA differentiation, such as *TP53TG1, LINC01833,* and *SNHG18*, found specifically enriched in the floor-plate clusters, as well as two antisense transcripts of the *NR2F1* and *OTX2* coding genes, which play a key role in cortical development and VM floor-plate formation, respectively [49]. Our dataset also includes significantly enriched lncRNAs not previously linked to functionally mature DA cells, such as *LINC01111*, *RFPL1S*, and *AL365361.1*. It also confirms the expression of lncRNAs already associated with DA tissue, including *MIAT*, involved in DA signaling via modulation of DA transmission and neurobehavioral phenotypes [50]. Using a microfluidic approach enabled us to analyze a sufficiently large number of cells and more accurately redefine the feature expression map of lncRNAs which until now were thought to be mainly expressed in late stages of VM differentiation. *NEAT1*, for example, known to exert a neuroprotective role in SNc, was also found highly expressed in our floor-plate subclusters, suggesting its potential role in DA commitment [51]. The imprinted lncRNA *Meg3* also displayed a particular cell-type-specific expression pattern robustly expressed in DA clusters, hinting at its involvement as a critical regulator of DA neuron specification, possibly through crosstalk with its coding neighbor gene *DLK1*. In this scenario, integrating single-cell transcriptomics and epigenomics technologies, such as assay for transposase-accessible chromatin using sequencing (ATAC-seq), will bring valuable insights into the complex and intricate regulatory network involving coding and noncoding genes during stem-cell DA differentiation.

Taken together, these findings provide a valuable transcriptomic dataset of coding and noncoding genes in human DA neurogenesis that may lead to the identification of novel cell types and a better definition of molecular diversity in progenitor and mature DA populations.

Supplementary Materials: The following are available online at https://www.mdpi.com/2073-4409/10/1/137/s1, Figure S1: Gene expression and functional analysis of VM-patterned hPSCs, Figure S2: Cell-type identification based on scRNAseq and immunocytochemistry, Figure S3: Differentially expressed lncRNAs based on cell-type and time-point, Table S1: RT-qPCR primer list, Table S2: LncRNAs deregulated in 60 vs. 16 time points, and Table S3: LncRNAs deregulated in DA vs. FP cell-types.

Author Contributions: Conceptualization, M.P. and A.F.; methodology, M.P., A.F. and F.N.; formal analysis, F.N., A.F., E.S., P.S., M.B., Y.S. and D.H.G.; investigation, F.N., E.S., P.S., M.B., Y.S. and D.H.G.; resources, M.P. and A.F.; data curation, A.F. and F.N.; writing—original draft preparation, M.P. and A.F.; supervision, M.P. and A.F; funding acquisition, M.P. All authors have read and agreed to the published version of the manuscript.

Funding: The research leading to these results has received funding from the New York Stem Cell Foundation (MP), the European Research Council (ERC Grant Agreement no. 771427, MP), the Swedish Research Council (Grant Agreements 2016-00873 (MP)), the Swedish Parkinson Foundation (Parkinsonfonden, MP), the Swedish Brain Foundation (Hjärnfonden FO2019-0301, MP), the Strategic Research Area at Lund University MultiPark (Multidisciplinary research in Parkinson's disease) and KAW (2018.0040). M. Parmar is a New York Stem Cell Foundation–Robertson Investigator.

Institutional Review Board Statement: Not applicable.

Informed Consent Statement: Not applicable.

Data Availability Statement: The data presented in this study are available in supplementary material.

Acknowledgments: We thank Ulla Jarl, Marie Persson Vejgården, and Mikael Sparrenius for technical assistance; and Bengt Mattsson for his valuable help with microscopy and figure preparation.

Conflicts of Interest: The authors declare no conflict of interest.

References

1. Barker, R.A.; Drouin-Ouellet, J.; Parmar, M. Cell-based therapies for Parkinson disease—past insights and future potential. *Nat. Rev. Neurol.* **2015**, *11*, 492–503. [CrossRef] [PubMed]
2. Barker, R.A.; Parmar, M.; Studer, L.; Takahashi, J. Human Trials of Stem Cell-Derived Dopamine Neurons for Parkinson's Disease: Dawn of a New Era. *Cell Stem Cell* **2017**, *21*, 569–573. [CrossRef] [PubMed]
3. Parmar, M. Towards stem cell based therapies for Parkinson's disease. *Development* **2018**, *145*, dev156117. [CrossRef] [PubMed]
4. Barker, R.A.; TRANSEURO consortium. Designing stem-cell-based dopamine cell replacement trials for Parkinson's disease. *Nat. Med.* **2019**, *25*, 1045–1053. [CrossRef]
5. Kriks, S.; Shim, J.-W.; Piao, J.; Ganat, Y.M.; Wakeman, D.R.; Xie, Z.; Carrillo-Reid, L.; Auyeung, G.; Antonacci, C.; Buch, A.; et al. Dopamine neurons derived from human ES cells efficiently engraft in animal models of Parkinson's disease. *Nat. Cell Biol.* **2011**, *480*, 547–551. [CrossRef] [PubMed]
6. Grealish, S.; Diguet, E.; Kirkeby, A.; Mattsson, B.; Heuer, A.; Bramoulle, Y.; Van Camp, N.; Perrier, A.L.; Hantraye, P.; Björklund, A.; et al. Human ESC-Derived Dopamine Neurons Show Similar Preclinical Efficacy and Potency to Fetal Neurons when Grafted in a Rat Model of Parkinson's Disease. *Cell Stem Cell* **2014**, *15*, 653–665. [CrossRef]
7. Kikuchi, T.; Morizane, A.; Doi, D.; Magotani, H.; Onoe, H.; Hayashi, T.; Mizuma, H.; Takara, S.; Takahashi, R.; Inoue, H.; et al. Human iPS cell-derived dopaminergic neurons function in a primate Parkinson's disease model. *Nat. Cell Biol.* **2017**, *548*, 592–596. [CrossRef]
8. Kirkeby, A.; Nolbrant, S.; Tiklova, K.; Heuer, A.; Kee, N.; Cardoso, T.; Ottosson, D.R.; Lelos, M.J.; Rifes, P.; Dunnett, S.B.; et al. Predictive Markers Guide Differentiation to Improve Graft Outcome in Clinical Translation of hESC-Based Therapy for Parkinson's Disease. *Cell Stem Cell* **2017**, *20*, 135–148. [CrossRef]
9. Nolbrant, S.; Heuer, A.; Parmar, M.; Kirkeby, A. Generation of high-purity human ventral midbrain dopaminergic progenitors for in vitro maturation and intracerebral transplantation. *Nat. Protoc.* **2017**, *12*, 1962–1979. [CrossRef]
10. Tiklová, K.; Nolbrant, S.; Fiorenzano, A.; Björklund Åsa, K.; Sharma, Y.; Heuer, A.; Gillberg, L.; Hoban, D.B.; Cardoso, T.; Adler, A.F.; et al. Author Correction: Single cell transcriptomics identifies stem cell-derived graft composition in a model of Parkinson's disease. *Nat. Commun.* **2020**, *11*, 1. [CrossRef]
11. La Manno, G.; Gyllborg, D.; Codeluppi, S.; Nishimura, K.; Salto, C.; Zeisel, A.; Borm, L.E.; Stott, S.R.; Toledo, E.M.; Villaescusa, J.C.; et al. Molecular Diversity of Midbrain Development in Mouse, Human, and Stem Cells. *Cell* **2016**, *167*, 566–580.e19. [CrossRef] [PubMed]
12. Vallejos, C.A.; Risso, D.; Scialdone, A.; Dudoit, S.; Marioni, J.C. Normalizing single-cell RNA sequencing data: Challenges and opportunities. *Nat. Methods* **2017**, *14*, 565–571. [CrossRef] [PubMed]

13. The FANTOM consortium; Carninci, P.; Kasukawa, T.; Katayama, S.; Gough, J.; Frith, M.C.; Maeda, N.; Oyama, R.; Ravasi, T.; Lenhard, B.; et al. The Transcriptional Landscape of the Mammalian Genome. *Science* **2005**, *309*, 1559–1563. [CrossRef]
14. Rinn, J.L.; Kertesz, M.; Wang, J.K.; Squazzo, S.L.; Xu, X.; Brugmann, S.A.; Goodnough, L.H.; Helms, J.A.; Farnham, P.J.; Segal, E.; et al. Functional Demarcation of Active and Silent Chromatin Domains in Human HOX Loci by Noncoding RNAs. *Cell* **2007**, *129*, 1311–1323. [CrossRef]
15. Flynn, R.A.; Chang, H.Y. Long Noncoding RNAs in Cell-Fate Programming and Reprogramming. *Cell Stem Cell* **2014**, *14*, 752–761. [CrossRef]
16. Fiorenzano, A.; Pascale, E.; Gagliardi, M.; Terreri, S.; Papa, M.; Andolfi, G.; Galasso, M.; Tagliazucchi, G.M.; Taccioli, C.; Patriarca, E.J.; et al. An Ultraconserved Element Containing lncRNA Preserves Transcriptional Dynamics and Maintains ESC Self-Renewal. *Stem Cell Rep.* **2018**, *10*, 1102–1114. [CrossRef]
17. Grace, A.; Onn, S. Morphology and electrophysiological properties of immunocytochemically identified rat dopamine neurons recorded in vitro. *J. Neurosci.* **1989**, *9*, 3463–3481. [CrossRef]
18. Marques, S.; Zeisel, A.; Codeluppi, S.; Van Bruggen, D.; Falcão, A.M.; Xiao, L.; Li, H.; Häring, M.; Hochgerner, H.; Romanov, R.A.; et al. Oligodendrocyte heterogeneity in the mouse juvenile and adult central nervous system. *Science* **2016**, *352*, 1326–1329. [CrossRef]
19. Birtele, M.; Sharma, Y.; Storm, P.; Kajtez, J.; Sozzi, E.; Nilsson, F.; Wahlestedt, J.N.; Stott, S.; He, X.L.; Mattsson, B.; et al. Single cell transcriptional and functional analysis of human dopamine neurons in 3D fetal ventral midbrain organoid like cultures. *bioRxiv* **2020**. [CrossRef]
20. Ang, C.E.; Ma, Q.; Wapinski, O.L.; Fan, S.; Flynn, A.R.; Lee, Q.Y.; Coe, B.P.; Onoguchi, M.; Olmos, V.H.; Do, B.T.; et al. The novel lncRNA lnc-NR2F1 is pro-neurogenic and mutated in human neurodevelopmental disorders. *eLife* **2019**, *8*, 41770. [CrossRef]
21. Prajapati, B.; Fatma, M.; Maddhesiya, P.; Sodhi, M.K.; Fatima, M.; Dargar, T.; Bhagat, R.; Seth, P.; Sinha, S. Identification and epigenetic analysis of divergent long non-coding RNAs in multilineage differentiation of human Neural Progenitor Cells. *RNA Biol.* **2019**, *16*, 13–24. [CrossRef] [PubMed]
22. Ng, S.-Y.; Johnson, R.; Stanton, L.W. Human long non-coding RNAs promote pluripotency and neuronal differentiation by association with chromatin modifiers and transcription factors. *EMBO J.* **2011**, *31*, 522–533. [CrossRef] [PubMed]
23. Zhang, Y.; Jin, T.; Shen, H.; Yan, J.; Guan, M.; Jin, X. Identification of Long Non-Coding RNA Expression Profiles and Co-Expression Genes in Thyroid Carcinoma Based on The Cancer Genome Atlas (TCGA) Database. *Med Sci. Monit.* **2019**, *25*, 9752–9769. [CrossRef]
24. Joshi, P.; Jallo, G.; Perera, R.J. In silico analysis of long non-coding RNAs in medulloblastoma and its subgroups. *Neurobiol. Dis.* **2020**, *141*, 104873. [CrossRef] [PubMed]
25. Muret, K.; Désert, C.; Lagoutte, L.; Boutin, M.; Gondret, F.; Zerjal, T.; Lagarrigue, S. Long noncoding RNAs in lipid metabolism: Literature review and conservation analysis across species. *BMC Genom.* **2019**, *20*, 1–18. [CrossRef]
26. Lyu, Y.; Bai, L.; Qin, C. Long noncoding RNAs in neurodevelopment and Parkinson's disease. *Anim. Model. Exp. Med.* **2019**, *2*, 239–251. [CrossRef]
27. Simchovitz, A.; Hanan, M.; Niederhoffer, N.; Madrer, N.; Yayon, N.; Bennett, E.R.; Greenberg, D.S.; Kadener, S.; Soreq, H. NEAT1 is overexpressed in Parkinson's disease substantia nigra and confers drug-inducible neuroprotection from oxidative stress. *FASEB J.* **2019**, *33*, 11223–11234. [CrossRef]
28. Li, L.; Zhuang, Y.; Zhao, X.; Li, X.-K. Long Non-coding RNA in Neuronal Development and Neurological Disorders. *Front. Genet.* **2019**, *9*, 744. [CrossRef]
29. Li, X.L.; Subramanian, M.; Jones, M.F.; Chaudhary, R.; Singh, D.K.; Zong, X.; Gryder, B.; Sindri, S.; Mo, M.; Schetter, A.; et al. Long Noncoding RNA PURPL Suppresses Basal p53 Levels and Promotes Tumorigenicity in Colorectal Cancer. *Cell Rep.* **2017**, *20*, 2408–2423. [CrossRef]
30. Sun, C.; Huang, L.; Li, Z.; Leng, K.; Xu, Y.; Jiang, X.-M.; Cui, Y. Long non-coding RNA MIAT in development and disease: A new player in an old game. *J. Biomed. Sci.* **2018**, *25*, 1–7. [CrossRef]
31. Yan, H.; Rao, J.; Yuan, J.; Gao, L.; Huang, W.; Zhao, L.; Ren, J. Long non-coding RNA MEG3 functions as a competing endogenous RNA to regulate ischemic neuronal death by targeting miR-21/PDCD4 signaling pathway. *Cell Death Dis.* **2017**, *8*, 1–15. [CrossRef] [PubMed]
32. Pan, S.; Shen, M.; Zhou, M.; Shi, X.; He, R.; Yin, T.; Wang, M.; Guo, X.; Qin, R.Y. Long noncoding RNA LINC01111 suppresses pancreatic cancer aggressiveness by regulating DUSP1 expression via microRNA-3924. *Cell Death Dis.* **2019**, *10*, 1–16. [CrossRef] [PubMed]
33. Diaz-Lagares, A.; Crujeiras, A.B.; Lopez-Serra, P.; Soler, M.; Setien, F.; Goyal, A.; Sandoval, J.; Hashimoto, Y.; Martinez-Cardús, A.; Gomez, A.; et al. Epigenetic inactivation of the p53-induced long noncoding RNA TP53 target 1 in human cancer. *Proc. Natl. Acad. Sci. USA* **2016**, *113*, E7535–E7544. [CrossRef] [PubMed]
34. Zheng, R.; Yao, Q.; Li, X.; Xu, B. Long Noncoding Ribonucleic Acid SNHG18 Promotes Glioma Cell Motility via Disruption of α-Enolase Nucleocytoplasmic Transport. *Front. Genet.* **2019**, *10*, 1140. [CrossRef] [PubMed]
35. Ouyang, T.; Zhang, Y.; Tang, S.; Wang, Y. Long non-coding RNA LINC00052 regulates miR-608/EGFR axis to promote progression of head and neck squamous cell carcinoma. *Exp. Mol. Pathol.* **2019**, *111*, 104321. [CrossRef] [PubMed]

36. Cooper, O.; Hargus, G.; Deleidi, M.; Blak, A.; Osborn, T.; Marlow, E.; Lee, K.; Levy, A.; Pérez-Torres, E.; Yow, A.; et al. Differentiation of human ES and Parkinson's disease iPS cells into ventral midbrain dopaminergic neurons requires a high activity form of SHH, FGF8a and specific regionalization by retinoic acid. *Mol. Cell. Neurosci.* **2010**, *45*, 258–266. [CrossRef] [PubMed]
37. Fasano, C.A.; Chambers, S.M.; Lee, G.; Tomishima, M.J.; Studer, L. Efficient Derivation of Functional Floor Plate Tissue from Human Embryonic Stem Cells. *Cell Stem Cell* **2010**, *6*, 336–347. [CrossRef]
38. Kirkeby, A.; Parmar, M. Building authentic midbrain dopaminergic neurons from stem cells—Lessons from development. *Transl. Neurosci.* **2012**, *3*, 314–319. [CrossRef]
39. Daadi, M.M.; Weiss, S. Generation of Tyrosine Hydroxylase-Producing Neurons from Precursors of the Embryonic and Adult Forebrain. *J. Neurosci.* **1999**, *19*, 4484–4497. [CrossRef]
40. Wang, K.C.; Chang, H.Y. Molecular Mechanisms of Long Noncoding RNAs. *Mol. Cell* **2011**, *43*, 904–914. [CrossRef]
41. Fiorenzano, A.; Pascale, E.; Patriarca, E.J.; Minchiotti, G.; Fico, A. LncRNAs and PRC2: Coupled Partners in Embryonic Stem Cells. *Epigenomes* **2019**, *3*, 14. [CrossRef]
42. Grassi, D.A.; Brattås, P.L.; Jönsson, M.E.; Atacho, D.; Karlsson, O.; Nolbrant, S.; Parmar, M.; Jakobsson, J. Profiling of lincRNAs in human pluripotent stem cell derived forebrain neural progenitor cells. *Heliyon* **2020**, *6*, e03067. [CrossRef] [PubMed]
43. Liu, S.J.; Nowakowski, T.J.; Pollen, A.A.; Lui, J.H.; Horlbeck, M.A.; Attenello, F.J.; He, D.; Weissman, J.S.; Kriegstein, A.R.; Diaz, A.; et al. Single-cell analysis of long non-coding RNAs in the developing human neocortex. *Genome Biol.* **2016**, *17*, 1–17. [CrossRef] [PubMed]
44. Alessio, E.; Buson, L.; Chemello, F.; Peggion, C.; Grespi, F.; Martini, P.; Massimino, M.L.; Pacchioni, B.; Millino, C.; Romualdi, C.; et al. Single cell analysis reveals the involvement of the long non-coding RNA Pvt1 in the modulation of muscle atrophy and mitochondrial network. *Nucleic Acids Res.* **2019**, *47*, 1653–1670. [CrossRef] [PubMed]
45. Jiang, S.; Cheng, S.-J.; Ren, L.-C.; Wang, Q.; Kang, Y.-J.; Ding, Y.; Hou, M.; Yang, X.; Lin, Y.; Liang, N.; et al. An expanded landscape of human long noncoding RNA. *Nucleic Acids Res.* **2019**, *47*, 7842–7856. [CrossRef] [PubMed]
46. Zhou, J.; Xu, J.; Zhang, L.; Liu, S.; Ma, Y.; Wen, X.; Hao, J.; Li, Z.; Ni, Y.; Li, X.; et al. Combined Single-Cell Profiling of lncRNAs and Functional Screening Reveals that H19 Is Pivotal for Embryonic Hematopoietic Stem Cell Development. *Cell Stem Cell* **2019**, *24*, 285–298.e5. [CrossRef]
47. Jönsson, M.E.; Wahlestedt, J.N.; Åkerblom, M.; Kirkeby, A.; Malmevik, J.; Brattås, P.L.; Jakobsson, J.; Parmar, M. Comprehensive analysis of microRNA expression in regionalized human neural progenitor cells reveals microRNA-10 as a caudalizing factor. *Development* **2015**, *142*, 3166–3177. [CrossRef]
48. Fico, A.; Fiorenzano, A.; Pascale, E.; Patriarca, E.J.; Minchiotti, G. Long non-coding RNA in stem cell pluripotency and lineage commitment: Functions and evolutionary conservation. *Cell. Mol. Life Sci.* **2019**, *76*, 1459–1471. [CrossRef]
49. Vernay, B.; Koch, M.; Vaccarino, F.; Briscoe, J.; Simeone, A.; Kageyama, R.; Ang, S.-L. Otx2 Regulates Subtype Specification and Neurogenesis in the Midbrain. *J. Neurosci.* **2005**, *25*, 4856–4867. [CrossRef]
50. Ip, J.Y.; Sone, M.; Nashiki, C.; Pan, Q.; Kitaichi, K.; Yanaka, K.; Abe, T.; Takao, K.; Miyakawa, T.; Blencowe, B.J.; et al. Gomafu lncRNA knockout mice exhibit mild hyperactivity with enhanced responsiveness to the psychostimulant methamphetamine. *Sci. Rep.* **2016**, *6*, 27204. [CrossRef]
51. Cai, L.; Tu, L.; Li, T.; Yang, X.; Ren, Y.; Gu, R.; Zhang, Q.; Yao, H.; Qu, X.; Wang, Q.; et al. Downregulation of lncRNA UCA1 ameliorates the damage of dopaminergic neurons, reduces oxidative stress and inflammation in Parkinson's disease through the inhibition of the PI3K/Akt signaling pathway. *Int. Immunopharmacol.* **2019**, *75*, 105734. [CrossRef] [PubMed]

PAPER II

Stem Cell Reports
Article
ISSCR
OPEN ACCESS

Age-related pathological impairments in directly reprogrammed dopaminergic neurons derived from patients with idiopathic Parkinson's disease

Janelle Drouin-Ouellet,[1,6,*] Emilie M. Legault,[1,6] Fredrik Nilsson,[2] Karolina Pircs,[2] Julie Bouquety,[1] Florence Petit,[1] Shelby Shrigley,[2] Marcella Birtele,[2] Maria Pereira,[2] Petter Storm,[2] Yogita Sharma,[2] Andreas Bruzelius,[2] Romina Vuono,[3,4] Malin Kele,[5] Thomas B. Stoker,[3] Daniella Rylander Ottosson,[2] Anna Falk,[5] Johan Jakobsson,[2] Roger A. Barker,[3] and Malin Parmar[2,*]

[1]Faculty of Pharmacy, Université de Montréal, Montreal, QC H3T 1J4, Canada
[2]Department of Experimental Medical Science, Wallenberg Neuroscience Center, Division of Neurobiology and Lund Stem Cell Center, Lund University, BMC A11 and B10, S-221 84 Lund, Sweden
[3]Wellcome-MRC Cambridge Stem Cell Institute & John van Geest Centre for Brain Repair, Department of Clinical Neurosciences, University of Cambridge, Forvie Site, Cambridge CB2 0PY, UK
[4]Medway School of Pharmacy, University of Kent, Chatham Maritime, Chatham ME4 4TB, UK
[5]Department of Neuroscience, Karolinska institutet, Stockholm, Sweden
[6]These authors contributed equally
*Correspondence: janelle.drouin-ouellet@umontreal.ca (J.D.-O.), malin.parmar@med.lu.se (M.P.)
https://doi.org/10.1016/j.stemcr.2022.08.010

SUMMARY

We have developed an efficient approach to generate functional induced dopaminergic (DA) neurons from adult human dermal fibroblasts. When performing DA neuronal conversion of patient fibroblasts with idiopathic Parkinson's disease (PD), we could specifically detect disease-relevant pathology in these cells. We show that the patient-derived neurons maintain age-related properties of the donor and exhibit lower basal chaperone-mediated autophagy compared with healthy donors. Furthermore, stress-induced autophagy resulted in an age-dependent accumulation of macroautophagic structures. Finally, we show that these impairments in patient-derived DA neurons leads to an accumulation of phosphorylated alpha-synuclein, the classical hallmark of PD pathology. This pathological phenotype is absent in neurons generated from induced pluripotent stem cells from the same patients. Taken together, our results show that direct neural reprogramming can be used for obtaining patient-derived DA neurons, which uniquely function as a cellular model to study age-related pathology relevant to idiopathic PD.

INTRODUCTION

Parkinson's disease (PD) is a neurodegenerative disorder that has a major pathology within the midbrain dopaminergic (DA) neurons and involves the aggregation of the misfolded protein alpha-synuclein (αSYN). How the disease arises and develops is currently unknown and no cure exists. There is an urgent need for better treatments and disease modifying therapies, but their development is hampered by a poor understanding of the pathogenesis of PD and lack of appropriate model systems, in particular ones that capture age, the biggest risk factor for developing this condition.

To better recapitulate disease relevant features and age, we have established a protocol for making induced neurons (iNs) that can be directly generated from adult human dermal fibroblasts (aHDFs). This type of direct neural conversion offers several advantages. In particular, such cells retain many important aspects of the aging signatures of the starting fibroblasts, including age-related changes in the epigenetic clock, the transcriptome and microRNAs, the reactive oxygen species level, DNA damage and telomeres length, as well as in their metabolic profile and mitochondrial defects (Huh et al., 2016; Kim et al., 2018; Mertens et al., 2015, 2021; Tang et al., 2017).

The idiopathic nature of most PD cases, coupled to the late age at onset, complicates the study of pathophysiology as it is challenging to design and interpret models of idiopathic PD. For example, animal models depend on toxin-induced mitochondrial damage or overexpression of αSYN at non-physiological levels (i.e., levels that exceed what is observed in idiopathic PD patients). Patient-derived induced pluripotent stem cells (iPSCs) are frequently used to study cellular features of PD (Brazdis et al., 2020; Lang et al., 2019) but fail to capture the age and epigenetic signatures of the patient (Lapasset et al., 2011; Mertens et al., 2015, 2021; Miller et al., 2013; Tang et al., 2017).

In this study, we investigated iNs using specific combinations of transcription factors and fate determinants without a pluripotent intermediate (Ambasudhan et al., 2011) as a mean to better recapitulate disease-relevant features of idiopathic PD. While it is possible to generate iNs with a DA-like phenotype (Caiazzo et al., 2011; Jiang et al., 2015; Li et al., 2019; Pereira et al., 2014; Pfisterer et al., 2011), current protocols are not efficient enough to

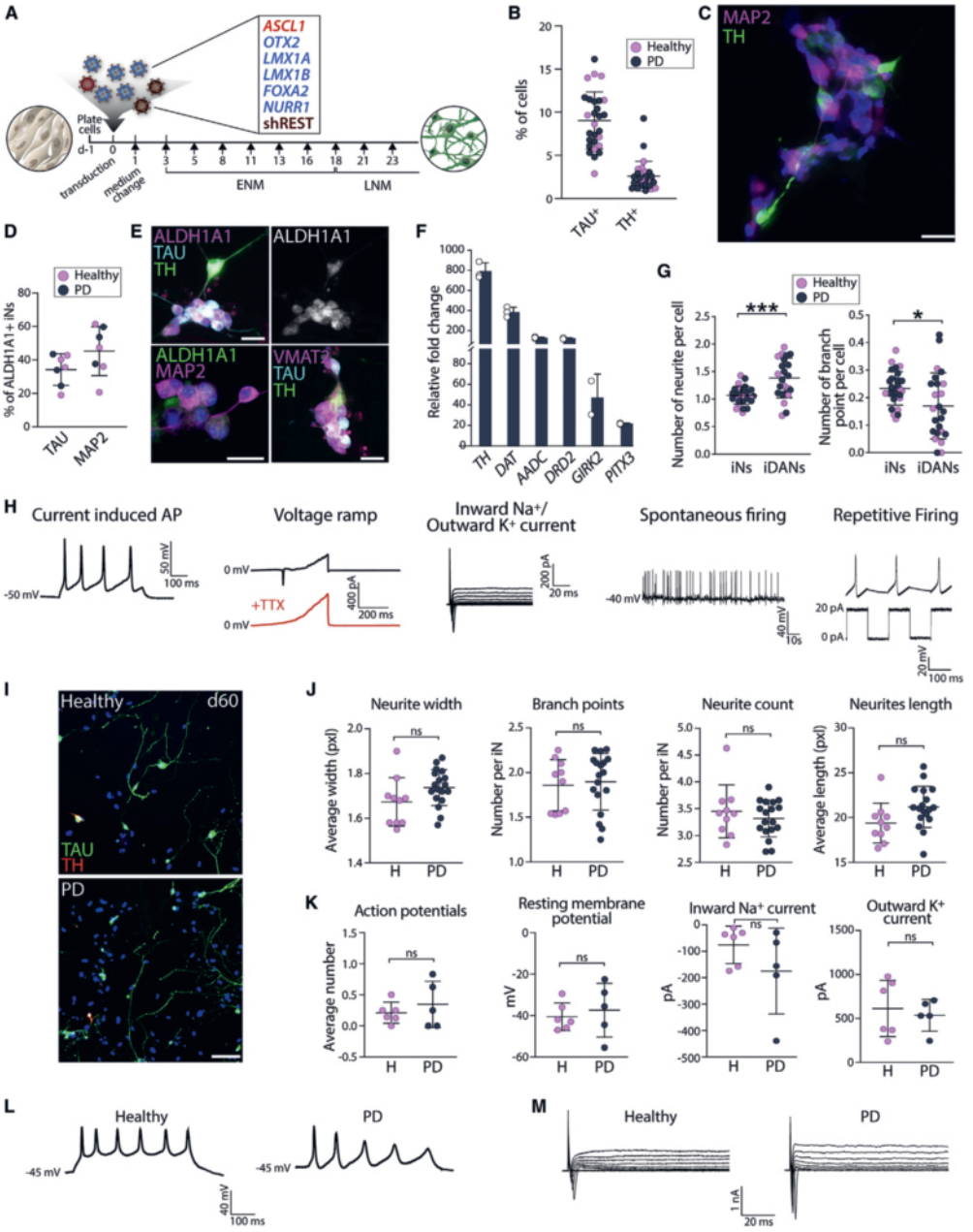

(legend on next page)

generate DA neurons from aHDFs of elderly donors in numbers required for further downstream experimental studies. Therefore, we first identified a combination of reprogramming factors that resulted in the efficient generation of subtype-specific and functional induced DA neurons (iDANs) when converting aHDFs from aged individuals. Subsequently, we used this protocol to convert iDANs from idiopathic PD patient-derived aHDFs as well as age- and sex-matched controls.

When analyzing the patient-derived neurons, we found stress-induced chaperone-mediated autophagy (CMA) and macroautophagy impairments in the idiopathic PD iNs but not in control iNs or in parental aHDFs of the patients. This type of pathology has previously only been captured in genetic PD variants using iPSC-based models (Sánchez-Danés et al., 2012; Schöndorf et al., 2014), and we hypothesized that the ability to do so in idiopathic PD iNs as reported here is related to maintenance of donor age in the iNs. To test this, we established iPSCs from a subset of the same patients. This analysis confirmed that fibroblast-derived iNs maintain expression of age-associated genes and express mature isoforms of TAU (4R), whereas iPSC-derived iNs do not. In line with this, we were able to detect αSYN pathology in directly converted patient-derived neurons but not in iPSC-generated patient-derived neurons. This study thus reports PD-associated phenotypes in directly converted neurons from patient aHDFs and provides a new model to study idiopathic forms of PD.

RESULTS

Generation of functional iDANs from aHDFs of adult donors

To enable a cell-based model of idiopathic PD using iNs with characteristics of aged DA neurons, we screened 10 different reprogramming factors (*Ascl1*, *Lmx1a*, *Lmx1b*, *Foxa2*, *Otx2*, *Nr4a2* (*Nurr1*), *SMARCA1*, *CNPY1*, *EN1*, *PAX8*) that were selected based on their (1) role during normal DA neurogenesis (Luo and Huang, 2016), (2) expression in the normal human fetal ventral midbrain (Nelander et al., 2013), (3) value in predicting functional DA differentiation from hPSCs (Kirkeby et al., 2017), and/or (4) role on midbrain-specific chromatin modeling (Metzakopian et al., 2015). All factors were expressed in combination with the knockdown of the RE1-silencing transcription factor (*REST*) according to our published protocol for high efficiency reprograming of aHDFs (Drouin-Ouellet et al., 2017). Three of the screened combinations gave rise to a significant proportion of tyrosine hydroxylase (TH)-expressing neurons: sh*REST*, *Ascl1*, *Lmx1a*, *Lmx1b*, *Foxa2*, *Otx2* (2.21% ± 2.02), sh*REST*, *Ascl1*, *Lmx1a*, *Lmx1b*, *Foxa2*, *Otx2*, *SMARCA1* (7.50% ± 3.55%), and sh*REST*, *Ascl1*, *Lmx1a*, *Lmx1b*, *Foxa2*, *Otx2*, *Nr4a2* (Figures 1A and S1A). The best TH-positive cell yield was obtained with the last combination, which gave rise to up to 70.3% ± 0.3% of cells expressing the neuronal marker TAU, of which 16.1% ± 2.01% also expressed TH (Figure S1A),

Figure 1. Generation of iDANs from Parkinson's disease and heathy donor lines

(A) Reprogramming iDANs from adult fibroblasts.

(B) Quantification of TAU-positive and TH-positive cells (mean average of 2,575 TAU-positive and 32 TH-positive cells assessed per line, n = 28 lines). Data are expressed as mean ± the SD.

(C) TAU-positive and TH-positive iDANs. Cells are counterstained with DAPI (in blue). Scale bar, 25 μm.

(D) Quantification of ALDH1A1 and TAU or MAP2 double-positive cells (mean average of 1,652 TAU-positive and 1,258 MAP2-positive cells assessed per well from four replicates per line, n = 7 lines (lines #4, #8, #9, #10, #26, #27, and #28). Data are expressed as mean ± the SD.

(E) TAU-positive, MAP2-positive, and TH-positive iNs and iDANs expressing ALDH1A1 and VMAT2. Cells are counterstained with DAPI (in blue). Scale bars, 25 μm.

(F) Gene expression quantification of DA genes relative to parental fibroblast levels (from two to three well replicates [white dots] from line #2). Data are expressed as mean ± the SD.

(G) Quantification of the neurite profile in TAU-positive and TH-negative (iNs) versus TAU and TH double-positive cells (iDANs) from healthy and Parkinson's disease lines (mean average of 2,575 TAU-positive and 32 TH-positive cells assessed per line, n = 28 lines). Two-tailed unpaired t test with Welch's correction: ***p = 0.0004, df = 30.82; *p = 0.0245, df = 32.94. Data are expressed as mean ± the SD.

(H) Patch clamp recordings of iDANs from line #2 (at day 65).

(I) Double TAU-positive and TH-positive H-iDANs and PD-iDANs at day 60. Scale bar, 100 μm.

(J) Quantification of the neurite profile in TAU-positive H-iNs and PD-iNs (experiment has been repeated independently three times, mean average of 2,142 TAU-positive cells assessed per line, n = 10 healthy and n = 18 Parkinson's disease lines). Data are expressed as mean ± the SD.

(K) Quantification of voltage-clamp recordings of evoked action potentials (n = 8–10 neurons per line, n = 5–6 lines per group), resting membrane potential of H-iNs and PD-iNs (n = 4–9 neurons per line, n = 5–6 lines per group), inward and outward currents (n = 4–9 neurons per line, n = 5–6 lines per group). Lines #1, #2, #4, #5, #6, #8, #13, #16, #17, #24, #28 were used for patch clamp experiments. Data are expressed as mean ± the SD.

(L) Voltage-clamp recordings of repetitive evoked action potentials.

(M) Representative traces of membrane sodium and potassium currents following voltage depolarization steps in H-iNs and PD-iNs. APs, action potentials; ns, not significant; TTX, tetrodotoxin.

with an average TAU purity of 9.1% ± 3.3% and TH purity of 2.6% ± 1.7% (Figures 1B and 1C) when reprogramming all lines used in the study (see Table 1), and showed robust upregulation of DA genes as measured by RT-qPCR (Figure S1B).

Further characterization of the iNs obtained using this reprogramming factor combination showed that, in addition to TH, 35.38% ± 9.05% of the TAU-positive and 45.20% ± 14.65% of the MAP2-positive cells were also expressing ALDH1A1 (Figure 1D), which is found in a subset of A9 DA neurons that are more vulnerable to loss in PD (Poulin et al., 2014), as well as VMAT2, a key DA neuronal marker (Figure 1E). Gene expression profiling of 76 neuronal genes relating to dopaminergic, glutamatergic, and GABAergic neuronal subtypes confirmed an upregulation of key genes related to DA patterning and identity (*FOXA1*, *OTX1*, *SHH*, *PITX3*), as well as DA synaptic function, including the receptors *DRD1* to *DRD5*; the DA transporter *SLC6A3* (*DAT*); the enzymes *DDC*, *MAOA*, and *ALDH1A1*; and the A9-enriched DA marker *KCNJ6* (*GIRK2*) (Figures 1F, S1C, and S1D). Thus the iDANs expressed the key markers of the AT-DAT^{high} subgroup of the DA sublineage as identified in Tiklová et al. (2019). Finally, to get a better idea of the identity of the cells that did not convert to iNs, we performed a triple staining using MAP2 to identify iNs, as well as GFAP and collagen 1 to identify potential glial cells and cells that remained fibroblasts. We observed that some MAP2-negative cells are expressing either collagen 1 or GFAP alone, or together (Figure S1E).

Morphologically, the iNs are quite immature at this stage (i.e., day 25–30), but high-throughput image acquisition analysis showed that TH-positive iNs express significantly more neurites compared with non-TH iNs but had significantly fewer branch points (Figure 1G). Patch-clamp electrophysiological recordings 65 days post transduction confirmed that the reprogrammed cells had functionally matured (Figure 1H). They were able to fire repetitive action potentials upon injection of current as well as exhibited inward-sodium, outward-potassium currents with depolarizing steps. When a continuous depolarizing voltage ramp was applied, inward currents were seen across the membrane and could be blocked by the neurotoxin tetrodotoxin, indicating an involvement of voltage-gated sodium channels in these currents. Without any injection of current or voltage, the cells displayed spontaneous firing, and 43.8% of iNs also showed rebound action potentials and/or pacemaker-like activity typical of mesencephalic DA neurons (Figure 1H). Based on this, we refer to the cells as iDANs.

Generation of functional iDANs from aHDFs of idiopathic Parkinson's disease patients

Using this new iDAN reprogramming method, we next converted aHDFs of 18 idiopathic PD patients and 10 age- and sex-matched healthy donors (Table 1). We found that the aHDFs obtained from PD patients reprogrammed at a similar efficiency to those obtained from healthy donors (Figure 1B) and displayed a similar neuronal morphological profile (Figures 1I and 1J). When measuring their functional properties using patch clamp electrophysiological recordings, we confirmed that iNs derived from healthy donors (H-iNs) and from PD patients (PD-iNs) displayed similar functionalities in terms of the number of current-induced action potentials, resting membrane potential, and the inward-sodium, outward-potassium currents (Figures 1K–1M).

PD-iDANs show altered chaperone-mediated autophagy

To assess the presence of age- and PD-related pathological impairments in iDANs derived from idiopathic PD patients, we focused on autophagy, a lysosomal degradation pathway that is important in cellular homeostasis and the efficiency of which decreases with age (Rubinsztein et al., 2011). We first looked for CMA alterations as this is one type of autophagy that has been suggested to be implicated in the pathophysiology of PD (Cuervo et al., 2004). During CMA, HSC70 recognizes soluble proteins carrying a KFERQ-like motif and guides them to the transmembrane LAMP2a receptor. Thereafter, the protein cargo is translocated into the lysosomal lumen and, as such, the level of LAMP2a determines the rate of CMA (Klionsky et al., 2016). To induce autophagy, cells were cultured under starvation conditions, which promotes the recycling of non-essential proteins and organelles for reuse (Klionsky et al., 2016). After validating that the starvation regimen had no impact on the number of neurons and induced changes in LAMP2a and HSC70 expression using western blot (WB) (Figures S2A–S2C), we assessed CMA expression using a high-content imaging approach, which allowed us to analyze cytoplasmic puncta in parental aHDFs, iNs (TAU positive and TH negative), and iDANs (TAU positive and TH positive) in a quantitative manner, and also to determine their subcellular location. When investigating this in parental aHDFs and PD-iNs at baseline and in the context of starvation using an antibody specific to the "a" isoform of LAMP2, we observed a slight reduction in LAMP2a-positive cytoplasmic puncta in healthy donors' parental aHDFs, which was also seen in PD patients' aHDFs, although this was not significant (Figures S2F and S2G). Moreover, we did not observe a difference in LAMP2a-positive cytoplasmic puncta in the neurites of TAU-positive iNs upon starvation in both H-iNs and PD-iNs (Figures S2J and S2K). However, when looking specifically at iDANs, we observed a lower number of LAMP2a-positive cytoplasmic puncta in the neurites at baseline in the PD-iDANs compared with H-iDANs, suggesting a lower

Table 1. Demographics, clinical, and genotype data of the study participants

Line ID	Group	Sex	Age at biopsy	MAPT haplotype	Age at onset (years)	Disease duration (years)	[a]UPDRS motor decline	[a]MMSE score decline	iPSC lines
1	healthy	M	69	H1/H1					
2	healthy	F	67	H1/H1					
3	healthy	M	80	H2/H2					
4	healthy	F	75	H1/H1					healthy 4
5	healthy	M	70	H1/H2					healthy 5
6	healthy	F	70	H1/H2					
7	healthy	M	71	H1/H1					
8	healthy	F	61	H1/H2					healthy 8
9	healthy	F	66	H2/H2					
10	healthy	F	58	H1/H1					
	ratio F:M/ mean ± SD	6:4	68.7 ± 6.3						
11	PD	M	56	H1/H1	34	23	−0.32	0	
12	PD	M	60	H1/H1	48	12	−0.43	0	
13	PD	F	77	H2/H2	65	12	1.48	0	
14	PD	F	67	H1/H1	56	12	0.76	−0.07	
15	PD	F	59	H1/H1	45	15	−1.39	0	
16	PD	F	80	H1/H2	69	11	0.39	−0.07	
17	PD	M	80	H2/H2	49	33	1.70	0	
18	PD	F	87	H1/H1	72	15	0.25	−0.12	
19	PD	F	77	H1/H1	56	24	−0.42	−0.25	
20	PD	M	75	H1/H1	63	13	−1.18	0	
21	PD	M	77	H1/H1	66	11	−1.68	0	
22	PD	F	71	H1/H1	62	14	0	−0.47	
23	PD	M	72	H1/H1	70	2	1.71	−0.44	
24	PD	M	81	H1/H1	76	6	1.88	0.14	
25	PD	F	44	H1/H1	40	5	−3.56	0.15	
26	PD	F	79	H1/H1	NA	NA	NA	NA	PD 26
27	PD	F	68	H1/H1	55	15	1.65	0	
28	PD	M	57	H1/H1	50	8	NA	NA	PD 28
	ratio F:M/mean ± SD	10:8	70.4 ± 11.2		57.4 ± 11.9	12.5 ± 7.1	0.05 ± 1.5	−0.07 ± 0.18	

MMSE, Mini-Mental State Examination; NA, not available; UPDRS, Unified Parkinson's Disease Rating Scale.
[a]Average rate of decline per year over a minimum of 2 years.

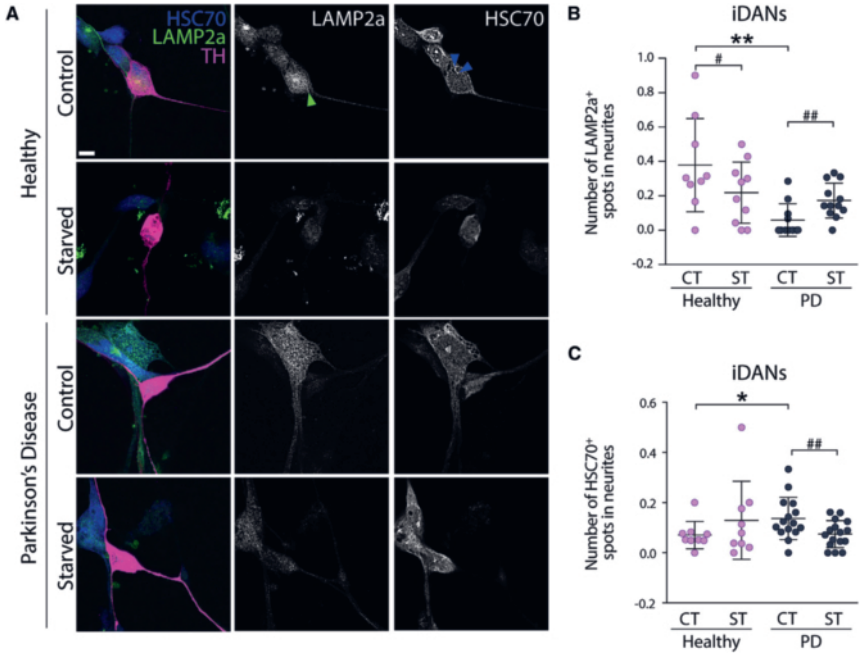

Figure 2. Chaperone-mediated autophagy impairment in PD-iDANs

(A) LAMP2a-positive dot expression and spot detection analysis of LAMP2a-positive (green arrowhead) and HSC70-positive (blue arrowheads) puncta in TH-positive iDANs. Scale bar, 10 μm.

(B) Quantification of LAMP2a-positive puncta in the neurites of TH-positive iDANs (mean average of 14 TH-positive cells assessed per line, n = 10 healthy and n = 18 Parkinson's disease lines). Kruskal-Wallis test, Dunn's multiple comparisons test: *p = 0.0067. Healthy: two-tailed paired t test, $^{\#}$p = 0.0194, df = 8. Parkinson's disease: Wilcoxon matched pairs signed rank test, $^{\#\#}$p = 0.0098, rs = 0.339. Data are expressed as mean ± the SD.

(C) Quantification of HSC70-positive puncta in neurites of TH-positive iDANs (mean average of 95 TH-positive cells assessed per line, n = 8–9 healthy and n = 16 Parkinson's disease lines). Mann-Whitney U test: *p = 0.0128, U = 26.5. Wilcoxon matched pairs signed rank test: $^{\#\#}$p = 0.0031, rs = 0.395. CT, control; H, healthy; PD, Parkinson's disease; ST, starved. Data are expressed as mean ± the SD.

basal rate of CMA in PD-iDANs (Figures 2A and 2B). Importantly, starvation induced a decrease in LAMP2a-positive cytoplasmic puncta in neurites only in H-iDANs, suggesting that PD-iDANs have an altered response to starvation, and that this alteration is specific to the DA subtype (Figures 2A and 2B). We next looked at HSC70 expression, the main chaperone responsible for the degradation of αSYN via CMA (Cuervo and Wong, 2014). Both parental aHDFs from healthy and PD donors showed a decrease in HSC70 expression in response to starvation (Figures S2H and S2I). While the number of HSC70-positive puncta in the neurites of starved H-iDANs increased (154.0% ± 117.2% of the non-starved condition), starvation-induced autophagy led to a decrease of HSC70-positive puncta in PD-iDANs (55.9% ± 28.1% of the non-starved condition) (Figure 2C). At baseline, an increase in the colocalization between HSC70 and αSYN was observed in iDANs from the PD group compared with healthy controls (Figure S2O). However, this was not accompanied by a decrease in αSYN in PD-iDANs following starvation (Figures S2P and S2Q). Taken together, these results suggest that there is both an alteration in baseline CMA as well as stress-induced autophagy that is specific to idiopathic PD-derived iDANs.

Altered macroautophagy response to stress-induced autophagy in iNs from PD patients

CMA preferentially degrades specific proteins, rather than organelles and other macromolecules (Salvador et al., 2000). However, while there is considerable crosstalk between CMA and macroautophagy, starvation predominantly induces macroautophagy, a process involving the formation of double-membraned autophagosomes that

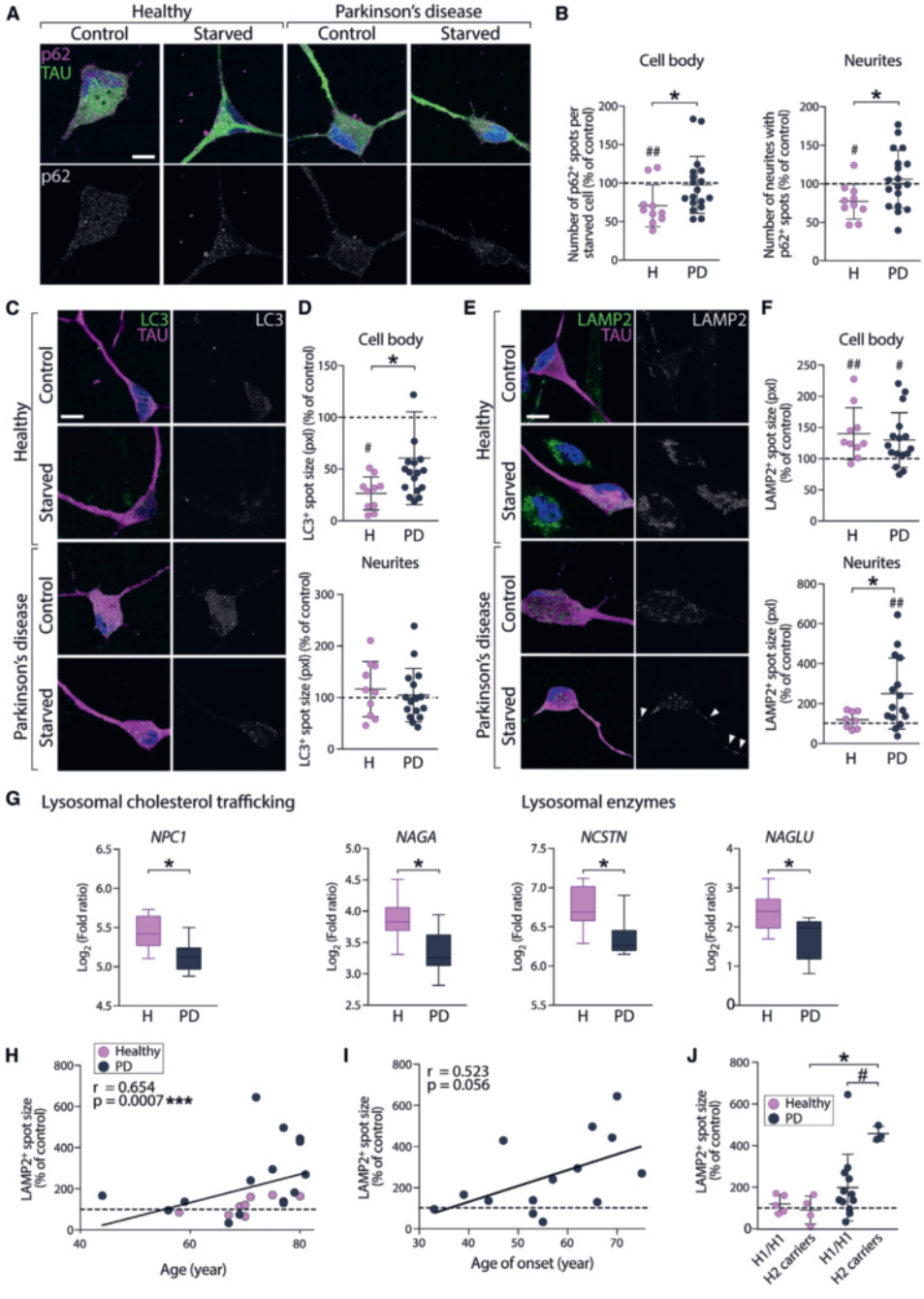

(legend on next page)

fuse with lysosomes, resulting in degradation of their contents. Given that we observed CMA alteration in PD-iDANs in response to starvation, we sought to further investigate whether there is an impairment in macroautophagy in PD-iNs. To validate the activation of macroautophagy upon starvation, we first looked at the cargo receptor p62, which decreases in the context of nutrient deprivation (Pircs et al., 2012). In the parental aHDFs, our starvation regimen induced a decrease in p62-positive cytoplasmic puncta in both healthy and PD donor-derived lines (Figures S3A and S3B). This decrease was also observed in H-iNs (70.6% ± 27.2% of the non-starved condition in the cell body and 77.1% ± 22.8% in neurites) (Figures 3A and 3B). However, once converted to neurons, the majority of PD lines failed to degrade p62 upon starvation, resulting in an accumulation of p62-positive puncta in PD-iNs compared with H-iNs, which was observed in all TAU-positive iNs, regardless of the neuronal subtype or neuronal compartment (97.5% ± 37.1% of the non-starved condition in the cell body and 106.0% ± 37.4% in neurites) (Figures 3A and 3B; see representative images of the puncta quantified in Figures S3G–S3I). We then assessed more specifically microtubule-associated protein 1 light chain 3 beta (LC3) to identify autophagic structures (Pircs et al., 2018). We found that starvation significantly reduced the size of LC3-positive cytoplasmic puncta in the cell bodies of H-iNs (26.5% ± 15.9% of the non-starved condition). However, LC3-positive cytoplasmic puncta in the cell body of PD-iNs were not significantly smaller after starvation (56.5% ± 44.2% of the non-starved condition). When comparing the level of size reduction of LC3-positive cytoplasmic puncta in the cell body after starvation, PD-iNs failed to reduce puncta size to the level that was seen in the H-iN group (Figures 3C and 3D), whereas no effect of starvation was observed in the neurites of H-iNs and PD-iNs (116.3% ± 53.6% of the non-starved condition for H-iNs, and 104.4% ± 51.8% for PD-iNs). Furthermore, this difference in macroautophagy between H-iNs and PD-iNs in the cell bodies was a cell-type-specific feature as it was not seen in the parental aHDFs (Figures S3C and S3D).

Once autophagosomes have enclosed their autophagy substrates, they can fuse with endosomes or lysosomes to form amphisomes and autolysosomes. We thus used LAMP2 (detecting all three isoforms: LAMP2a, LAMP2b, and LAMP2c) to visualize these structures. LAMP2-positive cytoplasmic puncta decreased upon starvation in the parental aHDFs of PD lines (Figures S3E and S3F). However, while an increase of the size of these structures upon starvation was similar in the cell bodies of both H- and PD-iNs (140.1% ± 41.6% of the non-starved condition for H-iNs and 130.06% ± 43.8% for PD-iNs), in the neurites, the size of LAMP2-positive puncta was unaffected by starvation in H-iNs (118.9% ± 42.3% of the non-starved condition), whereas they were significantly bigger in PD-iNs (251.8% ± 177.7% of the non-starved condition) (Figures 3E and 3F). Unlike the altered CMA

Figure 3. Accumulation of p62, LC3, and LAMP2 in PD-iNs upon starvation

(A) p62-positive dot expression in TAU-positive iNs. Scale bar, 10 μm.

(B) Quantification of p62-positive puncta in TAU-positive iNs (mean average of 577 TAU-positive cells assessed per line, n = 10 healthy and n = 18 Parkinson's disease lines). Cell body: Mann-Whitney test, *p = 0.0400; healthy, two-tailed paired t test, $^{\#\#}$p = 0.0056, df = 9. Neurite: unpaired t test, *p = 0.0357, df = 26, healthy, two-tailed paired t test, $^{\#}$p = 0.0128, df = 9. Data were normalized as percentage of control condition (not starved) and are expressed as mean ± the SD.

(C) LC3-positive dot expression in TAU-positive iNs. Scale bar, 10 μm.

(D) Quantification of LC3-positive puncta in TAU-positive iNs (mean average of 479 TAU-positive cells assessed per line, n = 10 healthy and n = 18 Parkinson's disease lines). Cell body: two-tailed Mann-Whitney U test, *p = 0.0311, U = 51; healthy, two-tailed paired t test, $^{\#\#}$p = 0.0051, df = 9. Data were normalized as percentage of control condition (not starved) and are expressed as mean ± the SD.

(E) LAMP2-positive dot expression in TAU-positive iNs. Scale bar, 10 μm.

(F) Quantification of LAMP2-positive puncta in TAU-positive iNs (mean average of 202 TAU-positive cells assessed per line, n = 10 healthy and n = 17 Parkinson's disease lines). Cell body: healthy, two-tailed paired t test, $^{\#\#}$p = 0.0078, df = 8; Parkinson's disease, $^{\#}$p = 0.0295, df = 13. Neurites: two-tailed unpaired t test with Welch's correction, *p = 0.0136, U = 24; *p = 0.0125, df = 18.23. Parkinson's disease: two-tailed paired t test, $^{\#\#}$p = 0.0042, df = 16.75. Data were normalized as percentage of control condition (not starved) and are expressed as mean ± the SD.

(G) Boxplots of $\log_2$ fold changes in expression of genes associated with lysosomal functions (adjusted p value <0.09, n = 10 healthy and n = 10 Parkinson's disease lines). Data are expressed as mean ± the SD.

(H) Accumulation of LAMP2-positive puncta upon stress-induced autophagy is associated with the age of the donor (n = 23 lines). Spearman's rank correlation: ***p = 0.0007; 95% confidence interval, 0.3199–0.8437.

(I) Association between accumulation of LAMP2-positive puncta upon stress-induced autophagy and the age of onset of Parkinson's disease (n = 14 Parkinson's disease lines). Spearman's rank correlation: p = 0.056; 95% confidence interval, 0.01127–0.8263.

(J) More pronounced accumulation of LAMP2-positive puncta upon stress in *MAPT H2* carrier Parkinson's disease patients. Kruskal-Wallis test, Dunn's multiple comparisons test: *p = 0.0265. Two-tailed Mann-Whitney U test: $^{\#}$p = 0.0250, U = 3. Data are expressed as mean ± the SD. CT, control; H, healthy; PD, Parkinson's disease; ST, starved.

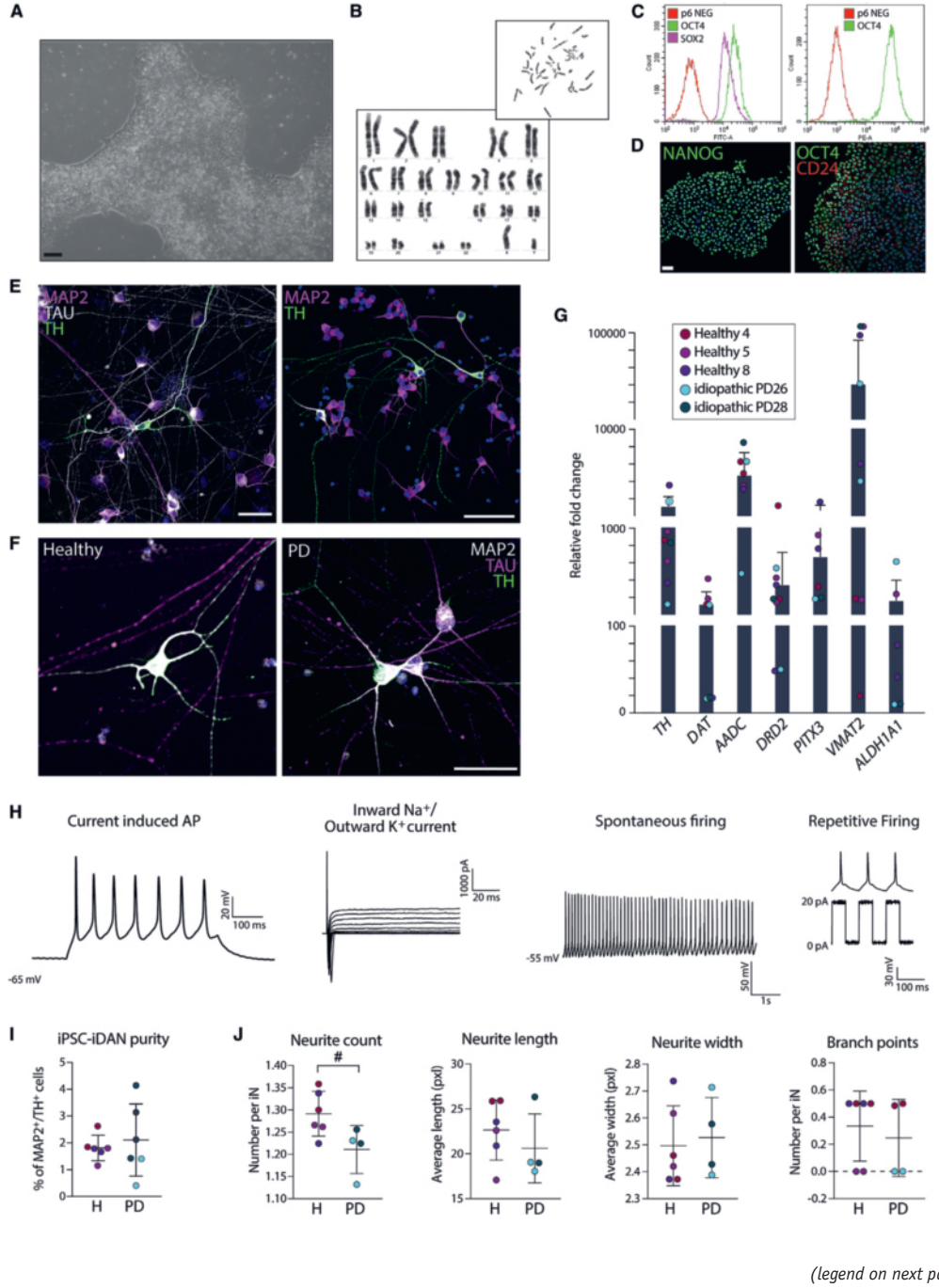

(legend on next page)

response (Figures 2A–2C), these phenotypes were present in all iNs and not just DA neurons (Figure S4). Blocking the autophagic flux using bafilomycin A1 led to an accumulation of LC3-positive puncta in the cell body of H-iNs. However, this accumulation of autophagosomes was absent in PD-iNs (Figures S6C–S6E), indicating possible impairment at early steps of the autophagic process, as also supported by a downregulation of early autophagy-related genes in PD-iNs (Figure S6F).

To assess whether this altered autophagy response could be due to basal changes in the transcriptome of PD-iNs, we performed RNA sequencing (RNA-seq) analysis on the iNs and the parental aHDFs. This analysis confirmed there was a major change in gene expression profile as aHDFs were reprogrammed toward a neuronal phenotype (Figure S5). Moreover, gene set enrichment analysis (GSEA) using Kyoto Encyclopedia of Genes and Genomes (KEGG) pathways identified genes in the lysosome pathway (hsa014142) to be significantly enriched (adjusted p value = 0.026) (Figure S6A). When analyzing specifically the lysosomal genes, we found that the lysosomal cholesterol trafficking gene *NPC1* involved in the inherited metabolic disease Niemann-Pick, type C (Park et al., 2003) as well as three other lysosomal enzymes (*NAGA*, *NCSTN*, *NAGLU*) were downregulated in PD-iNs compared to H-iNs (Figure 3G), supporting the data suggesting that there are alterations in lysosomal functions at baseline and in line with observations that these inherited disorders can lead to parkinsonian states clinically and pathologically (Winder-Rhodes et al., 2012). Importantly, when analyzing expression of these genes between the healthy controls and PD patients in parental aHDFs, they were not differentially expressed (Figure S6B).

Age-related correlation in disease-associated impairments and accumulation of phosphorylated αSYN

Recent reports have shown that age-associated properties of the human donors are maintained in iNs but not in iPSC-derived neurons (Capano et al., 2022; Huh et al., 2016; Kim et al., 2018; Mertens et al., 2015, 2021; Tang et al., 2017). We therefore assessed whether the accumulation of lysosomal structures in H- and PD-iNs was associated with the age of the donor. We found a positive correlation between the age and the accumulation of lysosomes in neurites (Figure 3H), and a trend toward a positive correlation of this accumulation with age of onset at diagnosis (Figure 3I). This was more pronounced in lines derived from patients carrying the H2 haplotype of *MAPT*, which has previously been associated with a more rapid progression and cognitive decline in PD and other neurodegenerative disorders (Figure 3J) (Valenca et al., 2016; Vuono et al., 2015).

To further study donor age and how this affects disease-related pathology, we next established iPSC lines from the aHDFs of two patients (with a high amount of pathology as quantified in the iNs derived from same patient's aHDFs) and three controls (see Table 1). The cells were reprogrammed into iPSCs using the StemRNA 3rd Generation Reprogramming Kit (Figure 4A). Quality control analysis confirmed that the iPSCs retained a normal karyotype (Figure 4B), and expression of pluripotency markers was confirmed using immunocytochemistry and flow analysis (Figures 4C and 4D). We then confirmed that the same protocol developed for the fibroblast-to-iDAN conversion (Figure 1A) also converted iPSCs to functional iDANs (Figures 4E and 4F). iPSC-iDANs expressed high levels of DA-related genes (Figure 4G) and were functionally mature (Figure 4H). Similarly to fibroblast-derived iDANs, there was no difference in neuronal purity, although a slightly lower neurite count was observed in iPSC-derived iDANs from PD patients (Figures 4I and 4J).

Next, we used RNA-seq from iNs derived from aHDFs (Fib-iNs) and iNs derived from iPSCs (iPSC-iNs) from the same individuals to assess age-related aspects in the resulting neurons (Figure 5A). First, GSEA was performed to determine if any molecular features relating to cellular

Figure 4. Generation of iDANs from iPSCs of healthy donors and idiopathic PD patients

(A) Brightfield images of fibroblasts reprogrammed to iPSCs using a StemRNA 3rd Generation Reprogramming Kit. Scale bar, 100 μm.
(B) Cells retained a normal karyotype.
(C) FACS quantification of stem cell markers OCT4, SOX2, and CD24.
(D) Immunofluorescence staining showing that cells express stem cell markers NANOG, OCT4, and CD24. Scale bar, 50 μm.
(E) MAP2-positive, TAU-positive, and TH-positive iPSC-iDANs. Cells are counterstained with DAPI (in blue). Scale bars, 100 μm.
(F) Representative images of MAP2-positive, TAU-positive, and TH-positive iPSC-iDANs derived from healthy donors and PD patients. Cells are counterstained with DAPI (in blue). Scale bars, 25 μm.
(G) Quantitative RT-PCR gene expression quantification of DA genes relative to parental iPSC levels (nine clones from five lines). Refer to Table 1 for information on each donor from which the iPSC cell lines were derived. Data are expressed as mean ± the SD.
(H) Patch clamp recordings of iDANs reprogrammed from RC17 embryonic stem cells at day 35 (n = 8 neurons).
(I) Quantification of double-MAP2-positive and TH-positive cells (from two clones; six well replicates). Data are expressed as mean ± the SD.
(J) Quantification of neurite profile in TAU-positive H-iNs and PD-iNs derived from iPSCs (from two clones; six well replicates). Data are expressed as mean ± the SD.

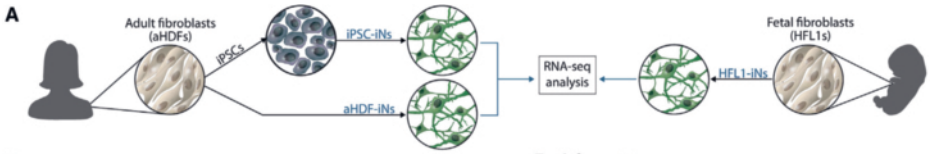

B

Description	Set size	Enrichment Score	NES	*p* value	*p*-adjust
GO_MULTICELLULAR_ORGANISM_AGING	28	-0.627	-1.872	0.003	0.015
GO_AGING	265	0.296	1.120	0.217	0.460
GO_NEGATIVE_REGULATION_OF_CELL_AGING	21	-0.432	-1.201	0.230	0.460
GO_REGULATION_OF_CELL_AGING	42	-0.320	-1.015	0.425	0.594
GO_POSITIVE_REGULATION_OF_CELL_AGING	12	-0.372	-0.887	0.581	0.594
GO_CELL_AGING	96	-0.249	-0.935	0.594	0.594

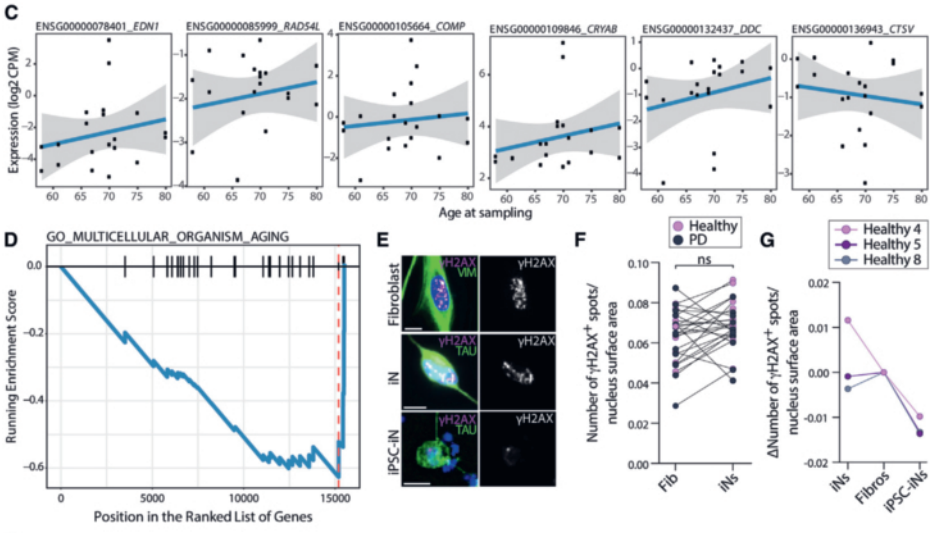

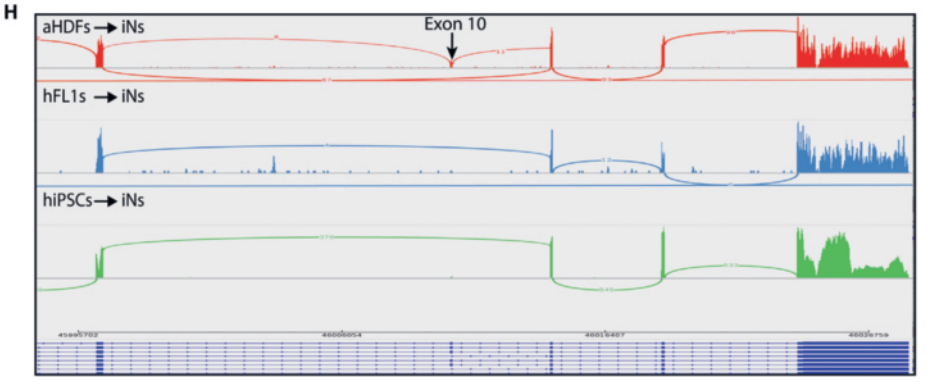

(legend on next page)

aging were associated with the donor age in Fib-iNs. Genes were ranked based on their association (using the Pearson correlation coefficient) with age at sampling and six gene sets related to aging were extracted from the Gene Ontology database. Despite the limited age span of the donors included in this analysis (58–80 years old), we observed a positive correlation between donor age with expression of an age-related gene signature (normalized enrichment score 1.4, adjusted p value = 0.015) in Fib-iNs (adjusted p value = 0.4; Figures 5B–5D). To complement the GSEA data, we also looked at DNA damage, another independent marker of cellular aging, using γH2AX. This analysis comparing the number of γH2AX spots in the nucleus of parental aHDFs with reprogrammed iNs showed a maintenance of the number of γH2AX spots after 27 days of conversion, which was not the case following reprograming of these same cell lines to iPSC-iNs, indicating a rejuvenation of the cells during reprograming to pluripotency (Figures 5E–5G). Next, we looked at the presence of the isoforms of TAU expressed in adult mature neurons. There are three TAU isoforms with three repeats (3R) and three with four repeats (4R). Neurons generated from iPSCs very strongly express the 3R isoforms but do not express the 4Rs at the protein level, even after 1 year of *in vitro* maturation (Sposito et al., 2015), reflecting the expression of only the 3Rs of TAU at the human embryonic stage. This analysis showed that exon 10 (giving rise to 4R isoforms) is only expressed in iNs from aHDFs (in ∼40% of transcripts), and not in iNs derived from fetal fibroblasts or from iPSCs (Figure 5H). Moreover, the 3R/4R ratio for aHDFs was 23%, whereas it was <1% for hFL1s. Taken together, this analysis suggests that donor age is at least partially maintained during iN conversion but erased during iPSC reprogramming, similar to other reports (Capano et al., 2022; Mertens et al., 2015; Tang et al., 2017).

Phosphorylated αSYN is a hallmark of PD pathology and this has been recapitulated in some iPSC-based cellular models of genetic forms of PD (Kouroupi et al., 2017; Lin et al., 2016) but not idiopathic PD. We therefore sought to investigate whether alterations in stress-induced autophagy observed in Fib-iNs from idiopathic PD patients could lead to changes in the levels of phosphorylated αSYN at the serine 129 site (pSer129 αSYN). We found that while a concurrent activation of macroautophagy by starvation and a blockage of the flux with bafilomycin A1 did not induce significant changes in pSer129 αSYN in H-iNs (83.1% ± 53.9% of the starved condition), it did lead to an increase in the number of PD-iNs with pSer129 αSYN-positive cytoplasmic dots (126.5% ± 54.0% of the starved condition) (Figures 6A and 6B). This increase was also observed when looking specifically at PD-iDANs (128.1% ± 21.4% of the starved condition), compared with H-iDANs, which again did not show any changes in pSer129 αSYN upon bafilomycin A1 treatment (98.2% ± 16.0% of the starved condition) (Figures 6D and 6E). Positive correlation between the accumulation of 81A-positive puncta in two independent experiments evaluating the pSer129 αSYN spot expression in iNs and in iDANs showed that the same cell lines are prone to pSer129 αSYN accumulation independently of the neuronal subtype, and demonstrates the reproducibility of these experiments (Figure S6G). Interestingly, for some of the results including pSer129 αSYN, p62, and LAMP2 accumulation, subanalyses allowed a stratification of the PD patient population based on their age and age at onset (Figures S3J and S6I). Finally, to assess whether elevated basal levels of total αSYN could explain the elevated levels of pSer129 αSYN observed in lines starved and treated with bafilomycin A1, we plotted the measure of the total αSYN fluorescence intensity against the pSer129 αSYN expression

Figure 5. Assessment of cellular aging

(A) Overview of RNA-seq experiment.

(B) Gene set enrichment analysis (GSEA) showing enrichment scores of pathways related to cell aging.

(C) Top genes showing a clear increase in expression with age were extracted from the Gene Ontology database and queried against using GSEA (as implemented in the clusterProfiler R package). Five out of six of these gene sets showed negative enrichment scores, indicating association of aging with donor age in this dataset.

(D) Multicellular organism aging showing a significant enrichment score.

(E) Representative image of γH2AX expression in TAU-positive iNs, parental fibroblasts and iPSC-iNs, all from line #18 (87 years old). Scale bar, 10 μm.

(F) Quantification of γH2AX-positive puncta in TAU-positive iNs and parental fibroblasts (mean average of 1,327 fibroblasts and 1,210 TAU-positive cells assessed per line, n = 26 lines). Two-tailed paired t test: p = 0.071, df = 25.

(G) Quantification of γH2AX-positive puncta in TAU-positive iNs, parental fibroblasts and iPSC-iNs (mean average of n = 329 fibroblasts, n = 833 TAU-positive iNs, and n = 24 iPSC-iNs assessed per line, n = 3 lines). Refer to Table 1 for the information of each donor from which the iPSC cell lines were derived.

(H) Sashimi plots visualizing splice junctions and genomic coordinates from merged bam files from adult Fib-iNs (red) and fetal Fib-iNs (blue) indicating that expression of exon 10 (4R isoforms) is only present in iNs from adult fibroblasts. Height of bars indicates expression level and the number on the lines gives number of reads spanning that splice junction. ns, not significant; Vim, vimentin.

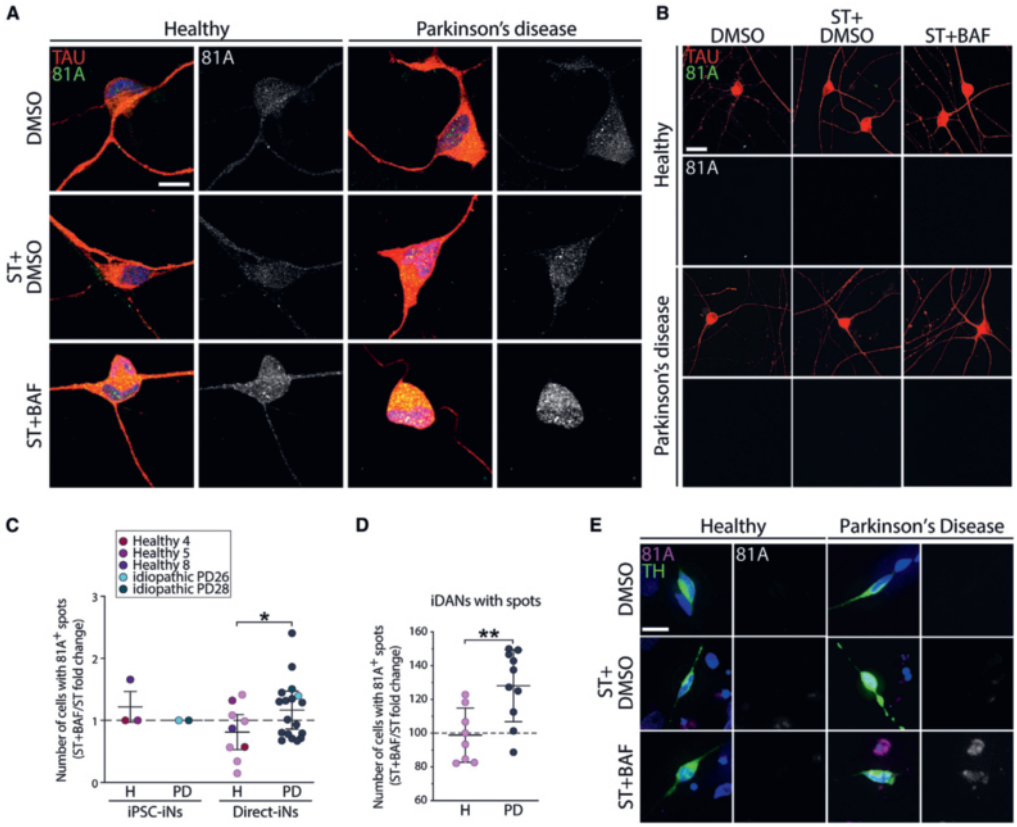

Figure 6. Autophagy impairments lead to an accumulation of phosphorylated αSYN in PD-iNs and PD-iDANs

(A) Confocal images of 81A-positive dot expression in TAU-positive iNs directly reprogrammed from fibroblasts. Scale bar, 10 μm.

(B) Fluorescent images of 81A-positive dot expression in TAU-positive iNs reprogrammed from iPSCs. Scale bar, 25 μm.

(C) Quantification of TAU-positive iNs with 81A-positive (pSer129 αSYN) puncta in the cell body (iPSCs-iNs: mean average of 180 TAU-positive cells assessed per line, n = 3 healthy and n = 2 PD lines. Direct-iNs: mean average of 1,461 TAU-positive cells assessed per line, n = 9 healthy and n = 18 PD lines). Two-tailed unpaired t test: *p = 0.0329, df = 25. Refer to Table 1 for the information of each donor from which the iPSC cell lines were derived. Data are expressed as mean ± the SD.

(D) Quantification of TAU-positive/TH-positive iDANs with 81A-positive puncta in the cell body (mean average of 28 TAU-positive/TH-positive cells assessed per line, n = 8 healthy and n = 10 PD lines). Two-tailed unpaired t test: **p = 0.0054, df = 16. Data are expressed as mean ± the SD.

(E) 81A-positive dot expression (in magenta) in TH-positive iDANs (in green) directly reprogrammed from fibroblasts. Scale bar, 25 μm.

BAF, bafilomycin A1; H: healthy; PD, Parkinson's disease; ST, starved.

measured in iDANs. There was no correlation between basal total αSYN levels and the bafilomycin A1-induced accumulation of pSer129 αSYN in iDANs (Figure S6H), suggesting that the increase seen in the PD group is not due to higher basal αSYN expression (Figures S2L–S2N). When assessing iN reprogrammed from iPSCs established from the two PD lines showing the most pSer129 αSYN accumulation in fibroblast-derived iNs and iDANs as well as three control lines (Table 1), we could not detect any pSer129 αSYN puncta in the resulting iPSC-iNs in these lines (Figures 6B and 6C), supporting that the maintenance of age in iNs is important for modeling the αSYN pathophysiology of idiopathic PD.

DISCUSSION

We report on an improved cellular model of idiopathic PD using a *REST* knockdown approach to enable neuronal gene transcription in aHDFs (Drouin-Ouellet et al., 2017), combined with an optimal combination of DA fate determinants (*Lmx1a*, *Lmx1b*, *Foxa2*, *Otx2*, *Nr4a2*). This new direct reprogramming approach increased the efficiency, subtype identity, and functional maturation of iDANs during direct conversion, making it possible to perform studies at a scale suitable for disease modeling, drug screening, and other biomedical applications. The model is much less labor intensive and cost-effective than iPSC-modeling, which allowed us to compare iNs from 18 different idiopathic PD patients that were all processed at the same time. Moreover, it maintains the donor's age and reflect pathological changes after only 25 days.

We observed alterations in stress-induced autophagy across the different patient-derived iNs compared with healthy donor lines. We found that blocking the autophagic flux through the inhibition of the fusion of autophagosomes with lysosomes resulted in accumulation of pSer129 αSYN in PD-iNs and PD-iDANs. These impairments of autophagy-lysosomal function may reflect the effect of the important presence of variants of genes related to lysosomal storage disorders in the PD patient population. Indeed, a recent study reported that more than half of the cases in a PD patient cohort harbored one or more putative damaging variants among the lysosomal storage disorders genes, suggesting the possibility that these variants may interact in a multi-hit, combinatorial manner to degrade lysosomal function, causing the accumulation of αSYN and increasing susceptibility to PD (Robak et al., 2017). Future studies using lines derived from patients with strong genetic forms of PD will also help our understanding of the phenotypes found in the idiopathic PD lines and how they relate to different pathways disrupted in familial PD.

Disease-associated impairment could not be detected in the parental aHDFs, nor in the same cells when they were first reprogrammed to pluripotency and then converted to DA neurons. This shows that direct conversion of aHDFs, where age-related aspects of the donor are maintained, provides a faithful cell-based model of idiopathic PD. Importantly, our cellular model showed that iNs from different patients are not impaired to the same degree. We found that the degree of impairment relates, at least to some extent, to the age of the donor, the age at PD onset, and the *MAPT* haplotype. This effect of age and genetic variance on disease pathology has not been recapitulated in cellular models before, and suggests that direct conversion to iDANs could be used for differential diagnostics, drug screening, and disease modeling of late-onset neurogenerative diseases while also capturing the heterogeneity of disease that is apparent clinically.

In this respect, our results demonstrate the utility of establishing models of neurodegenerative disorders with cells that resemble the subtype and functionality of the affected neurons in individual patients as closely as possible. For example, we could not detect any autophagy-related impairment in the aHDFs prior to conversion, clearly demonstrating that the reprogramming to neurons is essential to reveal disease-related phenotypes. Also, specific CMA impairments were detected only in iNs with a DA phenotype.

While it is hard to draw exact parallels between stem-cell derived neurons formed via developmental principles and directly converted neurons, both systems have their own merits. Of importance here is that the aging signature of the donor cell is maintained during direct conversion when postmitotic neurons are formed without a proliferative intermediate. Our data support the maintenance of donor age, which uniquely allows for modeling age-related aspects of PD. Future studies using this cellular model will thus contribute to a deeper understanding of the age-associated pathology of PD along with the cellular basis of disease subtypes and variable progression and, by so doing, allow us to better develop and assess novel therapeutic interventions.

EXPERIMENTAL PROCEDURES

Cell lines

aHDFs were obtained from the Parkinson's Disease Research Clinic at the John van Geest Centre for Brain Repair (Cambridge, UK) and used under full local ethical approvals: REC 09/H0311/88 (University of Cambridge) and CERSES-18-004-D (University of Montreal) (Table 1). The subjects' consent was obtained according to the declaration of Helsinki. Cell lines used in this study will be made available to others subject to appropriate ethical approval and an MTA from the requestor. For biopsy sampling information see Drouin-Ouellet et al. (2017).

Neural reprogramming

For direct neural reprogramming, aHDFs were plated at a density of 26,300 cells/cm^2 in 24-well plates (Nunc) according to a previously published protocol (Shrigley et al., 2018). Prior to plating, the wells were coated overnight with either 0.1% gelatin (Sigma), or a combination of polyornithine (15 μg/mL), fibronectin (0.5 ng/μL), and laminin (5 μg/mL). To assess the reprogramming efficiency of each line, all 28 lines were reprogrammed at the same time with the same virus mixture, and this was repeated three times using different batches of virus for each of the eight lentiviral vectors required for the iDAN reprogramming.

Starvation and bafilomycin A1 treatment

On day 28 following viral transduction, iNs were starved for 4 h by replacing the culture medium with HBSS and Ca^{2+}/Mg^{2+} and

compared with the condition without starvation, where cells were left in their original culture medium. The duration of starvation treatment was chosen based on a starvation curve performed on the iNs (0, 2, and 4 h), which showed clear increases in p62 and LC3 expression by WB in the absence of neuronal cell death (Figures S2D and S2E). For the experiment with bafilomycin A1, cells were starved in HBSS Ca^{2+}/Mg^{2+} containing bafilomycin A1 (100 nM; Sigma Aldrich) for 2 h and compared with cells incubated in HBSS Ca^{2+}/Mg^{2+} containing dimethyl sulfoxide (DMSO; vehicle). This regimen was chosen based on the increase of LC3-II and the LC3-II/LC3-I ratio as assessed by WB. At the end of the incubation period, cells were fixed in 4% paraformaldehyde.

High-content screening quantifications

The total number of DAPI-positive, TAU-positive, and TH-positive cells per well, as well as the average fluorescence intensity for αSYN, was quantified using the Cellomics Array Scan (Array Scan VTI, Thermo Fisher). Average dot number and size were measured in those neurons in which the cytoplasm and neurites were defined by TAU or TH staining. Puncta of p62, LC3, LAMP2, LAMP2a, HSC70, αSYN, and 81A were detected (using a spot-detection program) and measured in each case. Images with cells with extreme values were manually verified to make sure that poor focus was not underlying these results. The primary antibodies used are listed in Table S1. Cell images in Figures 2, 3A, 3C, 3E, 6A, 6B, and 6E are representatives images acquired by confocal microscopy (Zeiss LSM800) at 63×.

Statistical analysis

All data are expressed as mean ± the SD. Whenever the analysis is performed with one cell line, three to four well replicates were used. In case of experiments using multiple cell lines, we used a minimum of n = 6 to account for inter-individual variation. A Shapiro-Wilk normality test was used to assess the normality of the distribution. When a normal distribution could not be assumed, a non-parametric test was performed. Groups were compared using a one-way ANOVA with a Bonferroni post hoc or a Kruskal-Wallis test with a Dunn's multiple comparisons tests. To determine whether there was a significant difference between two sets of observations repeated on the same lines, a paired sample t test was also performed. In cases of only two groups, they were compared using a Student's t test. An F test was used to compare variance and, in cases of unequal variance, a Welch's correction test was then performed. Statistical analyses were conducted using the GraphPad Prism 7.0. An alpha level of $p < 0.05$ was set for significance.

See supplemental experimental procedures for further details.

Data and code availability

The accession number for the RNA-seq dataset reported in this paper is GEO: GSE125239.

SUPPLEMENTAL INFORMATION

Supplemental information can be found online at https://doi.org/10.1016/j.stemcr.2022.08.010.

AUTHOR CONTRIBUTIONS

J.D.-O., K.P., J.J., R.A.B., and M. Parmar designed the research. J.D.-O., E.M.L., F.N., K.P., J.B., F.P., M.B., S.S., M. Pereira, A.B., M.K., R.V., T.B.S., and K.P. performed the research. D.R.O., A.F., and R.A.B. contributed new reagents/analytic tools. J.D.-O., E.M.L., F.N., K.P., J.B., F.P., M.B., S.S., P.S., Y.S., R.V., and K.P. analyzed data. J.D.-O. and M. Parmar wrote the first draft of the paper.

ACKNOWLEDGMENTS

We thank Marie Persson Vejgården, Sol Da Rocha Baez, Ulla Jarl (Lund University), as well as Dr. Anna Hammarberg at the MultiPark Cellomics platform at Lund University and Simon-Pierre Gravel (U. Montreal) for their valuable help with high content imaging. This research has received funding from the NYSCF, the ERC FP/2007–2013 NeuroStemcellRepair (no. 602278 and ERC no. 771427), the Swedish Research Council (2016-00873), Parkinsonfonden, Hjärnfonden (FO2019-0301), Olle Engkvist Foundation 203-0006 (J.J.), the Strategic Research Areas at Lund University MultiPark and StemTherapy, the Cure Parkinson's Trust in the UK (RAB), and Parkinson Canada (2018-00236) (J.D.-O.). This research was also supported by the Canada Research Chair Program and the NIHR Cambridge Biomedical Research Centre (BRC-1215-20014). The views expressed are those of the authors and not necessarily those of the NIHR or the Department of Health and Social Care. This research was funded in part by the Wellcome Trust 203151/Z/16/Z. For the purpose of open access, the author has applied a CC BY public copyright license to any author-accepted manuscript version arising from this submission. R.A.B. was a NIHR Senior Investigator. M. Parmar is an NYSCF - Robertson Investigator. J.D.-O. is a Canada Research Chair and received support from FRQS in partnership with Parkinson Québec (#268980) and the Canada Foundation for Innovation (#38354). M.B. and S.S. were funded by the European Union Horizon 2020 Programme (H2020-MSCA-ITN-2015; no. 676408). E.M.L. is supported by an FRQS Graduate Scholarship in partnership with Parkinson Canada.

CONFLICTS OF INTERESTS

M. Parmar, J.J., and J.D.-O. are co-inventors of the patent application PCT/EP2018/062261 owned by New York Stem Cell Foundation. M. Parmar is the owner of Parmar Cells AB.

Received: August 24, 2021
Revised: August 25, 2022
Accepted: August 25, 2022
Published: September 22, 2022

REFERENCES

Ambasudhan, R., Talantova, M., Coleman, R., Yuan, X., Zhu, S., Lipton, S.A., and Ding, S. (2011). Direct reprogramming of adult human fibroblasts to functional neurons under defined conditions. Cell Stem Cell *9*, 113–118.

Brazdis, R.M., Alecu, J.E., Marsch, D., Dahms, A., Simmnacher, K., Lörentz, S., Brendler, A., Schneider, Y., Marxreiter, F., Roybon, L., et al. (2020). Demonstration of brain region-specific neuronal

vulnerability in human iPSC-based model of familial Parkinson's disease. Hum. Mol. Genet. *29*, 1180–1191.

Caiazzo, M., Dell'Anno, M.T., Dvoretskova, E., Lazarevic, D., Taverna, S., Leo, D., Sotnikova, T.D., Menegon, A., Roncaglia, P., Colciago, G., et al. (2011). Direct generation of functional dopaminergic neurons from mouse and human fibroblasts. Nature *476*, 224–227.

Capano, L.S., Sato, C., Ficulle, E., Yu, A., Horie, K., Kwon, J.S., Burbach, K.F., Barthélemy, N.R., Fox, S.G., Karch, C.M., et al. (2022). Recapitulation of endogenous 4R tau expression and formation of insoluble tau in directly reprogrammed human neurons. Cell Stem Cell *29*, 918–932.e8.

Cuervo, A.M., Stefanis, L., Fredenburg, R., Lansbury, P.T., and Sulzer, D. (2004). Impaired degradation of mutant alpha-synuclein by chaperone-mediated autophagy. Science *305*, 1292–1295.

Cuervo, A.M., and Wong, E. (2014). Chaperone-mediated autophagy: roles in disease and aging. Cell Res. *24*, 92–104.

Drouin-Ouellet, J., Lau, S., Brattås, P.L., Rylander Ottosson, D., Pircs, K., Grassi, D.A., Collins, L.M., Vuono, R., Andersson Sjöland, A., Westergren-Thorsson, G., et al. (2017). REST suppression mediates neural conversion of adult human fibroblasts via microRNA-dependent and -independent pathways. EMBO Mol. Med. *9*, 1117–1131.

Huh, C.J., Zhang, B., Victor, M.B., Dahiya, S., Batista, L.F., Horvath, S., and Yoo, A.S. (2016). Maintenance of age in human neurons generated by microRNA-based neuronal conversion of fibroblasts. Elife *5*, e18648.

Jiang, H., Xu, Z., Zhong, P., Ren, Y., Liang, G., Schilling, H.A., Hu, Z., Zhang, Y., Wang, X., Chen, S., et al. (2015). Cell cycle and p53 gate the direct conversion of human fibroblasts to dopaminergic neurons. Nat. Commun. *6*, 10100.

Kim, Y., Zheng, X., Ansari, Z., Bunnell, M.C., Herdy, J.R., Traxler, L., Lee, H., Paquola, A.C.M., Blithikioti, C., Ku, M., et al. (2018). Mitochondrial aging defects emerge in directly reprogrammed human neurons due to their metabolic profile. Cell Rep. *23*, 2550–2558.

Kirkeby, A., Nolbrant, S., Tiklova, K., Heuer, A., Kee, N., Cardoso, T., Ottosson, D.R., Lelos, M.J., Rifes, P., Dunnett, S.B., et al. (2017). Predictive markers guide differentiation to improve graft outcome in clinical translation of hESC-based therapy for Parkinson's disease. Cell Stem Cell *20*, 135–148.

Klionsky, D.J., Abdelmohsen, K., Abe, A., Abedin, M.J., Abeliovich, H., Arozena, A.A., Adachi, H., Adams, C.M., Adams, P.D., Adeli, K., et al. (2016). Guidelines for the use and interpretation of assays for monitoring autophagy (3rd edition). Autophagy *12*, 1–222.

Kouroupi, G., Taoufik, E., Vlachos, I.S., Tsioras, K., Antoniou, N., Papastefanaki, F., Chroni-Tzartou, D., Wrasidlo, W., Bohl, D., Stellas, D., et al. (2017). Defective synaptic connectivity and axonal neuropathology in a human iPSC-based model of familial Parkinson's disease. Proc. Natl. Acad. Sci. USA *114*, E3679–E3688.

Lang, C., Campbell, K.R., Ryan, B.J., Carling, P., Attar, M., Vowles, J., Perestenko, O.V., Bowden, R., Baig, F., Kasten, M., et al. (2019). Single-cell sequencing of iPSC-dopamine neurons reconstructs disease progression and identifies HDAC4 as a regulator of Parkinson cell phenotypes. Cell Stem Cell *24*, 93–106.e6.

Lapasset, L., Milhavet, O., Prieur, A., Besnard, E., Babled, A., Aït-Hamou, N., Leschik, J., Pellestor, F., Ramirez, J.M., De Vos, J., et al. (2011). Rejuvenating senescent and centenarian human cells by reprogramming through the pluripotent state. Genes Dev. *25*, 2248–2253.

Li, H., Jiang, H., Yin, X., Bard, J.E., Zhang, B., and Feng, J. (2019). Attenuation of PRRX2 and HEY2 enables efficient conversion of adult human skin fibroblasts to neurons. Biochem. Biophys. Res. Commun. *516*, 765–769.

Lin, L., Göke, J., Cukuroglu, E., Dranias, M.R., VanDongen, A.M.J., and Stanton, L.W. (2016). Molecular features underlying neurodegeneration identified through in vitro modeling of genetically diverse Parkinson's disease patients. Cell Rep. *15*, 2411–2426.

Luo, S.X., and Huang, E.J. (2016). Dopaminergic neurons and brain reward pathways: from neurogenesis to circuit assembly. Am. J. Pathol. *186*, 478–488.

Mertens, J., Herdy, J.R., Traxler, L., Schafer, S.T., Schlachetzki, J.C.M., Böhnke, L., Reid, D.A., Lee, H., Zangwill, D., Fernandes, D.P., et al. (2021). Age-dependent instability of mature neuronal fate in induced neurons from Alzheimer's patients. Cell Stem Cell *28*, 1533–1548.e6.

Mertens, J., Paquola, A.C.M., Ku, M., Hatch, E., Böhnke, L., Ladjevardi, S., McGrath, S., Campbell, B., Lee, H., Herdy, J.R., et al. (2015). Directly reprogrammed human neurons retain aging-associated transcriptomic signatures and reveal age-related nucleocytoplasmic defects. Cell Stem Cell *17*, 705–718.

Metzakopian, E., Bouhali, K., Alvarez-Saavedra, M., Whitsett, J.A., Picketts, D.J., and Ang, S.L. (2015). Genome-wide characterisation of Foxa1 binding sites reveals several mechanisms for regulating neuronal differentiation in midbrain dopamine cells. Development *142*, 1315–1324.

Miller, J.D., Ganat, Y.M., Kishinevsky, S., Bowman, R.L., Liu, B., Tu, E.Y., Mandal, P.K., Vera, E., Shim, J.w., Kriks, S., et al. (2013). Human iPSC-based modeling of late-onset disease via progerin-induced aging. Cell Stem Cell *13*, 691–705.

Nelander, J., Grealish, S., and Parmar, M. (2013). Human foetal brain tissue as quality control when developing stem cells towards cell replacement therapy for neurological diseases. Neuroreport *24*, 1025–1030.

Park, W.D., O'Brien, J.F., Lundquist, P.A., Kraft, D.L., Vockley, C.W., Karnes, P.S., Patterson, M.C., and Snow, K. (2003). Identification of 58 novel mutations in Niemann-Pick disease type C: correlation with biochemical phenotype and importance of PTC1-like domains in NPC1. Hum. Mutat. *22*, 313–325.

Pereira, M., Pfisterer, U., Rylander, D., Torper, O., Lau, S., Lundblad, M., Grealish, S., and Parmar, M. (2014). Highly efficient generation of induced neurons from human fibroblasts that survive transplantation into the adult rat brain. Sci. Rep. *4*, 6330.

Pfisterer, U., Kirkeby, A., Torper, O., Wood, J., Nelander, J., Dufour, A., Björklund, A., Lindvall, O., Jakobsson, J., and Parmar, M. (2011). Direct conversion of human fibroblasts to dopaminergic neurons. Proc. Natl. Acad. Sci. USA *108*, 10343–10348.

Pircs, K., Nagy, P., Varga, A., Venkei, Z., Erdi, B., Hegedus, K., and Juhasz, G. (2012). Advantages and limitations of different

p62-based assays for estimating autophagic activity in Drosophila. PLoS One *7*, e44214.

Pircs, K., Petri, R., Madsen, S., Brattås, P.L., Vuono, R., Ottosson, D.R., St-Amour, I., Hersbach, B.A., Matusiak-Brückner, M., Lundh, S.H., et al. (2018). Huntingtin aggregation impairs autophagy, leading to argonaute-2 accumulation and global MicroRNA dysregulation. Cell Rep. *24*, 1397–1406.

Poulin, J.F., Zou, J., Drouin-Ouellet, J., Kim, K.Y.A., Cicchetti, F., and Awatramani, R.B. (2014). Defining midbrain dopaminergic neuron diversity by single-cell gene expression profiling. Cell Rep. *9*, 930–943.

Robak, L.A., Jansen, I.E., van Rooij, J., Uitterlinden, A.G., Kraaij, R., Jankovic, J., International Parkinson's Disease Genomics Consortium IPDGC, Heutink, P., and Shulman, J.M. (2017). Excessive burden of lysosomal storage disorder gene variants in Parkinson's disease. Brain *140*, 3191–3203.

Rubinsztein, D.C., Mariño, G., and Kroemer, G. (2011). Autophagy and aging. Cell *146*, 682–695.

Salvador, N., Aguado, C., Horst, M., and Knecht, E. (2000). Import of a cytosolic protein into lysosomes by chaperone-mediated autophagy depends on its folding state. J. Biol. Chem. *275*, 27447–27456.

Sánchez-Danés, A., Richaud-Patin, Y., Carballo-Carbajal, I., Jiménez-Delgado, S., Caig, C., Mora, S., Di Guglielmo, C., Ezquerra, M., Patel, B., Giralt, A., et al. (2012). Disease-specific phenotypes in dopamine neurons from human iPS-based models of genetic and sporadic Parkinson's disease. EMBO Mol. Med. *4*, 380–395.

Schöndorf, D.C., Aureli, M., McAllister, F.E., Hindley, C.J., Mayer, F., Schmid, B., Sardi, S.P., Valsecchi, M., Hoffmann, S., Schwarz, L.K., et al. (2014). iPSC-derived neurons from GBA1-associated Parkinson's disease patients show autophagic defects and impaired calcium homeostasis. Nat. Commun. *5*, 4028.

Shrigley, S., Pircs, K., Barker, R.A., Parmar, M., and Drouin-Ouellet, J. (2018). Simple generation of a high yield culture of induced neurons from human adult skin fibroblasts. J. Vis. Exp. *132*, 56904.

Sposito, T., Preza, E., Mahoney, C.J., Setó-Salvia, N., Ryan, N.S., Morris, H.R., Arber, C., Devine, M.J., Houlden, H., Warner, T.T., et al. (2015). Developmental regulation of tau splicing is disrupted in stem cell-derived neurons from frontotemporal dementia patients with the 10 + 16 splice-site mutation in MAPT. Hum. Mol. Genet. *24*, 5260–5269.

Tang, Y., Liu, M.L., Zang, T., and Zhang, C.L. (2017). Direct reprogramming rather than iPSC-based reprogramming maintains aging hallmarks in human motor neurons. Front. Mol. Neurosci. *10*, 359.

Tiklová, K., Björklund, Å.K., Lahti, L., Fiorenzano, A., Nolbrant, S., Gillberg, L., Volakakis, N., Yokota, C., Hilscher, M.M., Hauling, T., et al. (2019). Single-cell RNA sequencing reveals midbrain dopamine neuron diversity emerging during mouse brain development. Nat. Commun. *10*, 581.

Valenca, G.T., Srivastava, G.P., Oliveira-Filho, J., White, C.C., Yu, L., Schneider, J.A., Buchman, A.S., Shulman, J.M., Bennett, D.A., and De Jager, P.L. (2016). The role of MAPT haplotype H2 and isoform 1N/4R in parkinsonism of older adults. PLoS One *11*, e0157452.

Vuono, R., Winder-Rhodes, S., de Silva, R., Cisbani, G., Drouin-Ouellet, J., REGISTRY Investigators of the European Huntington's Disease Network, Spillantini, M.G., Cicchetti, F., and Barker, R.A. (2015). The role of tau in the pathological process and clinical expression of Huntington's disease. Brain *138*, 1907–1918.

Winder-Rhodes, S.E., Garcia-Reitböck, P., Ban, M., Evans, J.R., Jacques, T.S., Kemppinen, A., Foltynie, T., Williams-Gray, C.H., Chinnery, P.F., Hudson, G., et al. (2012). Genetic and pathological links between Parkinson's disease and the lysosomal disorder Sanfilippo syndrome. Mov. Disord. *27*, 312–315.

PAPER III

Journal of Parkinson's Disease 11 (2021) 515–528
DOI 10.3233/JPD-202366
IOS Press

Research Report

Grafts Derived from an α-Synuclein Triplication Patient Mediate Functional Recovery but Develop Disease-Associated Pathology in the 6-OHDA Model of Parkinson's Disease

Shelby Shrigley[a,b], Fredrik Nilsson[a,b], Bengt Mattsson[a], Alessandro Fiorenzano[a,b], Janitha Mudannayake[a,b], Andreas Bruzelius[a,b], Daniella Rylander Ottosson[a,b], Anders Björklund[a], Deirdre B. Hoban[a,b,1] and Malin Parmar[a,b,1,*]

[a] *Wallenberg Neuroscience Center, Department of Experimental Medical Science, Lund University, Lund, Sweden*
[b] *Lund Stem Cell Center, Lund University, Lund, Sweden*

Accepted 3 December 2020
Pre-press 23 December 2020

Abstract.
Background: Human induced pluripotent stem cells (hiPSCs) have been proposed as an alternative source for cell replacement therapy for Parkinson's disease (PD) and they provide the option of using the patient's own cells. A few studies have investigated transplantation of patient-derived dopaminergic (DA) neurons in preclinical models; however, little is known about the long-term integrity and function of grafts derived from patients with PD.
Objective: To assess the viability and function of DA neuron grafts derived from a patient hiPSC line with an α-synuclein gene triplication (AST18), using a clinical grade human embryonic stem cell (hESC) line (RC17) as a reference control.
Methods: Cells were differentiated into ventral mesencephalic (VM)-patterned DA progenitors using an established GMP protocol. The progenitors were then either terminally differentiated to mature DA neurons *in vitro* or transplanted into 6-hydroxydopamine (6-OHDA) lesioned rats and their survival, maturation, function, and propensity to develop α-synuclein related pathology, were assessed *in vivo*.
Results: Both cell lines generated functional neurons with DA properties *in vitro*. AST18-derived VM progenitor cells survived transplantation and matured into neuron-rich grafts similar to the RC17 cells. After 24 weeks, both cell lines produced DA-rich grafts that mediated full functional recovery; however, pathological changes were only observed in grafts derived from the α-synuclein triplication patient line.
Conclusion: This data shows proof-of-principle for survival and functional recovery with familial PD patient-derived cells in the 6-OHDA model of PD. However, signs of slowly developing pathology warrants further investigation before use of autologous grafts in patients.

Keywords: Parkinson's disease, alpha-synuclein, cell transplantation, dopaminergic neurons

[1] These authors contributed equally to this work.

*Correspondence to: Professor Malin Parmar, Wallenberg Neuroscience Center, BMC A11, Lund University, 221 84 Lund, Sweden. Tel.: +46 46 222 06 20; E-mail: malin.parmar@med.lu.se.

INTRODUCTION

Parkinson's disease (PD) is one of the most common neurodegenerative disorders, affecting millions of people worldwide. It is characterized primarily by the loss of dopaminergic (DA) neurons in the substantia nigra *pars compacta*, degeneration of the nigrostriatal pathway, and the presence of pathological protein inclusions known as Lewy bodies. For decades cell replacement therapy, where the aim is to replace the lost DA neurons with new healthy ones, has been explored as a treatment for PD [1]. In early clinical trials, patients were transplanted with DA progenitors obtained from fetal ventral mesencephalic (VM) tissue [2, 3]. These efforts showed proof-of-principle for graft survival and long term clinical benefit, albeit with varying outcomes [4–8]. However, fetal tissue is scarcely available, and its use for transplantation is associated with a number of ethical and practical issues. Alternative cell sources are therefore required for wide use of cell replacement therapy in PD.

Recent advances in stem cell biology now make it possible to generate DA progenitors from human embryonic stem cells (hESCs) and human induced pluripotent stem cells (hiPSCs) *in vitro* with high similarity to authentic midbrain DA neurons [9–11]. These pluripotent stem cell-derived DA neurons represent a scalable source of cells that can be standardized, and quality controlled prior to transplantation. Additionally, the use of hiPSCs provides the option to use the patient's own cells for transplantation. Autologous cell replacement therapy has the advantage that the patient may not require immunosuppressive drugs, therefore avoiding any associated complications [12–16].

In some patients who received fetal VM transplants, postmortem analysis revealed the presence of slowly developing pathological or phosphorylated α-synuclein (pSyn) inclusions within the grafted cells [17–21]. Currently, it remains unclear if patient-derived VM progenitors would be inherently more susceptible to develop pathology in the grafted DA neurons than cells from healthy donors over time. A number of *in vitro* studies suggest that patient-derived DA neurons, especially those from familial forms of PD, are more vulnerable to dysfunction and protein inclusions due to their disease-specific backgrounds [22–26]. However, only a small number of studies have investigated transplantation of patient-derived DA neurons in preclinical models of PD using hiPSCs derived from sporadic PD patients [11, 27–29]. None of these studies reported any evidence of pathology in the transplant, however, given the extensive time it takes for pathology to develop in patients who received fetal VM transplants (>10 years), it may be too early to observe any pathological changes in cells from sporadic PD patients in these models.

In this study, we used a hiPSC line derived from an individual with a triplication mutation in *SNCA,* the gene encoding for α-synuclein (αSyn). Mutations in the *SNCA* gene have been linked to familial forms of PD [30–32] and variation at this locus (4q22) is also the most significant risk factor for sporadic PD [33, 34]. The αSyn triplication mutation leads to three copies of the gene on the first allele and one copy on the second allele, totaling 4 copies of the *SNCA* gene. This results in a doubling of messenger RNA and αSyn protein expression [26, 31, 35]. Since αSyn forms a major component of Lewy body pathology [36], and the triplication mutation is associated with early onset and rapidly progressing PD [31], we hypothesized that αSyn pathology, if present, would develop earlier in these grafts. Therefore, to investigate how cells with αSyn triplication mature and function, and if they develop any pathology after extended time periods after transplantation, we transplanted DA neurons derived from the Alpha Synuclein Triplication line AST18 [35] into the 6-hydroxydopamine (6-OHDA) preclinical model of PD. RC17, a clinical grade hESC line that has been extensively used in a number of pre-clinical studies [10, 37–39] was grafted in parallel as a control.

MATERIALS AND METHODS

Terminal differentiation of DA neurons

hESCs (RC17; Roslin Cells) and hiPSCs (AST18) were differentiated into DA neurons as described in Nolbrant et al. 2017 [10]. Pluripotent cells were maintained on laminin-521 in iPS brew. Cells were passaged approximately every 7 days (or when reaching confluency) with EDTA using a seeding density of 2,500 cells/cm^2 in iPS brew with Y-27632. For differentiation, on day 0 cells were plated on laminin-111 coated wells in differentiation medium (N2 medium + Y-27632 + SB431542 + Noggin + Shh-C2 4II + CHIR99021), they received a medium change on day 2, 4, and 7. On day 9 the medium was changed to N2 medium + FGF8b. Cells were replated on day 11 using replating medium (B27 medium + Y-27632 + BDNF + AA + FGF8b), they also received a medium change on day 14. On d16 cells were

replated using terminal differentiation medium (B27 medium + BDNF + AA + GDNF + cAMP + DAPT), cells received a medium change every 2-3 days. From day 25 onwards, only 75 % of the medium was replaced to reduce the risk of cell detachment. Cells were fixed and analyzed after 35 days in culture.

Electrophysiology

Electrophysiological recordings were performed on cells after 35 days in culture. Cells were cultured on coverslips and transferred to a recording chamber with constant flow of Krebs solution gassed with 95% O_2 and 5% CO_2 kept at room temperature (RT). The composition of the Krebs solution was (mM) 119 NaCl, 2.5 KCl, 1.3 MgSO4, 2.5 CaCl2, 25 Glucose and 26 NaHCO3. Multiclamp 700B (Molecular Devices) and pulled glass capillaries with a resistance of 3–7 MOhm filled with intracellular solution (mM) 122.5 potassium gluconate, 12.5 KCl, 0.2 EGTA, 10 Hepes, 2 MgATP, 0.3 Na3GTP and 8 NaCl adjusted to pH 7.3 with KOH were used for recordings. Data acquisition was performed with pClamp 10.2 (Molecular Devices); current was filtered at 0.1 kHz and digitized at 2 kHz. Cells with a neuronal morphology and clear from any surface debris were selected for recordings. Immediately after establishing whole-cell access resting membrane potential (RMP) was measured in current clamp mode, and cells were kept at a holding potential of –60 to –70 mV. 500 ms long current in rheobase injection steps from –20 to + 35pA at 5pA increments was performed for evoked action potentials. For measurements of inward sodium and delayed rectifying potassium currents cells were clamped at –70 mV and voltage-depolarizing steps were delivered for 100 ms at 10 mV increments. Data analysis was performed using Igor Pro 8.04 (Wavemetrics) with NeuroMatic package [40].

Immunocytochemistry

Cells were fixed in 4% PFA for 15 min and washed twice using 0.1 M phosphate-buffered saline with potassium (KPBS, pH = 7.4). Before staining cells were washed once with KPBS and then incubated in blocking solution (KPBS containing 0.1% Triton-X and 5% serum specific to the species of the secondary antibody) for 1 h. Following this, the primary antibody in blocking solution was added overnight at 4°C. The primary antibodies used were: rabbit anti-LMX1A (1:1000, Merck Millipore ab10533), mouse anti-FOXA2 (1:500, Santa Cruz Biotechnology sc101060), goat anti-OTX2 (1:2000, R&D Systems AF1979), rabbit anti-TH (1:1000, Merck Millipore ab152), mouse anti-TAU(HT7) (1:500, Thermo Fisher Scientific MN1000), chicken anti-MAP2 (1:10000, Abcam ab5392), goat anti-GIRK2 (1:200, Merck Millipore ab65096), and mouse anti-α-synuclein (1:250, BD Biosciences 610787). The next day cells were washed three times and incubated with fluorophore-conjugated secondary antibodies (1:200, Jackson ImmunoResearch Laboratories) and DAPI in blocking solution for 2 h at room temperature (RT). Cells were then washed with KPBS a further three times and stored at 4°C until analysis.

Animals

All procedures were performed in accordance with the European Union Directive (2010/63/EU) and approved by the local ethical committee at Lund University, as well as the Swedish Department of Agriculture (Jordbruksverket). Female Sprague-Dawley (SD) rats were purchased from Charles River Laboratories and female nude athymic rats (Hsd:RH-*Foxn*1^{rnu}) were purchased from Envigo. All rats were housed in ventilated cages with *ad libitum* access to food and water under a 12- h light/dark cycle.

In vivo experimental design

SD rats received a 6-OHDA medial forebrain bundle (MFB) lesion and the extent of the lesion was confirmed by amphetamine-induced rotation test after 4 weeks. Following this, the rats received cell transplantation surgery and were perfused 8 weeks later. SD rats received daily immunosuppression via intraperitoneal injection of cyclosporine (10 mg/ kg) to prevent graft rejection. Nude athymic rats received a 6-OHDA MFB lesion and the extent of the lesion was confirmed by the amphetamine-induced rotation test after 4 weeks. Following this, the rats received cell transplantation surgery and were perfused either 7 or 24 weeks later. Behavioural recovery was assessed by amphetamine-induced rotations at 16, 18, 20, 22, and 24 weeks post-transplantation.

Preparation of DA progenitor cells for transplantation

hESCs (RC17; Roslin Cells) and hiPSCs (AST18) were differentiated into VM-patterned progenitor cells as described in Nolbrant et al. 2017 [10] and

transplanted on day 16. All cell preparation batches passed quality control checks as in the protocol (Supplementary Figure 1).

Surgeries

All surgeries were performed under general anesthesia using a solution of fentanyl (0.36 mg/kg) and medetomidine hydrochloride (dormitor; 0.36 mg/kg). Animals were placed into a stereotaxic frame and the tooth bar was adjusted to the flathead position. For the lesion surgery, 3 μL of 6-OHDA (3.5 μg/μL of free base, dissolved in ascorbate-saline) was injected unilaterally into the MFB (AP –4.4, ML –1.1, DV –7.8) at a rate of 0.3 μL per minute. For the transplant surgery, 4 μL of cell suspension (75,000 c/μL) was injected unilaterally at four sites in the striatum (SD rats: AP + 0.5, ML –3.0, DV –4.5/–5.5 and AP + 1.2, ML –2.6, DV –4.5/–5.5; nude athymic rats: AP + 0.9, ML –3.0, DV –4.0/–5.0 and AP+1.4, ML –2.6, DV –4.0/–5.0) at a rate of 1 μL per minute. After surgery, anesthesia was reversed with atipamezole (antisedan; 0.28 mg/kg) and analgesia was administered using buprenorphine (temgesic; 0.04 mg/kg).

Behavioural testing

Rotational bias was assessed by amphetamine-induced rotations both before transplantation and at several timepoints after transplantation. Animals received an intraperitoneal injection of dexamphetamine solution (3.5 mg/kg) and were placed into automated rotometer bowls for 90 min (Omnitech Electronics Inc.). Full body turns towards the side of the lesion were given positive values and turns to the opposite side given negative values, with data expressed as net turns per minute. In the behavioural assessment, only animals with complete lesions (>4 net turns/min on the amphetamine rotation test at baseline) and confirmed TH^+ cell loss in the substantia nigra *post-hoc* were included, resulting in $n = 5$ for the RC17 and $n = 5$ for the AST18 group.

Immunohistochemistry

Rats were given terminal anesthesia with a lethal dose of sodium pentobarbitone injected intraperitoneally. Animals were transcardially perfused with physiological saline solution followed by ice-cold 4% PFA. Brains were post-fixed for 24 h in 4% PFA, transferred to 25% sucrose for 48 h and then sectioned coronally using a freezing microtome at a thickness of 35 μm (1:8 series). Immunohistochemistry was performed on free floating sections and all washing steps used 0.1 M phosphate-buffered saline with potassium (KPBS, pH = 7.4).

For DAB staining, sections were washed three times and then incubated in a quench solution for 15 min at RT. After washing a further three times, the sections were incubated in blocking solution (KPBS containing 0.25% Triton-X and 5% serum specific to the species of the secondary antibody) for 1 h. Following this, the primary antibody in blocking solution was added overnight at RT. The primary antibodies used were mouse anti-hNCAM (1:1000, Santa Cruz Biotechnology sc106) and rabbit anti-TH (1:2000, Merck Millipore ab152). The next day sections were washed twice and incubated in blocking solution for 30 min. The sections were incubated with secondary biotinylated antibodies (1:200, Vector Laboratories) for 1 h at RT. After washing a further three times, sections were incubated with avidin-biotin complex (ABC) for 1 h at RT for amplification. Next, sections were incubated in 0.05% DAB for 1–2 min before addition of 0.01% H_2O_2 for 1–2 min. After development, sections were mounted on gelatin-coated slides and then dehydrated in an ascending series of alcohols, cleared in xylene, and coverslipped with DPX mountant.

For fluorescent immunolabeling, sections were washed three times and then incubated in Tris-EDTA (pH 9.0) for 30 min at 80°C for antigen retrieval. After washing a further three times, the sections were incubated in blocking solution for 1 h. Following this, the primary antibody in blocking solution was added overnight at RT. The primary antibodies used were: rabbit anti-TH (1:2000, Merck Millipore ab152), sheep anti-TH (1:1000, Merck Millipore ab1542), mouse anti-α-synuclein (211) (1:2000, Santa Cruz sc12767), rabbit anti-IBA1 (1:1000 WAKO 019-19741), mouse anti-p-synuclein (81A) (1:10000, gift from Kelvin Luk University of Pennsylvania). The next day sections were washed twice and incubated in blocking solution for 30 min. The sections were incubated with fluorophore-conjugated secondary antibodies (1:200, Jackson ImmunoResearch Laboratories) for 1 h at RT. After washing a further three times, sections were mounted on gelatin-coated slides and coverslipped with PVA-DABCO containing DAPI (1:1000).

Graft quantifications

Photomicrographs of hNCAM stained coronal sections were taken at the level of the striatum. To

determine graft volume, the area of the graft core in every eighth section through the graft was measured using ImageJ (version: 2.0.0-rc-69/1.52p) and calibrated by associating the number of pixels with a known measurement, obtained from a scale taken as a photomicrograph using the same resolution and settings. The graft volume was calculated according to Cavalieri's principle, given the known distance between each section and the known section thickness. To determine the DA neuron yield, the number of DAB-stained TH^+ neurons in each section was counted manually using the Olympus AX70 inverted microscope at 20x magnification in brightfield. Final counts were adjusted for the number of series (1:8), and Abercrombie's formula was used for correction of cell counts in histological sections to get an estimate of the total number of TH^+ cells within the graft.

For the counts of $pSyn^+$ pathology inside TH^+ and $IBA1^+$ cells, fluorescent images were taken on a TCS SP8 laser scanning confocal microscope at 20X objective magnification, and collected in a 3D stack (775 × 775 μm x *ca*25 μm). The scan resolution was 2048x2048 and scanning speed 200 MHz interval of every 1 μm (z-stack). Microglia size was calculated by determining the total volume of stained $IBA1^+$ cells determined by threshold in the collected 3D stack, divided by the number of $IBA1^+$ cells in each stack. Microglia density was calculated by the number of microglia/stack. TH^+ and $IBA1^+$ cells were identified and assessed for co-expression of $pSyn^+$ inclusions using Volocity software. 15 animals were quantified (7 in the RC17 group and 8 in the AST18 group), with 5730 $IBA1^+$ cells counted in total (mean 382 $IBA1^+$ cells per animal) and 2703 TH^+ cells counted in total (mean 180 TH^+ cells per animal).

RESULTS

αSyn triplication does not significantly affect differentiation towards DA neurons in vitro

In order to confirm previous findings that the αSyn triplication line does not affect differentiation into DA neurons *in vitro* [35], we performed an experiment with both the AST18 and RC17 lines patterned towards a VM fate using our previously published GMP differentiation protocol [10]. Immunostaining on day 35 showed high expression of neuronal markers TAU and MAP2, as well as the DA marker TH in both cultures (Fig. 1A). Moreover, RC17-derived and AST18- derived cells expressed FOXA2 and GIRK2, indicating subtype-specific maturation (Fig. 1B, C). At this timepoint αSyn was expressed in both cultures (Fig. 1D).

We also assessed the functional maturity of the DA neurons at day 35 *in vitro* using whole-cell patch-clamp recordings. This revealed similar resting membrane potential, and both lines displayed the ability to produce evoked action potentials from current injection (Fig. 1E, F). Moreover, cells exhibited voltage gated sodium (Na^+) and potassium (*K*+) currents with no major differences between the cell lines (Fig. 1G). This demonstrates that both RC17- and AS T18-derived cells are capable of maturing into functional neurons under *in vitro* conditions in 35 days.

αSyn triplication VM progenitor cells survive intracerebral transplantation and generate neuron-rich grafts

Since AST18 cells have never been investigated after transplantation before, we first tested their capacity to survive and mature after intracerebral grafting. In this experiment, day 16 VM progenitors derived from either RC17 or AST18 were quality controlled according to Nolbrant et al. 2017 (Supplementary Figure 1) and transplanted into the striatum of 6-OHDA-lesioned, immunosuppressed SD rats. The animals in this group were sacrificed at 8 weeks post-transplantation, a timepoint when, based on previous studies, the DA neurons are expected to have formed in the grafts. The grafts were assessed using standard histology. All transplanted rats (3/3 in the RC17 group and 3/3 in the AST18 group) had surviving grafts. The grafts were neuron and DA rich, as evidenced by staining for hNCAM (Fig. 2A) that detects all human neurons, and the DA neuron marker TH (Fig. 2C), thus providing evidence that cells with αSyn triplication survive the transplantation procedure and also mature into DA neurons *in vivo*.

To substantiate these findings, we repeated the experiment in 6-OHDA-lesioned nude athymic rats, that do not require daily injections of cyclosporine, therefore allowing for functional studies that require a minimum of 18–20 weeks maturation after transplantation since human cells mature slowly. VM-patterned cells from both lines were transplanted in parallel and a total of 12 rats per cell line were grafted. Four animals in each group were analyzed at 7 weeks post-transplantation to confirm the earlier findings obtained in the immunosuppressed SD rats. All 4 animals in the RC17 group and all 4 animals in the AST18 group had surviving grafts that were neuron and TH rich (Fig. 2B, D). We performed

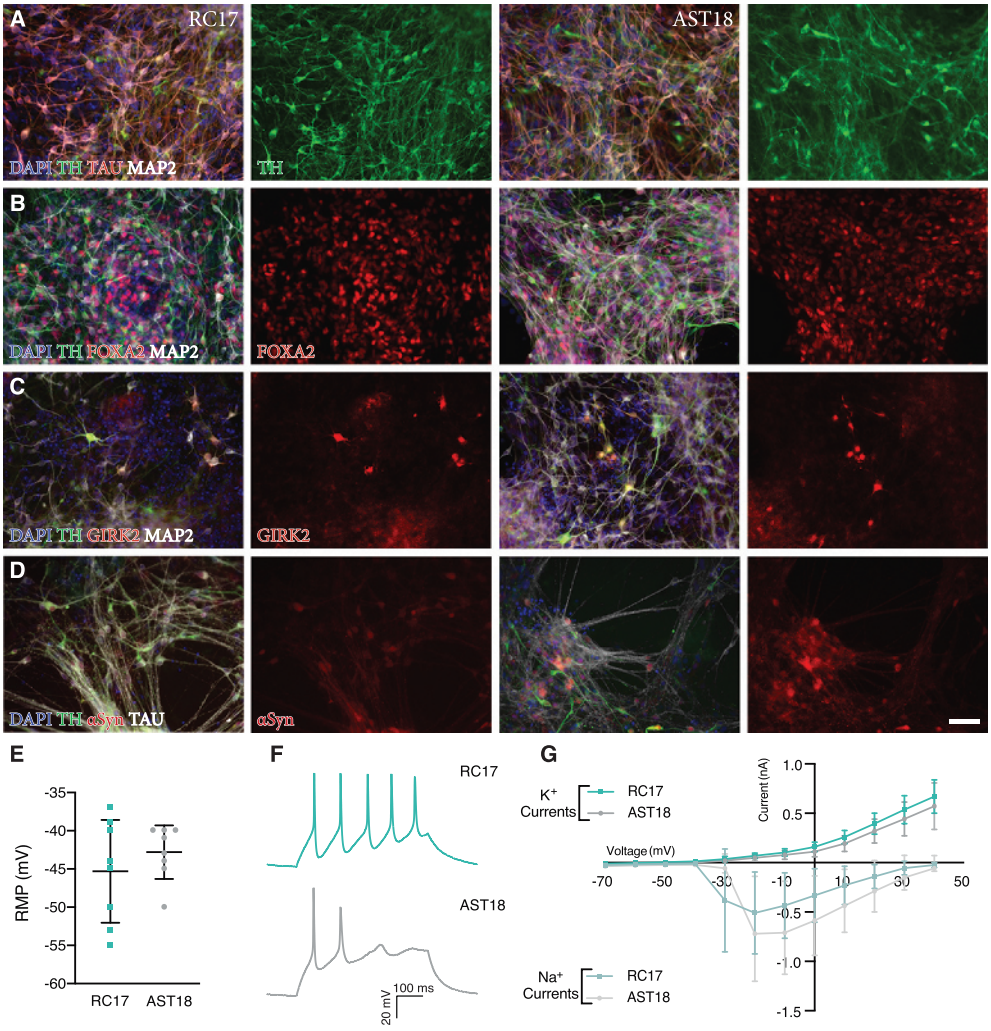

Fig. 1. Analysis of terminally differentiated DA neurons at day 35 *in vitro*. Immunostaining of VM-patterned neurons showing (A) high expression of neuronal markers TAU and MAP2, and DA marker TH. Immunostaining showing co-expression of (B) TH, FOXA2, and MAP2, (C) TH, GIRK2, and MAP2, and (D) TH, αSyn, and TAU. Scale bar 50 μm. (E) Resting membrane potential (RMP) at day 35 measured by whole-cell patch-clamp recordings showing no major difference between the cell lines, $n = 8$ in each group. (F) Representative trace of voltage responses from the whole-cell patch-clamp showing evoked action potentials from current injection. (G) Inward sodium (Na^+) and outward potassium (K^+) currents triggered by stepwise depolarization of the cell showing no major difference between the cell lines, $n = 8$ in each group. All data are expressed as mean ± the standard deviation.

quantification of graft size and TH^+ neuron content of all rats analysed at 7-8-weeks ($n = 7$ animals per group in total, combining grafts from both SD and nude athymic rats). Although their size and TH^+ neuron content varied markedly (Fig. 2E, F), as expected in xenografts of this type, the data confirmed that both RC17 and AST18 derived grafts had formed DA neurons with an appearance that is in line with previous reports. We also examined the grafts for αSyn and, as expected, we could observe αSyn expression in both RC17- and AST18- derived grafts at this time point (Fig. 2G).

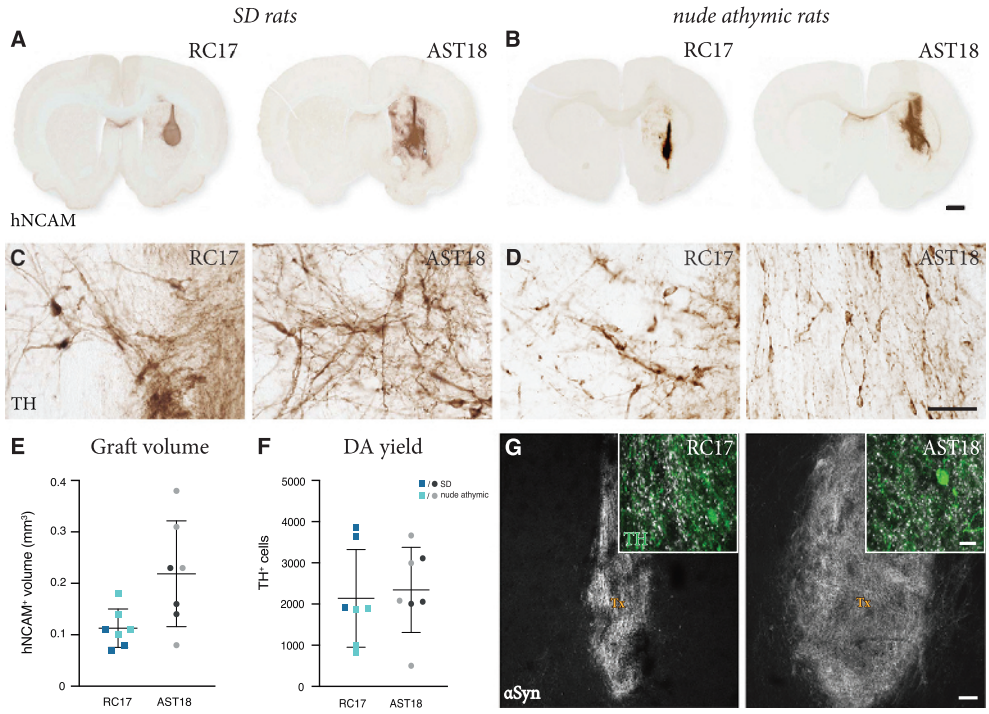

Fig. 2. Short term analysis of transplants. hNCAM immunostaining showing surviving grafts (A) in SD rats at 8 weeks and (B) in nude athymic rats at 7 weeks from both RC17 and AST18 VM progenitor cells, scale bar 1 mm. High magnification images of TH immunostaining (C) in SD rats at 8 weeks and (D) in nude athymic rats at 7 weeks, scale bar 50 μm. (E) Graft volume quantified showing no major difference between the cell lines in both experiments, $n = 3$ for SD rats (shown in dark blue and dark gray) and $n = 4$ for nude athymic rats (shown in light blue and light gray). (F) Quantification of TH^+ cells within the graft showing a similar number in grafts from both cell lines in both experiments, $n = 3$ for SD rats (shown in dark blue and dark gray) and $n = 4$ for nude athymic rats (shown in light blue and light gray). (G) Double staining for TH and human αSyn showing the distribution of αSyn within the transplant (Tx), scale bars 10 μm and 100 μm. All data are expressed as mean ± the standard deviation.

These results demonstrate that VM progenitors differentiated from an αSyn triplication patient hiPSC line survive and mature into neuron-rich grafts similar to RC17 hESCs after transplantation *in vivo*. This suggests that αSyn triplication does not significantly affect the ability of transplanted cells to undergo subtype-specific maturation into DA neurons in the rodent brain.

VM progenitor grafts derived from an αSyn triplication hiPSC line survive long term and are able to mediate functional recovery

Graft-induced functional recovery was assessed using the amphetamine-induced rotation test in the 6-OHDA lesioned nude athymic rats grafted with RC17-derived and AST18-derived DA progenitors. Animals were tested pre-transplantation (0 weeks) and again at 16, 18, 20, 22, and 24 weeks post-transplantation. Only rats with complete lesions (pre-transplant rotation score >4 net turns/min) and confirmed loss of nigral TH^+ neurons (*posthoc* histological analysis) (Fig. 3A) were included in this functional analysis, resulting in $n = 5$ in the RC17 group and $n = 5$ in the AST18 group. The rotation data showed that 5/5 of the RC17-derived grafts (Fig. 3B), and 4/5 of the AST18-derived grafts (Fig. 3C), mediated full functional recovery at the endpoint of experiment, i.e., 24 weeks post-transplantation and in a time course that is expected for human DA neurons [41, 42].

Histological analysis was performed on all animals at the end point of the experiment (i.e., also including those with a partial lesion at the start of

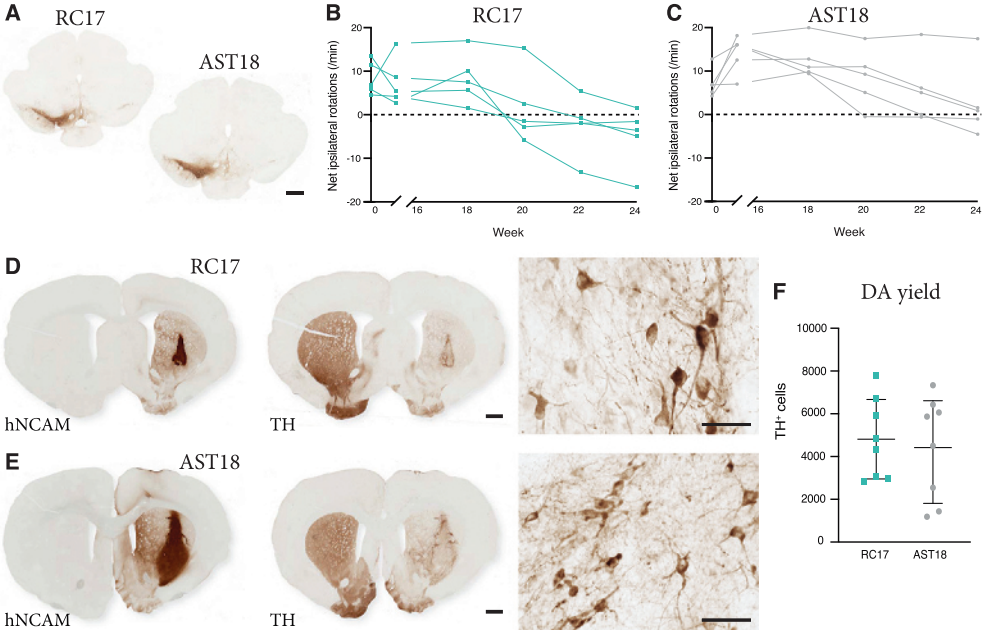

Fig. 3. Long term behavioural assessment and analysis of transplants. (A) TH immunostaining showing loss of nigral TH^+ neurons in the substantia nigra on the lesioned side of the brain, scale bar 1 mm. Net ipsilateral rotation scores at 0, 16, 18, 20, 22, and 24 weeks showing progressive recovery of rotational bias (B) in 5/5 animals in the RC17 group and (C) in 4/5 animals in the AST18 group. (D) hNCAM and TH immunostaining showing surviving grafts at 24 weeks from RC17 VM progenitor cells, scale bar 1 mm. High magnification images of TH immunostaining within the graft at 24 weeks, scale bar 50 μm. (E) hNCAM and TH immunostaining showing surviving grafts at 24 weeks from AST18 VM progenitor cells, scale bar 1 mm. High magnification images of TH immunostaining within the graft at 24 weeks, scale bar 50 μm. (F) Quantification of TH^+ cells within the grafts showing no major difference between the cell lines, $n = 8$ in each group. All data are expressed as mean ± the standard deviation.

the experiment). Graft survival was 8/8 in the RC17 group and 8/8 in the AST18 group as assessed by hNCAM and TH staining (Fig. 3D, E). TH immunostaining revealed a more mature neuronal morphology of the DA neurons in both RC17 and AST18 animals (Fig. 3D, E, high magnification) compared to what was observed after 7-8 weeks (Fig. 2C, D), with most mature TH^+ neurons located at the graft edge (Fig. 3D, E). Quantifications of TH^+ cells in the grafts showed similar DA content between RC17- and AST18-derived grafts (Fig. 3F). The quantifications also revealed that the one animal in the AST18 group that did not recover in the rotation test had a low number of DA neurons (1440 TH^+ cells) which is at the threshold for recovery in the rotation test [43].

Thus, both wt hESCs and hiPSCs with an αSyn triplication mutation generate functional grafts rich in TH^+ neurons capable of innervating the surrounding host striatum and mediating functional recovery.

Grafts derived from αSyn triplication VM progenitor cells show evidence of pathological changes

Finally, we performed a detailed investigation of any potential pathology in the AST18- vs the RC17-derived grafts at 24 weeks. For this purpose, grafts were immunolabeled for TH, the microglial marker IBA1, and pSyn (the phosphorylated, pathological form of αSyn which is the main component of Lewy bodies).

We detected a microglial response to the grafts derived from both cell lines, which is expected with a xenograft transplant (Fig. 4A-D). As illustrated in Fig. 4G, the overall density of $IBA1^+$ cells in the grafts was similar to that seen in the surrounding host striatum, and it did not differ between the two graft types. Next, we examined the microglia for expression of pSyn using confocal microscopy. We observed distinct $pSyn^+$ inclusions in $IBA1^+$ microglia within

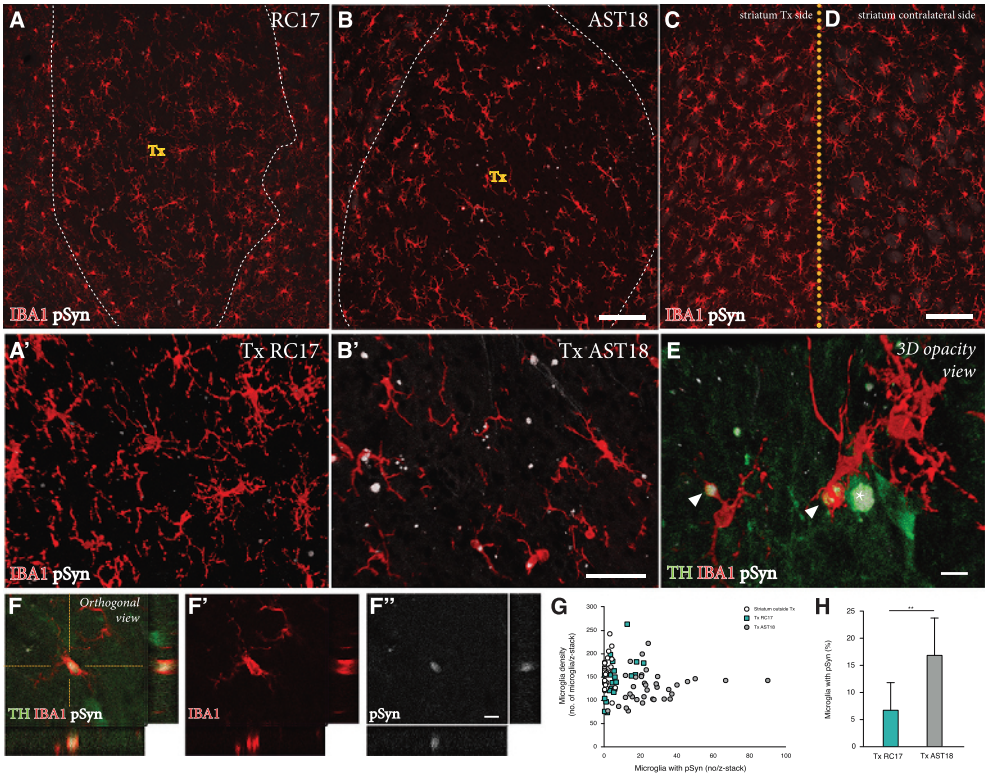

Fig. 4. Pathology in microglia 24 weeks after transplantation. IBA1 and pSyn immunostaining within the striatum from (A) RC17- and (B) AST18-derived grafts. The area of the transplant (Tx) is marked with dashed white lines, scale bar 100 μm. High magnification images of IBA1 and pSyn double staining within the (A') RC17 and (B') AST18 transplant, scale bar 50 μm. No pSyn+inclusions were detected in (C) the host striatum outside of the transplant area or (D) on the contralateral side, scale bar 100 μm. (E) Arrowheads indicating microglia with $pSyn^+$ inclusions, as well as an TH cell containing a $pSyn^+$ inclusion marked with an asterisk, scale bar 10 μm. (F,F',F'') Showing a microglial cell containing $pSyn^+$ inclusion as evidenced by orthogonal projection, scale bar 10 μ m. Quantifications showing (G) microglia density plotted against the number of microglia with $pSyn^+$ inclusions and (H) the percentage (%) of microglia with pSyn inclusions in RC17- and AST18-derived transplants (Tx) showing a significant difference between the groups ($t_{(13)} = 3.20$, $p = 0.007$).

the AST18-derived grafts (Fig. 4B, B' and 4E, F), which was markedly different from what we observed in the RC17-derived grafts (Fig. 4A, A'). The frequency of $IBA1^+$ microglia with $pSyn^+$ inclusions inside the grafts, as assessed in 3D stacks on the confocal microscope (Fig. 4H), showed a significant difference between the two graft types: much fewer in the RC17 grafts as compared to the AST18-derived grafts. No pSyn+inclusions were detected in the host striatum outside of the transplant area (Fig. 4C) or on the contralateral side (Fig. 4D).

To assess any potential disease-related pathology in the DA neurons within the grafts, we analysed the co-expression of TH and pSyn using confocal microscopy. In line with previous transplantation studies of RC17-derived DA transplants in the 6-OHDA model [44], we did not observe any pSyn pathology in TH^+ neurons in the RC17 group. However, we did find signs of $pSyn^+$ inclusions in a small number of the TH^+ neurons in AST18 grafts (Fig. 5A, B). Quantifications showed that 7% of the TH^+ neurons (99 out of 1437 TH^+ neurons counted in 8 different animals) in AST18-derived grafts contained $pSyn^+$ inclusions (Fig. 5C). The $pSyn^+$ inclusions in the AST18 grafts were most often found within small granular aggregates in the cytoplasm (Fig. 5D) or along neurites (shown by arrowheads in Fig. 5E). We also observed $pSyn^+$ inclusions in cells that displayed

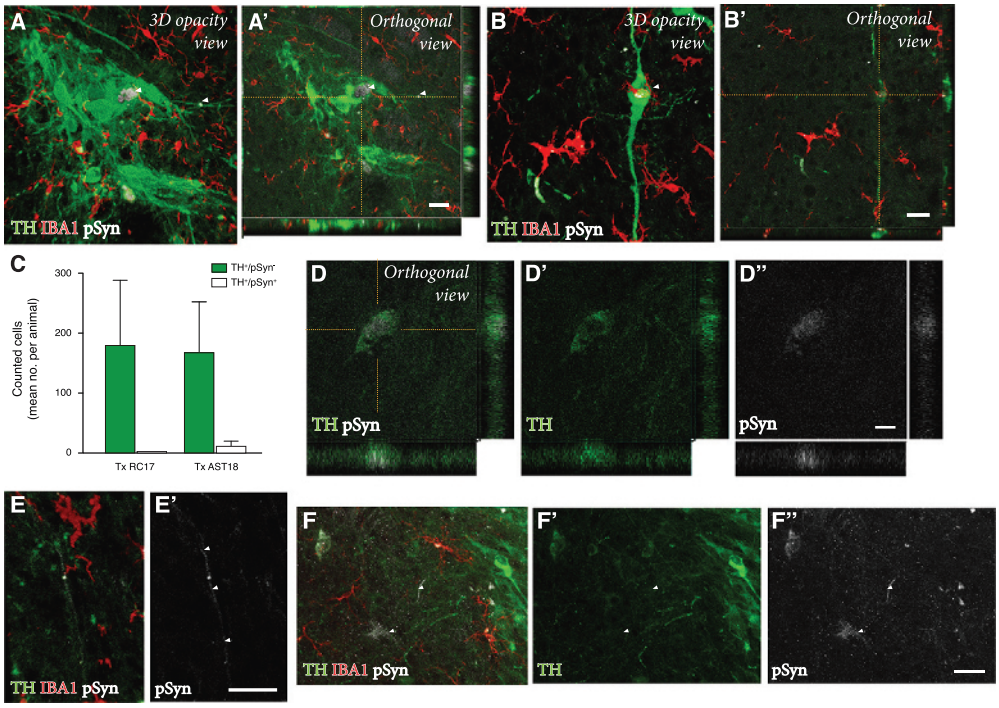

Fig. 5. Pathology in DA neurons 24 weeks after transplantation. (A, A', B, B') TH, IBA1, and pSyn triple immunostaining within the graft showing TH^+ neurons containing $pSyn^+$ inclusions as evidenced by orthogonal projections, scale bar 20 μm. (C) Quantification of the number of $pSyn^+$ inclusions in TH^+ neurons from both RC17 and AST18-derived grafts. TH and pSyn immunostaining showing (D, D', D") small granular aggregates of pSyn within a TH^+ neuron, scale bar 10 μ m, and (E, E') a TH-stained neurite containing $pSyn^+$ inclusions (indicated by arrowheads), scale bar 20 μm. (F) Granular aggregates of pSyn in a weakly stained DA neuron (shown by arrowheads) suggesting down-regulation of TH, scale bar 20 μm. All data are expressed as mean ± the standard deviation.

weak TH^+ staining (shown by arrowheads in Fig. 5F) indicative of TH down-regulation as part of a degenerative process.

DISCUSSION

Cell replacement therapy for PD was first explored decades ago, yet a scalable source of cells for transplantation has only recently become available due to advances in stem cell biology. It is now possible to efficiently generate transplantable progenitors, from both hESCs and hiPSCs, that give rise to functional midbrain DA neurons after transplantation into both rodent and primate models of PD [9–11, 28]. This pivotal development has led to the initiation of new clinical trials using allogeneic hiPSCs in Japan (CiRA trial) [45], HLA-matched hESCs in China [46], and others due to be initiated in the next few years in Europe and the United States [47, 48]. In these trials, PD patients will be transplanted with DA progenitors differentiated from either hESCs or hiPSCs (derived from donors without a PD disease background), and patients receiving allogeneic transplants will undergo 1 year of immunosuppression [47].

Personalised stem cell therapy for PD is an attractive future application that is actively under investigation. An autologous grafting strategy involves hiPSC generation, differentiation, and transplantation of the patients' own cells, and would remove the need for immune suppression. To date, one individual with sporadic PD has been reported to have received an autologous cell transplantation, approved by regulatory authorities as compassionate use [16], thereby showing feasibility of the approach. However, given post mortem evidence of slowly developing pSyn pathology in the recipients of fetal VM grafts [17–21], and the observation of disease-associated features appearing when patient-derived

hiPSCs are differentiated into DA neurons *in vitro* [22–26], a number of questions relating to the long-term integrity, stability and function of grafts from patient-derived cells remain to be answered.

One key issue to be addressed before initiating clinical trials based on autologous cells are whether patient-derived cells are more prone to develop pathology over extended time periods in the brain, and if they develop pathology in an accelerated manner in an autologous grafting paradigm compared to strategies where cells from healthy donors are used. So far, this has been investigated in very few transplantation studies using cell lines generated from sporadic PD patients. These studies demonstrate that DA progenitors derived from sporadic PD patients are capable of producing DA-rich grafts that mediate functional recovery both in rodent [27–29] and primate models of PD [11]. No obvious signs of pathology have been reported in these studies. However, in a clinical setting the graft should remain healthy and functioning for decades, and this is not possible to predict from these studies. In this study, we therefore used a hiPSC line from a patient with an αSyn triplication mutation with the idea that the pathological process is likely accelerated in these cells compared to cells from sporadic PD patients.

Previous studies have presented conflicting evidence about the DA differentiation efficiency of patient cell lines harboring the αSyn triplication mutation. One study reported that αSyn triplication impairs neuronal differentiation and maturation *in vitro* [49]. However, other studies have reported that patient cell lines with αSyn mutations differentiate with the same efficiency as healthy cell lines regardless of the *SNCA* genotype [22, 26, 35]. Here, we made a comparison of the AST18 cell line (derived from an αSyn triplication patient) with that of a clinical grade hESC line with no mutations in known PD related genes. We found no difference in how these cells responded to patterning factors, and both lines generated mature and functional DA neurons *in vitro*, which is in agreement with previous studies [22, 26, 35].

Furthermore, we next showed that αSyn triplication cells generate DA-rich grafts also after transplantation into the 6-OHDA preclinical model of PD. At early time points, these grafts behave *on par* with grafts derived from a healthy GMP-grade hESC stem cell line grafted in parallel, and in line with previous transplantation studies using fetal, hESC, and hiPSC-derived grafts [10, 11, 37, 38]. In addition, at 24 weeks post-transplantation grafts derived from an αSyn triplication patient mediated functional recovery, thereby supporting previous reports that patient-derived DA neurons function in preclinical PD models [27–29].

However, contrary to previous studies using cells derived from sporadic PD patients, we observed the appearance of pathological changes in grafts derived from an αSyn triplication patient in the form of $pSyn^+$ inclusions present in both reactive microglia and in the cell bodies and/or fibers of TH^+ neurons indicating that the pathological process is progressing. The dynamics and extent of TH down-regulation vs. DA neuron degeneration is not possible to experimentally assess in our study, but we did observe signs of TH down-regulation in affected cells (see for example Fig. 5F), similar to what has been shown for endogenous DA neurons in AAV-mediated overexpression of αSyn *in vivo* [50, 51].

In previous studies αSyn pathology has been observed in grafted DA neurons [17–21], but in all these cases the appearance of αSyn aggregates reflects transfer of pathology from the αSyn overexpressing host brain. In this study, αSyn triplication grafts show evidence of pathological changes at 24 weeks post-transplantation despite there being no ongoing pathology in the host brain. The development of αSyn pathology in these grafts is most probably due to the 2-fold increase in αSyn protein known to be expressed by these cells [26, 35] suggesting that cell intrinsic properties, and increased cellular levels of αSyn in particular, can lead to pathological changes within the grafts. Of particular note, is that the limited amount of pathology in the AST18-derived grafts was of no consequence to the function of the graft at this timepoint; however, it cannot be ruled out that the pathology may severely affect the graft and reduce its effectiveness over an extended period of time which cannot be modeled in a xenograft setting. Furthermore, this study was conducted in the 6-OHDA lesion model of PD [52], a toxin based system that induces profound loss of DA neurons accompanied by severe motor deficits, but does not reflect the progressive time course of the disease and lacks pathological hallmarks of the disease process. Therefore, the presence of pathology in the cells may in fact be more aggressive when exposed to the host environment of the PD patient brain, as would be the case in an autologous grafting paradigm. Future studies, therefore, need to investigate patient-derived grafts in more disease relevant models with the presence of proteinopathy and/or inflammation.

Even though this and future studies may indicate that PD patient-derived hiPSCs may not be suitable for immediate use in autologous therapy, there are several ongoing developments in the field that could be used in such cases. For monogenetic cases, gene correction strategies could be employed at the hiPSC stage of cell development [26]. Other examples are drugs or antibodies that prevent Lewy body formation and/or prevent the potential spread of αSyn from host to graft that are under development and could be used in combination with autologous grafting in both sporadic and familial patient groups [53, 54]. Future studies could also investigate the effect of engineering αSyn null cells for transplantation, as it has been suggested that cells lacking αSyn may be resistant to synuclein pathology [26, 55]. These developments could allow for autologous cell therapy and the associated benefits, while minimizing potential pathological effects on the grafted cells and ensuring their long-term function.

ACKNOWLEDGMENTS

We thank Dr. Tilo Kunath for kindly sharing the AST18 hiPSC line and Ulla Jarl, Sol da Rocha Baez, and Michael Sparrenius for excellent technical assistance. The research leading to these results has received funding from the New York Stem Cell Foundation, European Research Council (ERC) under ERC Grant Agreement 771427, Swedish Research Council (2016-00873 and 2018-02608), Swedish Parkinson Foundation (Parkinsonfonden), Swedish Brain Foundation, the Thorsten and Elsa Segerfalk Foundation, Strategic Research Area at Lund University Multipark, and Knut and Alice Wallenberg Stiftelse (KAW 2018-0040). Malin Parmar is a New York Stem Cell Foundation Robertson Investigator. Shelby Shrigley is funded by the European Union Horizon 2020 Programme (H2020-MSCA-ITN-2015) under the Marie Skłodowska-Curie Innovative Training Network and Grant Agreement 676408.

CONFLICT OF INTEREST

MP is the owner of Parmar Cells AB and co-inventor of the U.S. patent application US Patent App. 16/414,848 owned by Biolamina AB, US Patent App. 16/632,229 owned by Miltenyi Biotech and International Application No. PCT/EP2018/062261 owned by New York Stem Cell Foundation.

SUPPLEMENTARY MATERIAL

The supplementary material is available in the electronic version of this article: https://dx.doi.org/10.3233/JPD-202366.

REFERENCES

[1] Björklund A, Parmar M (2020) Neuronal replacement as a tool for basal ganglia circuitry repair: 40 years in perspective. *Front Cell Neurosci* **14**, 1-22.

[2] Lindvall O, Brundin P, Widner H, Rehncrona S, Gustavii B, Frackowiak R, Leenders K, Sawle G, Rothwell J, Marsden C, Björklund A (1990) Grafts of fetal dopamine neurons survive and improve motor function in Parkinson's disease. *Science* **247**, 574-577.

[3] Björklund A, Lindvall O (2017) Replacing dopamine neurons in Parkinson's disease: How did it happen? *J Parkinsons Dis* **7**, S21-S31.

[4] Piccini P, Pavese N, Hagell P, Reimer J, Björklund A, Oertel WH, Quinn NP, Brooks DJ, Lindvall O (2005) Factors affecting the clinical outcome after neural transplantation in Parkinson's disease. *Brain* **128**, 2977-2986.

[5] Olanow CW, Kordower JH, Lang AE, Obeso JA (2009) Dopaminergic transplantation for parkinson's disease: Current status and future prospects. *Ann Neurol* **66**, 591-596.

[6] Barker RA, Barrett J, Mason SL, Björklund A (2013) Fetal dopaminergic transplantation trials and the future of neural grafting in Parkinson's disease. *Lancet Neurol* **12**, 84-91.

[7] Kefalopoulou Z, Politis M, Piccini P, Mencacci N, Bhatia K, Jahanshahi M, Widner H, Rehncrona S, Brundin P, Björklund A, Lindvall O, Limousin P, Quinn N, Foltynie T (2014) Long-term clinical outcome of fetal cell transplantation for Parkinson disease two case reports. *JAMA Neurol* **71**, 83.

[8] Kordower JH, Goetz CG, Chu Y, Halliday GM, Nicholson DA, Musial TF, Marmion DJ, Stoessl AJ, Sossi V, Freeman TB, Olanow CW (2017) Robust graft survival and normalized dopaminergic innervation do not obligate recovery in a Parkinson disease patient. *Ann Neurol* **81**, 46-57.

[9] Kriks S, Shim J-W, Piao J, Ganat YM, Wakeman DR, Xie Z, Carrillo-Reid L, Auyeung G, Antonacci C, Buch A, Yang L, Beal MF, Surmeier DJ, Kordower JH, Tabar V, Studer L (2011) Dopamine neurons derived from human ES cells efficiently engraft in animal models of Parkinson's disease. *Nature* **480**, 547-551.

[10] Nolbrant S, Heuer A, Parmar M, Kirkeby A (2017) Generation of high-purity human ventral midbrain dopaminergic progenitors for *in vitro* maturation and intracerebral transplantation. *Nat Protoc* **12**, 1962-1979.

[11] Kikuchi T, Morizane A, Doi D, Magotani H, Onoe H, Hayashi T, Mizuma H, Takara S, Takahashi R, Inoue H, Morita S, Yamamoto M, Okita K, Nakagawa M, Parmar M, Takahashi J (2017) Human iPS cell-derived dopaminergic neurons function in a primate Parkinson's disease model. *Nature* **548**, 592-596.

[12] Emborg ME, Liu Y, Xi J, Zhang X, Yin Y, Lu J, Joers V, Swanson C, Holden JE, Zhang S-C (2013) Induced pluripotent stem cell-derived neural cells survive and mature in the nonhuman primate brain. *Cell Rep* **3**, 646-650.

[13] Morizane A, Doi D, Kikuchi T, Okita K, Hotta A, Kawasaki T, Hayashi T, Onoe H, Shiina T, Yamanaka S, Takahashi J (2013) Direct comparison of autologous and allogeneic

transplantation of iPSC-derived neural cells in the brain of a nonhuman primate. *Stem Cell Rep* **1**, 283-292.

[14] Hallett PJ, Deleidi M, Astradsson A, Smith GA, Cooper O, Osborn TM, Sundberg M, Moore MA, Perez-Torres E, Brownell A-L, Schumacher JM, Spealman RD, Isacson O (2015) Successful function of autologous iPSC-derived dopamine neurons following transplantation in a non-human primate model of Parkinson's disease. *Cell Stem Cell* **16**, 269-274.

[15] Morizane A, Kikuchi T, Hayashi T, Mizuma H, Takara S, Doi H, Mawatari A, Glasser MF, Shiina T, Ishigaki H, Itoh Y, Okita K, Yamasaki E, Doi D, Onoe H, Ogasawara K, Yamanaka S, Takahashi J (2017) MHC matching improves engraftment of iPSC-derived neurons in non-human primates. *Nat Commun* **8**, 385.

[16] Schweitzer JS, Song B, Herrington TM, Park T-Y, Lee N, Ko S, Jeon J, Cha Y, Kim K, Li Q, Henchcliffe C, Kaplitt M, Neff C, Rapalino O, Seo H, Lee I-H, Kim J, Kim T, Petsko GA, Ritz J, Cohen BM, Kong S-W, Leblanc P, Carter BS, Kim K-S (2020) Personalized iPSC-derived dopamine progenitor cells for Parkinson's disease. *N Engl J Med* **382**, 1926-1932.

[17] Kordower JH, Chu Y, Hauser RA, Freeman TB, Olanow CW (2008) Lewy body-like pathology in long-term embryonic nigral transplants in Parkinson's disease. *Nat Med* **14**, 504-506.

[18] Li J-Y, Englund E, Holton JL, Soulet D, Hagell P, Lees AJ, Lashley T, Quinn NP, Rehncrona S, Björklund A, Widner H, Revesz T, Lindvall O, Brundin P (2008) Lewy bodies in grafted neurons in subjects with Parkinson's disease suggest host-to-graft disease propagation. *Nat Med* **14**, 501-503.

[19] Li J-Y, Englund E, Widner H, Rehncrona S, Björklund A, Lindvall O, Brundin P (2010) Characterization of Lewy body pathology in 12- and 16-year-old intrastriatal mesencephalic grafts surviving in a patient with Parkinson's disease. *Mov Disord* **25**, 1091-1096.

[20] Chu Y, Kordower JH (2010) Lewy body pathology in fetal grafts. *Ann N Y Acad Sci* **1184**, 55-67.

[21] Li W, Englund E, Widner H, Mattsson B, van Westen D, Lätt J, Rehncrona S, Brundin P, Björklund A, Lindvall O, Li J-Y (2016) Extensive graft-derived dopaminergic innervation is maintained 24 years after transplantation in the degenerating parkinsonian brain. *Proc Natl Acad Sci U S A* **113**, 6544-6549.

[22] Byers B, Cord B, Nguyen HN, Schüle B, Fenno L, Lee PC, Deisseroth K, Langston JW, Pera RR, Palmer TD (2011) SNCA triplication Parkinson's patient's iPSC-derived DA neurons accumulate α-synuclein and are susceptible to oxidative stress. *PLoS One* **6**, e26159.

[23] Cooper O, Seo H, Andrabi S, Guardia-laguarta C, Sundberg M, Mclean JR, Carrillo-reid L, Xie Z, Hargus G, Deleidi M, Lawson T, Bogetofte H, Clark L, Moskowitz C, Mazzulli J, Chen L, Romero N, Jiang H, Uitti RJ, Huang Z, Scarffe L a, Dawson VL, Klein C, Feng J, Ross O a, Trojanowski JQ, Lee VM, Marder K, Surmeier DJ, Wszolek K, Przedborski S, Krainc D, Dawson TM, Isacson O (2012) Familial Parkinson's disease iPSCs show cellular deficits in mitochondrial responses that can be pharmacologically rescued. *Sci Transl Med* **4**, 141ra90.

[24] Sánchez-Danés A, Richaud-Patin Y, Carballo-Carbajal I, Jiménez-Delgado S, Caig C, Mora S, Di Guglielmo C, Ezquerra M, Patel B, Giralt A, Canals JM, Memo M, Alberch J, López-Barneo J, Vila M, Cuervo AM, Tolosa E, Consiglio A, Raya A (2012) Disease-specific phenotypes in dopamine neurons from human iPS-based models of genetic and sporadic Parkinson's disease. *EMBO Mol Med* **4**, 380-395.

[25] Schöndorf DC, Aureli M, McAllister FE, Hindley CJ, Mayer F, Schmid B, Sardi SP, Valsecchi M, Hoffmann S, Schwarz LK, Hedrich U, Berg D, Shihabuddin LS, Hu J, Pruszak J, Gygi SP, Sonnino S, Gasser T, Deleidi M (2014) iPSC-derived neurons from GBA1-associated Parkinson's disease patients show autophagic defects and impaired calcium homeostasis. *Nat Commun* **5**, 4028.

[26] Chen Y, Dolt KS, Kriek M, Baker T, Downey P, Drummond NJ, Canham MA, Natalwala A, Rosser S, Kunath T (2019) Engineering synucleinopathy-resistant human dopaminergic neurons by CRISPR-mediated deletion of the SNCA gene. *Eur J Neurosci* **49**, 510-524.

[27] Hargus G, Cooper O, Deleidi M, Levy A, Lee K, Marlow E, Yow A, Soldner F, Hockemeyer D, Hallett PJ, Osborn T, Jaenisch R, Isacson O (2010) Differentiated Parkinson patient-derived induced pluripotent stem cells grow in the adult rodent brain and reduce motor asymmetry in Parkinsonian rats. *Proc Natl Acad Sci U S A* **107**, 15921-15926.

[28] Kikuchi T, Morizane A, Doi D, Okita K, Nakagawa M, Yamakado H, Inoue H, Takahashi R, Takahashi J (2017) Idiopathic Parkinson's disease patient-derived induced pluripotent stem cells function as midbrain dopaminergic neurons in rodent brains. *J Neurosci Res* **95**, 1829-1837.

[29] Song B, Cha Y, Ko S, Jeon J, Lee N, Seo H, Park K, Lee I, Lopes C, Feitosa M, Luna MJ, Jung JH, Kim J, Hwang D, Cohen BM, Teicher MH, Leblanc P, Carter BS, Kordower JH, Bolshakov VY, Kong SW, Schweitzer JS, Kim K (2020) Human autologous iPSC–derived dopaminergic progenitors restore motor function in Parkinson's disease models. *J Clin Invest* **130**, 904-920.

[30] Polymeropoulos MH (1997) Mutation in the alpha-synuclein gene identified in families with Parkinson's disease. *Science* **276**, 2045-2047.

[31] Singleton A, Farrer M, Johnson J, Singleton A, Hague S, Kachergus J, Hulihan M, Peuralinna T, Dutra A, Nussbaum R, Lincoln S, Crawley A, Hanson M, Maraganore D, Adler C, Cookson M, Muenter M, Baptista M, Miller D, Blancato J, Hardy J, Gwinn-Hardy K (2003) a-Synuclein locus triplication causes Parkinson's disease. *Science* **302**, 841-841.

[32] Ibáñez P, Bonnet A-M, Débarges B, Lohmann E, Tison F, Agid Y, Dürr A, Brice A, Pollak P (2004) Causal relation between α-synuclein locus duplication as a cause of familial Parkinson's disease. *Lancet* **364**, 1169-1171.

[33] Satake W, Nakabayashi Y, Mizuta I, Hirota Y, Ito C, Kubo M, Kawaguchi T, Tsunoda T, Watanabe M, Takeda A, Tomiyama H, Nakashima K, Hasegawa K, Obata F, Yoshikawa T, Kawakami H, Sakoda S, Yamamoto M, Hattori N, Murata M, Nakamura Y, Toda T (2009) Genome-wide association study identifies common variants at four loci as genetic risk factors for Parkinson's disease. *Nat Genet* **41**, 1303-1307.

[34] Simón-Sánchez J, Schulte C, Bras JM, Sharma M, Gibbs JR, Berg D, Paisan-Ruiz C, Lichtner P, Scholz SW, Hernandez DG, Krüger R, Federoff M, Klein C, Goate A, Perlmutter J, Bonin M, Nalls MA, Illig T, Gieger C, Houlden H, Steffens M, Okun MS, Racette BA, Cookson MR, Foote KD, Fernandez HH, Traynor BJ, Schreiber S, Arepalli S, Zonozi R, Gwinn K, van der Brug M, Lopez G, Chanock SJ, Schatzkin A, Park Y, Hollenbeck A, Gao J, Huang X, Wood NW, Lorenz D, Deuschl G, Chen H, Riess O, Hardy JA, Singleton AB, Gasser T (2009) Genome-wide association

study reveals genetic risk underlying Parkinson's disease. *Nat Genet* **41**, 1308-1312.

[35] Devine MJ, Ryten M, Vodicka P, Thomson AJ, Burdon T, Houlden H, Cavaleri F, Nagano M, Drummond NJ, Taanman J-W, Schapira AH, Gwinn K, Hardy J, Lewis PA, Kunath T (2011) Parkinson's disease induced pluripotent stem cells with triplication of the α-synuclein locus. *Nat Commun* **2**, 440.

[36] Spillantini MG, Schmidt ML, Lee VM-Y, Trojanowski JQ, Jakes R, Goedert M (1997) a-Synuclein in Lewy bodies. *Nature* **388**, 839-840.

[37] Kirkeby A, Grealish S, Wolf DA, Nelander J, Wood J, Lundblad M, Lindvall O, Parmar M (2012) Generation of regionally specified neural progenitors and functional neurons from human embryonic stem cells under defined conditions. *Cell Rep* **1**, 703-714.

[38] Grealish S, Diguet E, Kirkeby A, Mattsson B, Heuer A, Bramoulle Y, Van Camp N, Perrier AL, Hantraye P, Björklund A, Parmar M (2014) Human ESC-derived dopamine neurons show similar preclinical efficacy and potency to fetal neurons when grafted in a rat model of Parkinson's disease. *Cell Stem Cell* **15**, 653-665.

[39] Cardoso T, Adler AF, Mattsson B, Hoban DB, Nolbrant S, Wahlestedt JN, Kirkeby A, Grealish S, Björklund A, Parmar M (2018) Target-specific forebrain projections and appropriate synaptic inputs of hESC-derived dopamine neurons grafted to the midbrain of parkinsonian rats. *J Comp Neurol* **526**, 2133-2146.

[40] Rothman JS, Silver RA (2018) NeuroMatic: An integrated open-source software toolkit for acquisition, analysis and simulation of electrophysiological data. *Front Neuroinform* **12**, 14.

[41] Brundin P, Strecker RE, Clarke DJ, Widner H, Nilsson OG, Åstedt B, Lindvall O, Björklund A (1988) Chapter 57: Can human fetal dopamine neuron grafts provide a therapy for Parkinson's disease? *Prog Brain Res* **78**, 441-448.

[42] Lelos MJ, Morgan RJ, Kelly CM, Torres EM, Rosser AE, Dunnett SB (2016) Amelioration of non-motor dysfunctions after transplantation of human dopamine neurons in a model of Parkinson's disease. *Exp Neurol* **278**, 54-61.

[43] Brundin P, Nilsson OG, Gage FH, Björklund A (1985) Cyclosporin A increases survival of cross-species intrastriatal grafts of embryonic dopamine-containing neurons. *Exp Brain Res* **60**, 204-208.

[44] Hoban DB, Shrigley S, Mattsson B, Breger LS, Jarl U, Cardoso T, Nelander Wahlestedt J, Luk KC, Björklund A, Parmar M (2020) Impact of α-synuclein pathology on transplanted hESC-derived dopaminergic neurons in a humanized α-synuclein rat model of PD. *Proc Natl Acad Sci U S A* **117**, 15209-15220.

[45] Doi D, Magotani H, Kikuchi T, Ikeda M, Hiramatsu S, Yoshida K, Amano N, Nomura M, Umekage M, Morizane A, Takahashi J (2020) Pre-clinical study of induced pluripotent stem cell-derived dopaminergic progenitor cells for Parkinson's disease. *Nat Commun* **11**, 3369.

[46] Safety and Efficacy Study of Human ESC-derived Neural Precursor Cells in the Treatment of Parkinson's Disease, https://clinicaltrials.gov/ct2/show/NCT03119636, Last updated April 18 2017, Accessed on September 18, 2020.

[47] Barker RA, Parmar M, Studer L, Takahashi J (2017) Human trials of stem cell-derived dopamine neurons for Parkinson's disease: Dawn of a new era. *Cell Stem Cell* **21**, 569-573.

[48] Barker RA (2019) Designing stem-cell-based dopamine cell replacement trials for Parkinson's disease. *Nat Med* **25**, 1045-1053.

[49] Oliveira LMA, Falomir-Lockhart LJ, Botelho MG, Lin K-H, Wales P, Koch JC, Gerhardt E, Taschenberger H, Outeiro TF, Lingor P, Schüle B, Arndt-Jovin DJ, Jovin TM (2015) Elevated α-synuclein caused by SNCA gene triplication impairs neuronal differentiation and maturation in Parkinson's patient-derived induced pluripotent stem cells. *Cell Death Dis* **6**, e1994-e1994.

[50] Ulusoy A, Decressac M, Kirik D, Björklund A (2010) Viral vector-mediated overexpression of α-synuclein as a progressive model of Parkinson's disease. *Prog Brain Res* **184**, 89-111.

[51] Volpicelli-Daley LA, Kirik D, Stoyka LE, Standaert DG, Harms AS (2016) How can rAAV-α-synuclein and the fibril α-synuclein models advance our understanding of Parkinson's disease? *J Neurochem* **139**, 131-155.

[52] Ungerstedt U, Arbuthnott GW (1970) Quantitative recording of rotational behavior in rats after 6-hydroxy-dopamine lesions of the nigrostriatal dopamine system. *Brain Res* **24**, 485-493.

[53] M. Danzer K, J. McLean P (2011) Drug targets from genetics: Alpha-synuclein. *CNS Neurol Disord Drug Targets* **10**, 712-723.

[54] Bengoa-Vergniory N, Faggiani E, Ramos-Gonzalez P, Kirkiz E, Connor-Robson N, Brown L V, Siddique I, Li Z, Vingill S, Cioroch M, Cavaliere F, Threlfell S, Roberts B, Schrader T, Klärner F, Cragg S, Dehay B, Bitan G, Matute C, Bezard E, Wade-Martins R (2020) CLR01 protects dopaminergic neurons *in vitro* and in mouse models of Parkinson's disease. *Nat Commun* **11**, 4885.

[55] Brundin P, Coetzee GA (2019) Genetically engineered stem cell-derived neurons can be rendered resistant to alpha-synuclein aggregate pathology. *Eur J Neurosci* **49**, 316-319.